Contents

List of figures

List of tables

Preface

In this report, the results of the author's MSc fieldwork are discussed. This fieldwork is part of the third and fourth year curriculum of Physical Geography at the Faculty of Geographical Sciences, Utrecht University, Utrecht, The Netherlands. At this faculty, the fieldwork report has the status of MSc Thesis.

The research was carried out in the surroundings of Sölden (Upper Tyrol, Austria) from June 28 to August 20, 1999, and was mainly done with Mr. A. Coevert (Faculty of Earth Sciences, Free University of Amsterdam). Minor parts of the fieldwork were carried out with Mss. M.F. Noomen and C.M.H. Kooijman. Mag. K. Pfeffer, dr. M.R. Hendriks, dr. Th.W.J. van Asch and dr. V.G. Jetten supervised the study.

The research was partly financed by the European Union, as it is part of the European research project GETS (Application of *G*eomorphology and *E*nvironmental Impact Assessment to *T*ransportation *S*ystems), with — amongst others — the research topic 'environmental impact assessment of ski runs'.

I would like to thank some persons for their support during the research. Als eerste natuurlijk Arthur Coevert, mijn veldwerkpartner gedurende zeven weken: hartelijk bedankt voor het naar boven dragen van die enorme hoeveelheden water zonder er psychisch noch lichamelijk onder te bezwijken: "Laat mij maar dragen, dat is goed voor mijn conditie." Karin Pfeffer danke ich für Ihre große Hilfsbereitheit während die Geländearbeit und danach. Besonders Ihre nicht ablassende Neugier war immer eine wichtige Stimulanz, die sie selbst nicht verlor wann sie zitterte vor Kälte (und das passierte regelmässig, oder?). Ook Theo van Asch gaf voortdurend blijk van een grote interesse voor het onderzoek: zelfs na acht uur zonder sigaretten ging het op die bepaald onsympathieke luchthaven van Miami nog over *subsurface flow* snelheden. Met de opmerkingen van Martin Hendriks (betreffende de Engelse grammatica) en Theo van Asch (betreffende het bodemfysisch en erosiegedeelte) is de definitieve versie vervolmaakt.

Verder bedank ik Christel Kooijman en Marleen Noomen voor het onbaatzuchtig delen van hun data. Jaap Cremer en Liz-Anne Strik worden bedankt voor het bij tijd en wijle krachtig relativeren van het onderzoek: "Niks aan het handje, we gaan volgend jaar lekker toch weer skiën." Martin — "Ik draag geen bergschoenen maar laarzen want ik ben hydroloog" — Hendriks en Victor — "Goh, best leuk hoor, met water en zand spelen"— Jetten worden bedankt voor het 'opsporen' van plekken voor afvoermetingen respectievelijk het bouwen van dammetjes aldaar. Alessandro Ghinoi è ringraziato per portare me all'ospedale, dopo che mi sono scontrato con la mia bicicletta durante la campagna.

Gerhard Markart (Institut für Lawinen- und Wildbachforschung, Innsbruck, Republik Österreich) und Günther Bunza (Bayerisches Landesamt für Wasserwirtschaft, München, Bundesrepublik Deutschland) möchte ich danken für die grosse Menge Literatur die sie mir geschickt haben.

Tot slot wil ik mijn ouders bedanken voor het gedeeltelijk betalen van het verblijf tijdens het veldwerk en Johan van Dommelen die ons van een prachtige metallic grijze Volvo 340 1.4 GL als veldwerkauto voorzag. En natuurlijk alle studiegenoten, medesporters, huisgenoten, zussen, vrienden en dergelijke die voor de broodnodige afleiding zorgden: "Zit je nou alweer / nog steeds achter die computer? Ga eens wielrennen / uit / de krant lezen / iets leuks doen!" Bedankt: Fleur, Thomas, Tjerk & Nynke, Sandra, Jeroen, Daniël, Evian & Johan, Cyrille & Stanley, Denise & Jasper, Ruben, Pepijn, Gea, Andrea & Pierre, Danielle, Arnold e.v.a.

Samenvatting

In juli en augustus 1999 is onderzoek gedaan naar de invloed van skiën op de oppervlaktewaterhydrologie en de bodem(erosie) in de omgeving van Sölden, Tirol, Oostenrijk. Sölden is een skidorp in het Ötztal op de grens van de Ötztaler en Stubaier Alpen. Binnen het onderzoek zijn 122 regenvalsimulaties uitgevoerd in combinatie met metingen van de belangrijkste bodemparameters en continue afvoermetingen van drie beken. De gegevens hieruit zijn bewerkt, statistisch onderzocht op verbanden en verschillen en indien nodig geï nterpoleerd. Met de geï nterpoleerde data en het erosie- en afvoermodel EUROSEM is onderzocht waar de bodem gevoelig is voor met name rill-erosie. Uit de analyses blijkt dat skiën in dit gebied indirect leidt tot compactie van de bodem (via beschadiging van de vegetatie) maar direct leidt tot een verlaging van het bodemvochtgehalte, hetgeen wellicht de oorzaak is van deze vegetatiebeschadigingen. De verticale doorlatendheid en de porositeit van de bodem worden echter niet aantoonbaar door skiën beï nvloed. Wel leidt skiën tot een grotere kans op oppervlakkige afstroming, wat bodemerosie met zich mee kan brengen als de vegetatiebedekking laag is. Dit wordt bevestigd door de modelresultaten en veldwaarnemingen die laten zien dat vooral kunstmatig opgebrachte bodems zonder vegetatiebedekking sterk erosiegevoelig zijn. Het verdient daarom aanbeveling om een goede vegetatiebedekking te handhaven, zodat de bodemcompactie tot een minimum beperkt wordt en het erosierisico laag blijft. Onder het huidige beleid van de skionderneming in het gebied wordt duurzaamheid voldoende gewaarborgd.

Summary

In July and August 1999, the influence of skiing on the catchment hydrology and soil (erosion) was investigated in the surroundings of Sölden, Tyrol, Austria. Sölden is a ski village located in the Ötztal valley in between the Ötztaler and Stubaier Alps. Within the research, 122 rainfall simulations were conducted, often in combination with measurements of the most important edaphic parameters. Also, continuous discharge measurements were carried out in three headwaters. The data that were output of these measurements were manipulated, subjected to statistical investigations in order to reveal differences and relationships and, if necessary, interpolated. With the interpolated data and the erosion- and runoff model EUROSEM it was investigated where the soil is sensitive to, in particular, rill erosion. It appears from the analyses that skiing only indirectly leads to compaction of the soil (via vegetation damage) but directly leads to a lowering of the soil moisture content, which may cause vegetation stress and damage. The vertical conductivity and the porosity of the soil are not affected by skiing. However, skiing increases the chance of overland flow, which, under circumstances with low vegetation cover, can lead to soil erosion. This is supported by the model results and field observations, which show the artificial soils without vegetation cover to be vulnerable to soil erosion. It is recommended that the vegetation cover be kept on a sufficiently high level, to protect the soil from compaction and to minimize the erosion hazard. When the present policy of the skiing companies in the area is maintained, sustainability is sufficiently secured.

Zusammenfassung

In Juli und August 1999 wurden Untersuchungen durchgeführt über die Einwirkung von Skifahren auf die Hydrologie und den Boden (beziehungsweise -erosion) in der Gegend von Sölden, Tirol, Österreich. Sölden ist ein skitouristisches Dorf im Ötztal, das zwischen den Ötztaler und Stubaier Alpen liegt. Im Rahmen der Untersuchungen wurden 122 Regenfallsimulationen in Kombination mit Messungen der wichtigsten Bodenparameter durchgeführt. Ausserdem wurden Abflussmessungen durchgeführt. Die ermittelten Daten wurden danach bearbeitet, statistisch ausgewertet und wenn notwendig interpoliert. Mit den interpolierten Daten und dem Erosions- und Abflussmodel EUROSEM wurde ermittelt, wo im Untersuchungsgebiet der Boden durch Erosion (vor allem Rinnenbildung) gefährdet ist. Die Analysen zeigen, dass Skifahren in diesem Gebiet nur indirekt (via Erschütterung der Vegetation) zu Kompaktion des Bodens, jedoch direkt zu einer Minderung des Wassergehaltes im Boden führt, was möglicherweise die Ursache der Vegetationsschädigungen bildet. Die vertikale Wasserleitfähigkeit und Porosität des Bodens werden allerdings nicht nachweislich vom Skifahren beeinflusst. Jedoch erhöht es die Wahrscheinlichkeit von oberirdischen Abfliessen, was Bodenerosion mit sich bringen kann, falls die Vegetationsbedeckung niedrig ist. Diese Ergebnis wird unterstützt von den Modelergebnissen und den Observationen im Gelände, die zeigen, dass künstliche Böden ohne Vegetationsbedeckung besonders erosionsempfindlich sind. Es ist gerade darum empfehlenswert, eine hohe Vegetationsbedeckung zu unterhalten, damit die Bodenkompaktion minimalisiert wird und das Erosionsrisiko niedrig bleibt. Die heutige Politik der Skiunternehmen genügt, um die Dauerhaftigkeit zu gewährleisten.

1 Introduction

1.1 Context

For ski areas in general, literature indicates that skiing, and especially the preparation of ski pistes with heavy machinery[1], can cause compaction of the soil (Giessübel 1988). This means an increase in bulk density and decrease in porosity (Rowell 1994; Verhees 1998; Van Dijck 2000) and decrease in infiltration capacity (Roels 1984; Fullen & Reed 1987). These changes may lead to serious overland flow (Karl & Toldrian 1973; Schauer 1981; Bunza 1984a; Bunza 1989; Bunza & Schauer 1989), (rill) erosion (Bunza 1984b; Cernusca 1984a, 1984b; Mosimann 1986; Bunza & Porzelt 1991), mass wasting (Löhmannsröben 1984; Löhmannsröben & Cernusca 1990; Markart *et al.* 1999) and vegetation stress (Löhmannsröben 1984; Giessübel 1988; Bringazi 1989; Löhmannsröben & Cernusca 1990; Neweseley *et al.* 1994; Neweseley 1997) on ski pistes. Besides, levelling of ski tracks leads to the loss of soil structure (Mosimann 1983, 1986; Ramskogler 1987), which may also lead to the above hazards, notably soil erosion (Mosimann 1981).

However, for Sölden, virtually no data are present to aid in the hazard risk assessment as this is part of the GETS research program (Section 1.3). Therefore, this and other studies were carried out to provide data with which the assessment can be made (see also Section 1.4).

1.2 Location of the study area

The study area is located at approximately 47° northern latitude and 11° eastern longitude, near the villages of Sölden (1368 m a.s.l.) and Hochsölden (2083 m a.s.l.) (see Figs. 1.1 & 1.2). Including the villages Ober-, Hoch- & Unter- Gurgl, Vent and Zwieselstein (Fig. 1.2), these villages make up the community of Sölden, which is part of the district / *Bezirk* of Imst, province / Land Tyrol[2], Western Austria (Fig. 1.1). See Fig. 6.1 for a map with the main features of the study area.

The valley in which the community is located is called Ötztal; the mountain region is called Ötztaler Alps, which is a distinct mountain range within the European Alps. For more information on — amongst others — geology and geomorphology of the study area and the Ötztaler Alps in general, one is referred to Chapter 2.

1.3 The GETS research program

As already mentioned in the preface, this study is part of the European GETS program. The GETS research program is funded by the European Union's TMR program. The Training and Mobility of Researchers program, as the TMR program is fully called, has the goal to bring young researchers in contact with laboratory facilities, computer modeling and several institutes throughout the European Union (Prakash 2000).

[1] When the word 'skiing' is used in the following, the whole range of piste preparation by snow bullies, levelling and the action of skiing itself are meant.

[2] In German: Tirol. When an English equivalent for a German topographical name exists, this will be used throughout the text.

Figure 1.1. Location of the study area in a larger framework. The fieldwork area is denoted with a black box in Tyrol.

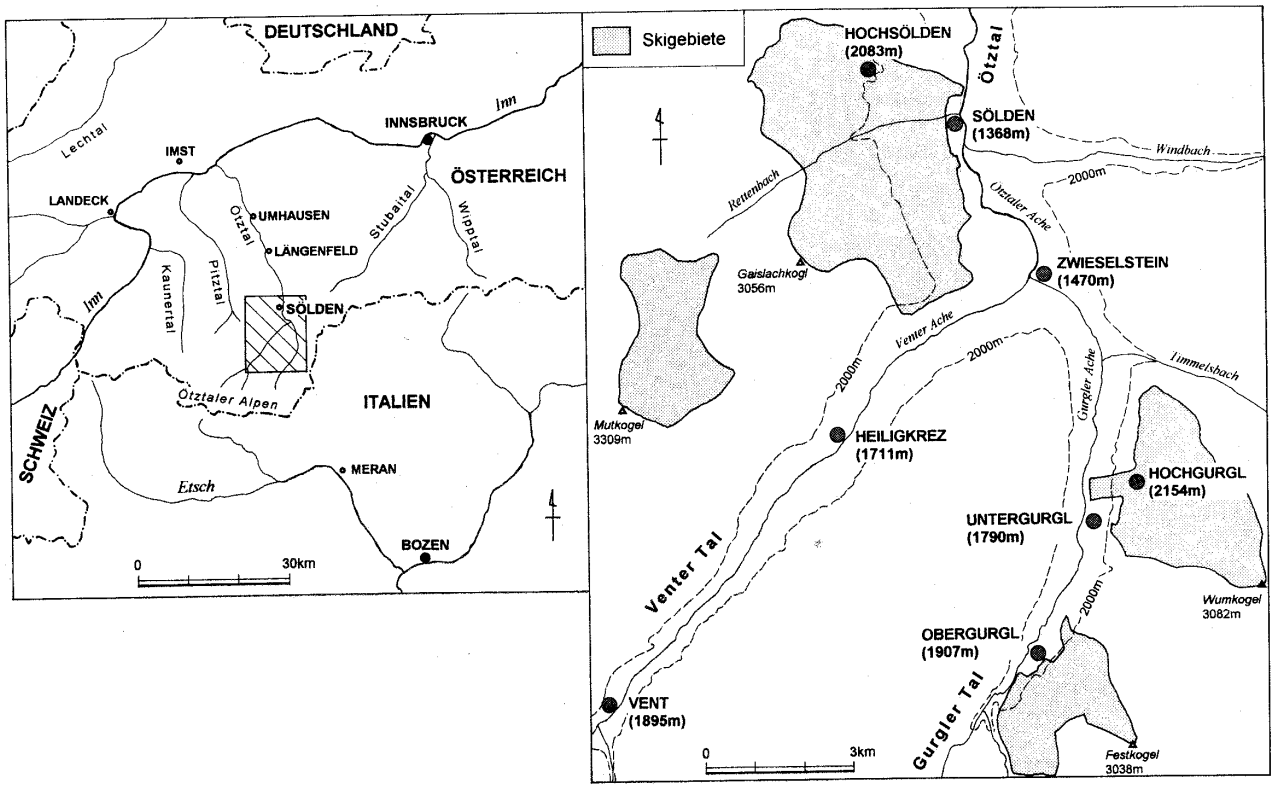

Figure 1.2. Location of the study area. The study area is located in the area west of Sölden, south of Hochsölden and east and northeast of the Gaislachkogl. Source: Kureha (1995, Fig. 7).

The present GETS program is an extended version of an earlier EU research program on geomorphology and environmental impact assessment (EIA for short). It applies the general procedures proposed in this earlier program to the assessment of transportation systems (for example, ski runs and lifts), thereby focusing on the use of computer models and GIS techniques. Because these computer simulations need validation, a few case studies in the European Union are selected to test the models and provide data for input. The current study is part of the Sölden case study, which

focuses on the assessment of the impact of ski tracks at different spatial scales and at different levels of implementation and development (Prakash 2000).

The overall research objectives of GETS are (Prakash 2000):

- development and improvement of methods for assessment of geomorphologic impacts and impacts of transport systems on the environment;
- recommendation of (computer) techniques and methods for EIA, which are applicable in a European context, e.g. a decision support system or GIS techniques;
- training of young researchers and promotion of contacts and collaboration between universities, (semi-)governmental institutes and public administrations;

The outcomes of the GETS investigations will be (Prakash 2000):

- maps with environmental and geomorphologic indicators[3] and the distribution of hazards and risks;
- estimations and comparisons of the impacts and a description of the causes and effects of the respective impacts;
- guides in decision-making, using mainly spatial decision-support tools (such as multi-criteria / multi-objective decision methods), cost-benefit analysis and concepts of environmental economics.

1.4 Utrecht's part in the GETS program and research questions

Within the overall GETS program, the task of Utrecht University is to assess the influence of the human impact (i.e., skiing) on the environment of the Sölden ski area in the light of the risks mentioned in Section 1.1 and the influence of the natural hazards and risks (e.g. avalanches, debris flows) on the location and planning of new ski tracks. The effects of skiing on the risk of mass wasting and vegetation growth potential in the Sölden ski area are investigated by Strik (2000) and Noomen & Kooijman (2000), respectively. This report focuses on the influence of skiing on the general soil condition and catchment hydrology of the Sölden ski area.

The following research questions are to be answered in this report:

1. Is there a clear and marked influence of skiing on the most important soil (hydrological) parameters, such as infiltration capacity, bulk density / porosity and soil moisture content?
2. Is there an increased risk of notably rill erosion or less severe erosion phenomena such as splash and wash erosion as an effect of skiing?
3. What is the influence of skiing on the catchment hydrology and catchment hydrological parameters such as amount of peak discharge, time to peak, runoff coefficient and amounts of either overland or subsurface flow?

A fourth research question was considered important enough to be investigated as well, but this question does not have a direct link to the GETS objectives or its expected outcomes, but it can be important for the next research question. The question was put forward by Van Asch (*pers. comm.*) as a verification of the research Van Dijck (2000) carried out in Southern France:

4. Is the influence of rainfall intensity on infiltration capacity indeed markedly positive?

A fifth research question was posed by Karssenberg (*pers. comm.*). While the answer to this question is rather important in perspective of the GETS objectives (especially in the light of modelling and the application of GIS techniques), it will be considered here as well:

[3] An indicator is an environmental parameter that can be influenced by human activity.

5. Is there a spatial correlation for the hydraulic conductivity present in the area and if so, is it possible to interpolate this important hydrological parameter? Is this interpolation still possible when the influence of rainfall intensity on infiltration capacity is indeed as remarkable as presently thought?

1.5 Fieldwork goals and setup

The goals of the fieldwork itself in the summer of 1999 were to:

- gather the soil physical parameters mentioned earlier on both ski tracks and undisturbed areas with which, after data manipulation, the first research question can be answered;
- gather additional soil and hydrological data needed to calibrate the runoff / erosion model EUROSEM (Morgan *et al.* 1998a, 1998b) with the infiltration equation by Smith & Parlange (1978) incorporated and combined with a rill initiation threshold formula, with which the second and third research question can be answered.

The fourth and fifth question can be answered using the data gathered to answer the other three questions.

The setup of the fieldwork, for which eight weeks were available, was to investigate the availability of water (needed for measurements as described in Section 3.1), to get a general impression of the area and to map the locations of the ski tracks and undisturbed areas in the first week. After this, it was tried to take samples in the whole skiing area (the area around Sölden and Hochsölden in Fig. 1.1) — whilst also considering the bordering natural areas — in order to get an overview of the total area for the considered parameters. With this general knowledge, in later phases of GETS, interesting sub areas for investigations on a more detailed scale can be selected.

During the total fieldwork period, measurements in mountain streams (described in Section 3.4 and 3.5) were carried out on both a random (discharge measurements) and continuous (water level measurements) basis. These random measurements could not be planned for they are linked to weather conditions and flow regimes. The three monitored headwaters had a catchment covered with forest and ski tracks, mainly ski tracks and some shrubs, and shrubs and ski tracks in equal portions, thereby enabling a comparison between different land uses (see also Table 6.1).

The report will continue with a description of the fieldwork area. After this, the methods and techniques that were used during the fieldwork are discussed, followed by a presentation and discussion of the results in several chapters (focusing on either hydrological or edaphic parameters and their interpolation). The report ends with the conclusions of the investigations; are all of the above stated questions answered to full satisfaction, or is it impossible to answer them due to inadequate techniques, too few or improper results or other reasons?

2 Description of the study area

In this chapter, an overview of the geology, geomorphology, climate, vegetation and some social-geographical aspects of the study area will be given.

The geological and geomorphological descriptions are representative for a wider region than the study area alone. In fact, most of the time they deal with the whole of the (Ötztaler) Alps. The same holds for the climate description, although to a lesser extent. For vegetation, only the more broadscaled vegetation patterns are discussed, because coworkers (Noomen & Kooijman 2000) give a more detailed description of the vegetation in the study area. To stress the importance of the ski pistes for the study area in a more economical and social sense, a short introduction to the development of the skiing tourism in the Ötztal in general and in Sölden in special will be given here.

2.1 History of tourism development in the Ötztal and Sölden

In the 18th century, the upper class in the cities of Germany and other central European countries start to get interested in alpinism (Hupke 1990). In the beginning, the tourism (mainly climbing and walking) only takes place in the summer season. Nevertheless, already before mid 19th century so, before the first alpine railroads came into existence (Haimayer 1984) , farmers in the Ötztal started to provide housing and feeding for the tourists (Hupke 1990)[4]. It is not till the end of the 19th century that the first skiers arrive in the Ötztal. However, already in the 1930s the winter season had become the main tourist season. The first ski lift in Sölden starts to work in 1948 (Hupke 1990), which is rather late, because in the 1930s one is already able to build ski lifts (Kureha 1995). Until this time, the developments can clearly be regarded as being of an initiating and discovering nature according to Bätzing (1991, *op. cit.* Kureha 1995). From 1955 on, tourism is rapidly developed in a quantitative sense: more ski lifts, pensions and hotels are built. In the 1970s, Sölden and Obergurgl are already the most important tourist places in the province Tyrol (Csikos 1975). From 1981 on, the development is more qualitatively oriented: better roads are provided and the comfort of hotels and pensions increases (Kureha 1995; Bätzing 1991, *op. cit.* Kureha 1995).

Nowadays, in Sölden more than 30 million people per year are transported by ski lifts to a still increasing number of ski pistes. The community of Sölden has in fact the largest lift capacity of all Austrian tourist communities (Kureha 1995).

2.2 Geology and geomorphology of the Ötztaler Alps

As already stated, the Ötztaler Alps are a distinct mountainous area within the European Alps (Fig. 2.1). Notably tectonics and rocks are quite different from other eastern alpine regions due to a largely independent formation, not to speak of the differences with the bordering Northern Alps (that are largely made up of limestone) and the Southern Alps (clearly separated from the Eastern Alps by the peradriatic strike-slip fault (Bögel & Schmidt 1976)). See Fig. 2.2 for the location of the separate alpine regions according to the terminology of Bögel & Schmidt (1976)[5].

[4] In German, this is called *Nebengeschäft*. This means that besides the income of farming the family also earnes an income with tourism business by running a restaurant, a hotel, a pension and alike. Nowadays, the more important part of the income is earned in tourism business but farming remains necessary to provide fresh food for the tourists.

[5] Throughout the text the classification of the Alps according to Bögel & Schmidt (1976) will be followed, as this is a general accepted one.

The Ötztaler Alps, together with the Silvretta Massif in the West and Stubaier Alps in the East, make up what is called in German the '*Altkristallin*' (literally translated in English: 'Old Crystalline') or *Ötztal Masse* (Ötztal Massif). This massif is located in the Central Eastern Alps (Fig. 2.2) and approximately one quarter of the province Tyrol exists of this massif (Purtscheller 1978).

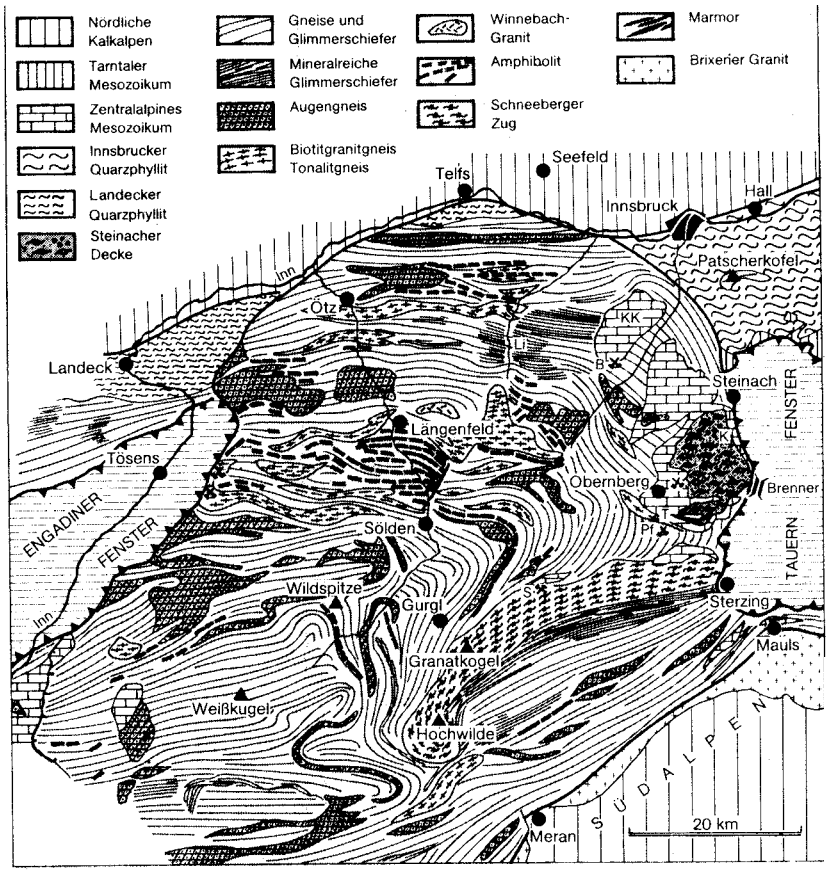

Figure 2.1. The A*ltkristallin,* a distinct Paleozoic mountainous area in the Eastern Alps. Sölden is located in the center of this area. Source: Bögel & Schmidt (1976, Fig. 32).

Figure 2.2. Three different classifications of the Alps. The Altkristallin from Fig. 2.1 is outlined with thicker lines. Source: Bögel & Schmidt (1976, Fig. 1).

The origin of this Altkristallin massif is as follows (general outline after Purtscheller (1978) and other authors):

1. Sedimentation of sands, marls and grauwacke in a syncline in a generally marine to lacustrine and sometimes even deltaic environment (Terwindt 1990) (Proterozoic, Cambrian and Ordovician, more than 450 million years ago).

2. Basaltic and andesitic vulcanism, which is due to the suturing of the Baltic and the Laurentic Plate (Late Ordovician-Early Silurian).

3. Intrusion of the massif by granite as part of the early phase of the Caledonian orogeny (the granite is dated as 486-415 million years old (Purtscheller 1978), corresponding with the Ordovician & Silurian eras).

4. First high pressure metamorphism of the Old Paleozoic and Young Proterozoic sedimentary and igneous rocks in the syncline during the Caledonian orogeny. This accompanies the formation of the Old Red Sandstone continent (Late Silurian - Early Devonian, a period of around 400 mln y bp) (Stanley 1989). Datings on rocks from the Ötztal and the Ventertal (a side valley from the Ötztal) indicate ages around 415 and 480 mln y bp (Purtscheller 1978), corresponding with the Early Ordovician / early Caledonian orogeny and Late Silurian / late Caledonian orogeny, respectively.

5. A retrograde phase takes place in between the Caledonian and Variscian orogeny, in which a broad tropical seaway developed that bordered the Old Red Sandstone continent (Stanley 1989) (Devonian).

6. Tectonical deformation and origination of the so called '*Schlingentektonik*'[6] (Fig. 2.3) in the south of the Ötztaler and Stubaier Alps in the early Variscian orogeny. During this orogeny the second and major metamorphosis of the Altkristallin takes place in the deep environment of the Earth's crust (Bögel & Schmidt 1976). Datings reveal rock ages of about 280 mln y bp (Purtscheller 1978), corresponding with the Late Carboniferous era. The end of this rather short but powerful orogeny can be dated before the ending of the Late Carboniferous, according to Von Klebelsberg (1935).

7. Intrusion of the metamorphosed mass by dikes (Perm, 250 mln y bp). These dikes exist of diabase, diabase porphyrite and gabbro (Von Klebelsberg 1935; Glauert 1975).

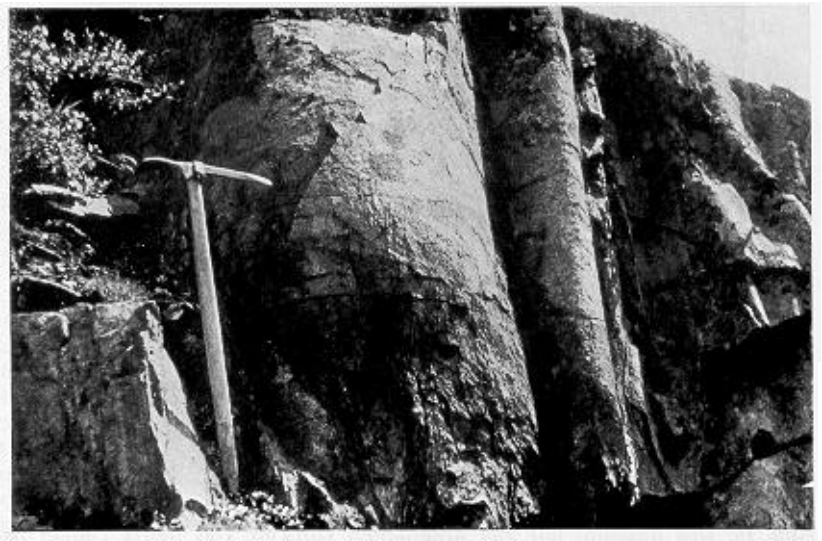

Figure 2.3. An example of *Schlingentektonik* as can be found in the surroundings of Sölden. Source: Purtscheller (1978, Fig. 17).

8. Sedimentation of the so called '*Brenner Mesozoikum*' at the margins of the Altkristallin by invasion of the sea. This invasion is invoked by the formation of a new geosyncline in conjunction with the rifting of the continent Pangea (Glauert 1975; Stanley 1989). The Brenner Mesozoikum constists of limestone and dolomites deposited during mainly during the Trias and Jura.

9. Alpine orogeny, starting in the Early Cretaceous according to Bauer (1988) and Bögel & Schmidt (1976) and about 100 to 90 mln y bp according to Purtscheller (1978). During this orogeny the whole Altkristallin massif is shifted to the North (Fig. 2.4),

[6] *Schlingentektonik* is the German name given by Sander (1912) and Schmidegg (1933) (Bögel & Schmidt 1976) to a fold with near vertical axes (Von Klebelsberg 1935). The name is more widely used for the resulting form than for the actual process.

thereby overriding younger and hardly metamorphosed Mesozoic rocks of the Pennine overfold like the '*Bündner Schiefer*' (schists) and '*Zentralgneiss*' (Central Gneiss) (Heißel 1975) (see also Fig. 2.1).

Next to the shifting, the Brenner Mesozoikum is faulted and folded, while the Altkristallin itself exhibits only some fault zones in which the metamorphic rocks are mylonitised (pulverized). In the case of the Altkristallin the Alpine orogeny ends around 120 to 70 mln y bp (Late Cretaceous to Paleocene), when the massif starts to cool down (Bögel & Schmidt 1976). Mineral datings listed in Purtscheller (1978) show the youngest minerals to be indeed some 77 million years old.

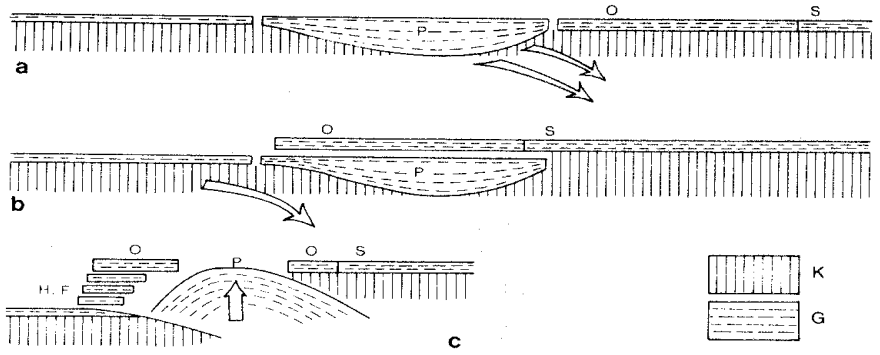

K = continental crust; G = sediments; H = Helvetic zone; F = Flysch. Source: Bögel & Schmidt (1976, Fig. 101).

Figure 2.4. The shifting to the north of the *Altkristallin*/ Ötztaler Alps (as indicated with an O) in the Alpine orogeny. In a, the Pennine Alps (P) subduct under the Eastern Alps (O). After this event, a new subduction takes place in the Tertiary (b), which leads to the upheaval of the

10. Development of the undulating relief[7] of the slightly elevated Altkristallin, starting in the Oligocene (Dongus 1984) and ending in the Pliocene (Glauert 1975). The radial drainage ('*Querentwasserung*') erodes the landscape and sheds molasse in a northerly direction (Glauert 1975).

11. Development of a downcutting valley system, which results in a more mountaineous relief (Miocene till now) (Dongus 1984; Bauer 1988). The valley erosion causes the so called Raxlandschaft to disappear before the beginning of the Pleistocene and also causes a shift from Querentwasserung to '*Längsentwasserung*' (parallel drainage) system (Glauert 1975; Dongus 1984) by a combination of fluvial erosion and faulting (Bauer 1988; Bätzing 1997).

12. Uplift of the whole Altkristallin massif (Fig. 2.5d). This is caused by the fact that the root of the Altkristallin - made up of relatively light felsic crust material - is subject to high pressure in a rather dense mafic environment. This high pressure and density difference cause the light material to be uplifted (Bauer 1988). The uplift takes place in several separate phases and starts in the Pliocene according to Schmidt (1922, *op. cit.* Von Klebelsberg 1935) or in the Miocene according to Glauert (1975) and has not ceased yet (Bauer, *pers. comm.*).

13. Shaping of the relief by flowing glaciers in the Pleistocene ice ages, resulting in the present-day mountainous relief with steep valley sides and shoulders (Glauert 1975; Dongus 1984). Besides shaping, sedimentation of morainic material (mainly ground moraine and rock flour) in hollows and at side valley outflow points takes place (Von Klebelsberg 1935).

[7] This is often called a '*Raxlandschaft*' (Glauert 1975; Dongus 1984; Bauer 1988). The name is derived from the landscape of the region Rax in Eastern Austria, which is a partly developed mountaineous area of moderate relief.

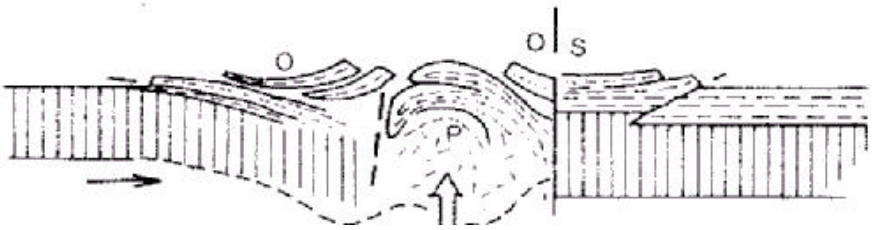

Figure 2.5. The uplift from the Eastern Alps through the rise of the lighter Pennine crust material. Source: Bögel & Schmidt (1976, Fig. 96d).

Petrology and mineralogy

The most common major rock species in the study area is paragneiss. Paragneiss is a group of metamorphic rock species, which in this case originates from the metamorphism of sedimentary rock during the Caledonian and / or Variscian orogeny.

Because the main sedimentary rock in the Ötztaler Alps during the metamorphism was grauwacke, which is very heterogeneous in mineral content, the newly formed paragneissic rocks are inhomogeneous as well (Purtscheller 1978). The most widespread paragneiss species is gray biotitic plagioklase gneiss (build up of quartz, plagioklase - albite to oligoklase -, biotite / chlorite and some muscovite). Another less well metamorphosed rock species derived from sedimentary rock is dark green Gneisglimmerschiefer (gneissose micaschist, with the same minerals as the biotitic plagioclase gneiss but also including granate, staurolith and disthen) (Bögel & Schmidt 1976; Purtscheller 1978). Both biotitic plagioclase gneiss and Gneisglimmerschiefer can be found throughout most of the study area (Fig. 2.6, see next page).

The second most widespread major rock species is orthogneiss, which originates from the metamorphism of igneous rocks. In the Ötztaler Alps, orthogneiss came into existence after metamorphism of felsic vulcanic rock, felsic tuff or granite (Tenschert 1974, *op. cit.* Purtscheller 1978). The main orthogneiss species in the study area are (Purtscheller 1978):

- biotitic granite gneiss, with merely quartz and biotite. It can only be found in the North of the study area between Grieskogl and the Ötztaler Ache;
- zweiglimmerige Augengneis (mica containing augengneiss), with quartz muscovite, biotite and microkline. It can be found at the Rettenbach glacier and in the proximity of Gaislachkogl and around Schwarze Schneide and Pitztaler Joch, according to Von Klebelsberg (1935);
- muscovite granite gneiss, with besides a large proportion of muscovite also K-feldspar. This species is mixed with the zweiglimmerige Augengneiss.

In the Ötztaler Alps migmatite, amphibolite, quartzphyllite (Bögel & Schmidt 1976) and even some marble (Von Klebelsberg 1935; Purtscheller 1978) can be found as well. However, these rock species cannot be found in the study area. Note that also the *Brenner Mesozoikum* is not represented in the study area.

Stuctural geology

In the study area, the main strike of the rock layers is East-West (in the Northern part) to Southeast-Nordwest (in the Southern part). The slope of the rock layers varies from nearly horizontal to rather flat in the North (0-30°) to near vertical due to the Schlingentektonik in the surroundings of Zwieselstein (Purtscheller 1978).

Geomorphology

In mountaineous areas, generally four geomorpological zones can be distinguished, each with its own distinct processes and forms (Bätzing 1997):

- Collin-montane zone (1300 up to more or less 2300 m high). In this zone, the main process is erosion by flowing water, which can be either sheet or stream erosion. However, in the study area these processes do not exhibit much power due to the presence of forest and shrubs (see also the section on vegetation). Yet, when they would be of importance, stream erosion would probably dominate over sheet erosion and would more likely lead to widening of the valleys than a deepening. Because of its reach of about one kilometer, it is the most important zone in the study area in an areal sense.
- Periglacial or solifluction zone (2300 up to approximately 2600 m high), the lowest actual mountain zone. As the name already indicates, in this zone the main process is solifluction, caused by freeze-thaw cycles. In this area also soil slips can be found, which are present at many places within the study area (Strik 2000). This zone can be separated from the higher zones because it is free of snow in summer.
- Glacial zone (2600 up to 2800 m). This zone exhibits a large number of glacial forms such as cirques (notably in the Rettenbachtal), end moraines (below Haimbachjoch, Fig. 2.7), rock glaciers (below Schwarzseekogl and in the Rettenbachtal), cirque lakes (Schwarzsee, Gaislacher See), transfluention passes (Timmelsjoch, 5 km SE of Sölden, Fig. 2.8) and other remnants of Pleistocene glaciers. Because of the dominance in the high-mountainous landscape of these artifacts, it is the most characteristic zone of the Alps (and for the study area as well, notwithstanding its coverage of only a relatively small area).

Figure 2.7. An end moraine as deposited by the Pleistocene glacier on the Tertiary terrace of Hochsölden. The person on the ridge indicates the scale.

- Nival zone or frost weathering zone (above 2800 m). The glaciers (often cirque/corrie glaciers) which are still active can be found in this zone. The major processes are frost weathering and hydration shattering, both causing large amounts of debris. In the Rettenbachtal alluvial fans, resulting from transport of physically weathered material, can be viewed (Fig. 2.9). In the inner part of this valley, debris flows are still active.

Figure 2.8. Transfluence pass (Timmelstal) of the Pleistocene glacier near the Austrian-Italian border. View is to the west.

Figure 2.9. View on the debris cones and steep alluvial fans in the Rettenbachtal. The view is to the south, the Rettenbachferner is in the upper right of the figure.

The traces of the destroyed Raxlandschaft are major geomorphological phenomena in the Eastern Alps in general and also in the study area. Nowadays, the remaining parts of this Tertiary landscape can be viewed as relatively flat areas at different levels of height. Because of their stepwise character (flat parts are separated from each other by steeper parts and are in itself stepped as well), the remnants are often called Piedmont steps (Bauer 1988). In the Quarternary, these flat areas represented shoulders and were further moulded by glaciers.

In the study area, the relatively flat area at Hochsölden (Fig. 2.10) is interpreted as such a Tertiary remnant (Heißel 1975). It is part of the '*Hochtalsystem*' (high valley system) or '*Hochtalboden*' (high valley surface) which borders the Ötztal at 1900 and 2500 m (Heißel 1975) a.s.l. and is one of the younger remnants of the Raxlandschaft (Bauer 1988). The flat areas in the east and south-east of the Gaislacher Kogl are located at the same level as the Hochsölden area and are therefore probably also member of this same system. Because of their flatness, these areas can stock large amounts of snow, firn or ice, dependent upon their level of height (Heißel 1975). This can be of hydrological importance as the melt of the snow in spring and summer releases large amounts of melt water.

In contrast to the flat area at Hochsölden stand the steep higher parts at the watershed of the Pollestal / Ötztal, in the back of the Rettenbachtal and at the

Gaislachkogl. Plucking by cirque glaciers often caused these steepenings, of which the cirque lakes are present-day witnesses. However, most of the time the main reason for the steepness of the high terrain is the resistance to weathering of the orthogneissic rocks, as is the case for the Gaislachkogl and the Rettenbachtal. This resistance causes the areas made up of orthogneiss to be higher and/or steeper than the surrounding area, thereby providing potentially glacierised surfaces (Heißel 1975). Because of their steepness and less fractured surface, the above mentioned areas can be major contributors to flood peaks, because water runs off fast and will not infiltrate easily.

Figure 2.10. The flat area in the center of the photo is the Tertiary terrace level of Hochsölden. Note that there is still some snow present at its upper part. The steep slopes to the left are the rims of the Pollestal and the watershed between the Ötztal and the Pollestal. The new ski area of the Schwarzseekogl is to the left and just outside this picture. The view is to the Northeast. The photo was taken at the Gaislachkogl.

2.3 Climate of the Ötztaler Alps and Sölden

Sölden has both a mountain climate and a humid sea climate (in the Köppen classification called EH and Cfb climate, respectively). In short, the climate of the study area can be characterized by a relatively dry winter and wet summer, rather low temperatures throughout the year (Fig. 2.11) and a major contribution of solar radiation to heat of soil and air. The different climatic variables (precipitation, temperature and radiation) will be treated separately here.

Precipitation

Sölden is located a few kilometers to the north of the central axis of the Alps, which is close to the border between the Eastern and Southern Alps (Fig. 2.2). This means that weather and climate are controlled by both northern influences and its central location in a high-mountainous area. The weather from the south, yet close by, has hardly any influence on the weather of the Ötztaler Alps. As the study area is fenced off from the eastern and western winds as well — by respectively the Silvretta and Stubaier Alps —, mainly the winds from the north control the local climate. These northern winds bring cool polar-maritime air with a large content of moisture (Fliri 1974). This results in rainy days throughout the year. Daily quantities are, however, relatively small: the average maximum amount of rain for one day is 50 to 70 mm in the center of the Alps; the absolute maximum in the period 1931-1960 is 100 to 125 mm (Fliri 1975). Therefore, rainfall intensities are usually not large. During the fieldwork period, the largest measured ten minutes intensity was 48 mm/h. Two times, ten minutes rainfall intensities of about 20-25 mm/h were measured.

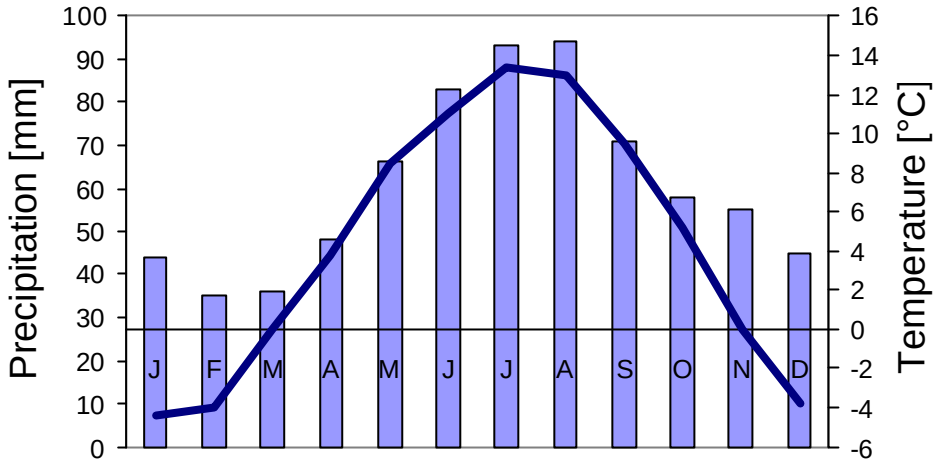

Figure 2.11. Yearly precipitation and temperature regime in Sölden. Data source: Kureha (1995, Fig. 8), measuring period for temperature: 1881 1930; measuring period for precipitation: 1901 1960.

The yearly precipitation peak occurs the summer months, as can be seen in Fig. 2.11; in Fig. 2.12, the values of Vent can be hold representative for Sölden. This maximum is caused by the prevalence of weather conditions (humid winds from the North and Northwest) that bring rain in this time of the year: approximately 50 out of 92 summer days in the North-Eastern Alps have rain-benefiting weather conditions (Fliri 1974). The relative absence of these weather conditions in winter leads to a minimum of precipitation during winter. The result of this is that about 39 % of the year's total precipitation in the Inn catchment falls in summer and only about 18 % of it in winter (Fliri 1974). Also, in at least half of all years, the winter is the driest season and the summer the wettest (Fliri 1974).

Notwithstanding the large number of rain days per year, the total precipitation per year in the study area is not very large when compared to other alpine regions (Fig. 2.12). The topographical location of Sölden near the central axis is quite important in this context, as with every kilometer moved to the centre of the Alps, on average 10 mm of yearly precipitation is lost (Fliri 1974). The yearly precipitation amounts to some 700 mm according to Kureha (1995, with 1901 - 1960 as measuring period) and to some 740 mm according to Fliri (1974, with 1931 - 1960 as measuring period). The average standard deviation of the total is relatively low and lies near 10 to 15 %, but is 35 % in summer. The relative low amount of precipitation results in a high index of 'hygric continentality'[8] in the southern Ötztaler Alps, which is defined as (Schiechtl 1975):

$$HK = \left(\frac{P}{h}\right) \cdot 100 \qquad \text{(Eq. 2.1)}$$

with: HK = hygric continentality [°]; P = yearly precipitation [mm]; h = height [m]. For Sölden, this value is close to 70°, whilst in the Rettenbachtal the HK is slightly above 70° (Schiechtl 1975). A value of >70° denotes 'very continental'.

[8] The continentality denotes the harshness of the climate: the higher the index of continentality is, the harsher the climate is perceived by human beings. In general, a continental climate refers to a relatively low rainfall amount and a high contrast between seasonal temperatures.

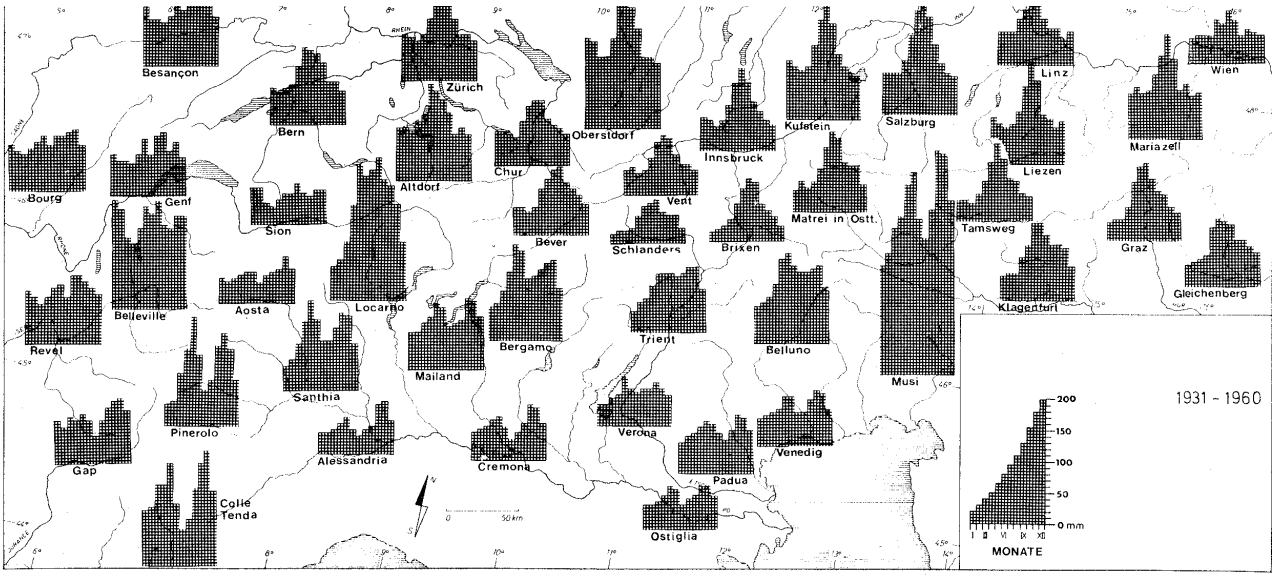

Figure 2.12. The precipitation regimes for different places in the Alps. Sölden is located between Vent and Innsbruck, in the dry part of the Alps. Source: Fliri (1974, Fig. 7).

Temperature and radiation

The air temperature is mainly controlled by outgoing (longwave) radiation from the ground surface and advection; general weather conditions as well as the shortwave radiation are relative unimportant (Fliri 1974; Glauert 1975). This is caused by the fact that the air is relatively dry and therefore unable to absorb much shortwave radiation. Therefore net longwave radiation accounts for up to 30 % of the energy input of the air (Glauert 1975). This is possible because due to a low average fractional cloud cover (however, in the fieldwork period this value amounted some 65 %), the ground receives a relative large amount of solar radiation. This is partly used for heating up the soil and partly emitted as longwave radiation, thereby warming up the air.

As can be seen in Fig. 2.11, in Sölden the amplitude of temperature is approximately 18 °C, with a minimum temperature in January of about -4.5 °C and a maximum temperature in July of about +13.5 °C. This amplitude is relatively high in comparison to other alpine regions due to the higher continentality of the region (Fliri 1975). The temperature continentality can also be expressed by indices. Conrad's index of continentality incorporates temperature and latitude:

$$k = \frac{1.7A}{[\sin(\varphi + 10)]} - 14 \qquad \text{(Eq. 2.2)}$$

with: k = index of continentality [ ]; A = yearly amplitude in temperature [°]; φ = latitude [°]. Sölden has an index of 22.9, Amsterdam (The Netherlands, Cfb climate) of 19.5 and Irkutsk (Central Siberia, Dw climate) of 78.4. Another, yet comparable, index of continentality is Gorczynski's:

$$K = 1.7 \cdot (A/\sin\varphi) - 20.4 \qquad \text{(Eq. 2.3)}$$

with: K = index of continentality [ ]. According to this equation, Sölden has a K of 21.4, Amsterdam of 17.1 and Irkutsk of 83.2.

The absolute variability of temperature in the Tyrolian Alps is not large: the standard deviation (F) lies between 0.9 °C in summer and 1.25 °C in spring; the skewness is -0.20 in winter and +0.33 in summer (Fliri 1974), indicating a nearly normal distribution. In addition, the spatial variation in temperature at the scale of the Ötztaler Alps and higher is not as high as that for precipitation, because the controlling variables radiation and advection are not much influenced by surface relief (Fliri 1974).

Hydrological implications

Temperature, radiation and precipitation all reach a peak in summer. Because high temperatures and radiation are by far the most important variables for snow melting, the snowmelt and precipitation peak partly overlap in time. This leads to a prolonged time of high discharges in spring and summer. An example of this can be seen in Fig. 2.13b, in which the relative discharge of the Inn river throughout the year is shown.

Because the daily maximum totals of precipitation as well as the maximum rainfall intensities are relatively low, all rain can be expected to infiltrate easily in areas where soils with reasonable conductivities are present. Only in the case of prolonged wet spells or rain in combination with snowmelt and frozen soil, Hortonian and notably saturation overland flow could be expected occur (see also Chapters 4 and 6).

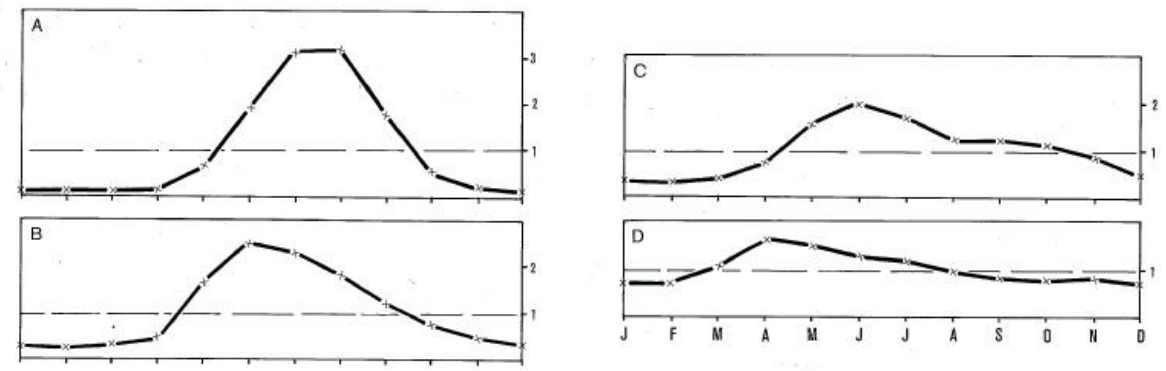

Figure 2.13. Regimes for four different rivers in the alpine region. A: Matter Visp at Randa (representative for a glacial regime); B: Inn at Innsbruck (representative for a nival regime in the highlands); C: Tessin at Bellinzona (northern Italy) (representative for a nival regime); D: Emme at Emmenmatt (northern Switzerland) (representative for a nival / pluvial regime). Source: Glauert (1975, Fig. 7).

2.4 Vegetation of the Ötztaler Alps

The large-scale diversity of vegetation in the Alps is controlled by four gradients (Bätzing 1997):

- hypsometric gradient. This gradient, referring to the change of height, is the most important. The existence of seven different vegetation zones (planar, collin, montane, subalpine, subnival and nival) is a direct consequence of this gradient in height, since height also influences climate, soil and geomorphologic processes.
- periphery-center gradient. This gradient denotes the differences in climatology between the margins and the center of the Alps: the margins exhibit far more precipitation, higher temperatures and a smaller amplitude than the centre (in which Sölden is located), with its higher continentality.
- planetarian gradient. This gradient would also influence the general vegetation characteristics of the area also if it would not be a mountainous area. It stands for a general decrease of temperature with an increase of distance to the equator.
- west-east gradient. This gradient is also not caused by the mountainous character of the area as well. It namely refers to the increase in continentality of the climate in Europe in eastern direction.

Vegetation zones

In the mountainous environment of the Alps, seven vegetation zones can be distinguished, a possible sub classification in lower, middle and higher sub zones for the montane, alpine and nival zones (Ernst 1984). Also other sub classifications (e.g.

Meurer (1984)) are possible. Of these seven zones, the Mediterranean (planar) and colline zone do not reach high enough to enter the study area: the colline zone reaches up to 1100 m a.s.l. in the Central Alps (Ernst 1984; Bätzing 1997). The nival zone is also not represented in the study area because its lower reach is too high.

The outline of the four vegetation zones given below follows Bätzing (1997). The heights are according to Bätzing (1997) and Ernst (1984); other authors are cited when needed:

- Montane zone (1100 up to 1700-1900 m). In the central alpine dry zone, in which the study area is located, this zone exhibits a forest of fir (*Abies alba*), spruce (*Picea abies*) and larch (*Larix decidua/Larix* ssp.). In its higher regions, pines (*Pinus sylvestris*) are also present. This zone is also called mountain forest zone (Ernst 1984), because it is largely dominated by forest (Tivy 1993), which is indeed the case for the study area. Nevertheless grassland is not only present in the immediate surroundings of Sölden (outside the study area), it is also present at the boundary with the lower reaches of the subalpine zone. It is not expected to be of natural origin (Noomen, *pers. comm.*). These alpine meadows are located around Hochsölden and are mainly used for haying.
- Subalpine zone (1700-1900 up to 2200-2400 m). In the study area, the forest- or timber-line is located in this zone: it lies at about 2000 m. Below the timberline, the zone is again forest-dominated. Its lower horizon is dominated by spruce and its middle horizon by larch and pine species (*Pinus cembra* and *Pinus arole* (Tivy 1993)). Its higher horizon is located above the timber-line and consists of dwarf shrubs (notably *Vaccinium* ssp.), rosette alpine herbs and heath (*Calluna vulgaris*) (Ernst 1984; Meurer 1984; Tivy 1993), with an understorey of mosses at some places. In the study area, these species are not mingled but concentrated in different areas within the upper subalpine zone. In non-skiing areas, dwarf trees (*Pinus mugo*) are present within the higher subalpine zone but real *krummholz* is hardly present in the study area.
- Alpine zone (2200-2400 up to about 2800 m). In theory, this zone exhibits heather at its lower reaches, but these plants do not reach high enough in the study area. In the remaining parts of the zone, grasses (in the study area mainly in the lower and steeper reaches) and sedges (at flatter places) dominate. According to Schiechtl (1975), in the Tyrolian Alps these are part of respectively the Festuceta (with *Festuca* ssp. as dominating species) and Primulo-Curvuletum associations.
- Subnival zone (2800 up to 3100 m). The more practical upper and lower boundaries of this zone are the perennial snow patches and the snow-line (Ernst 1984). This zone exhibits mainly mosses and lichens (e.g. *Rhizocarpon geographicum* and *Xanthoria elegans* (Rowell 1994)) and is only present in the fieldwork area in the surroundings of the Gaislachkogl (3054 m) and the Schwarzsee. In these high reaches, some pioneer vegetation is also present (Schiechtl 1975).

Hydrological implications

Vegetation is commonly known to be important for the transpiration of soil moisture. Transpiration can mount up to 4,7 mm / d for a spruce forest and up to 4,3 mm / d for a larch forest (Schiechtl 1975). This amount of transpiration in combination with a sloping terrain causes the chance of water logging of the soil to be rather low. Also, interception influences the hydrology of the area as well. The interception storage of the Tyrolean coniferous forests is 3-20 mm (Aulitzky 1970, *op. cit.* Schiechtl 1975) and even mosses

and lichens are able to intercept 3 to 10 mm of rain (Geiger 1961, *op. cit.* Schiechtl 1975)[9]. When forest is logged for the construction of ski pistes, the amount of transpiration and interception decreases. At the same time, the infiltration rate can decrease drastically, enabling the occurrence of overland flow. For example, according to data in Schiechtl (1975), for one hour of rainfall (i = 100 mm / h), 45 % of the rain runs off under heather, 80 % under alpine grasses and only 17 - 23 % under spruce forest. This influence of the vegetation on the infiltration rate of the soil is not directly but rather indirectly through its influence on the soil structure, moisture content, organic matter content and other soil (hydrological) variables.

[9] Interception measurements carried out during the fieldwork show interception storages of 1.4 to 1.8 mm for loosely packed moss.

3 Research methods and measuring techniques

In this chapter, the several research methods and measuring techniques that were used during the fieldwork itself and part of the data processing afterwards are treated. The theory behind a method or technique, how a method was applied and why a technique was used are explained. Alternatives are given and advantages and disadvantages of the techniques are discussed.

3.1 Infiltration measurements

The larger part of the research was dedicated to measurement of the (un)saturated hydraulic conductivity of the soil, *K* for short[10].

The reason for the large amount of time spent on measuring this parameter is that *K* is related to all five research questions as stated in section 1.4. It is both an important soil and hydrological variable, influencing the amount of peak discharge in headwaters and eventually rivers, the rise of the soil moisture content due to infiltration (important for plant growth) and the amount of overland flow.

There are several possible methods to measure the infiltration, e.g. the inversed auger hole method (Kessler & Oosterbaan 1974), double ring infiltration measurements, Kopecky ring infiltration measurements, ponded infiltration tests, disk permeameter or tension infiltrometer tests (Perroux & White 1988; Ankeny *et al.* 1988, 1991) and rainfall simulations.

It was decided to select the two last methods mentioned above: the tension infiltrometer and the rainfall simulator tests. These two methods were chosen because they both can handle unsaturated conditions and therefore the measurement of unsaturated *K* (K_{unsat}). This seems to be more appropriate in modelling than K_{sat}, because during natural rainfall the soil will nearly always remain unsaturated to a certain degree (Dikau 1986). Furthermore, with rainfall simulations, the hypothesis as mentioned in Section 1.4 that rainfall intensity positively influences infiltration capacity can be tested. This cannot be done using a tension infiltrometer, but with this apparatus one is in full control over the amount of negative pore pressure (i.e., the amount of 'water below saturation') in the soil.

However, the main disadvantages of a tension infiltrometer are the need for a completely level surface (without stones protruding through the surface), a low terrain inclination and a non-vegetated soil surface (Blijenberg, *pers. comm.*). Not one of these requirements is met in the fieldwork area, as can easily be deduced from the descriptions in Chapter 2. After one test with the disc permeameter, it already became clear that this apparatus could not function in the fieldwork area. It was therefore not used anymore and instead, all subsequent infiltration measurements were carried out with a rainfall simulator[11].

The apparatus that was used in rainfall simulations is the 09.06 Mini Rainfall Simulator, which is constructed by Eijkelkamp Agrisearch Equipment (Giesbeek, The Netherlands). See Fig. 3.1 for a side view with size measures and Figs. 3.2 & 3.3 for a front view. This apparatus was used because it is easy-to-handle on the rather steep slopes in a mountainous environment, it uses little water because of the small surface that is sprinkled, it is easy to install and has a low weight — the last argument was

[10] In the following, a subscript will denote the character of K; when there is not made use of a subscript, hydraulic conductivity is used in a general sense.

[11] More on rainfall simulators can be found in Parsons & Lascelles (2000).

considered important because it had to be taken from place to place on foot. One person can carry the apparatus because it fits in a large backpack. This last requirement (lightness) overruled all other requirements for rainfall simulators as stated in Hall (1970), Riezebos & Seyhan (1977), Imeson (1977) and Moore *et al.* (1981).

The rainfall simulator used here is of the drop forming type. Other light and useful rainfall simulators of this type are the ones constructed by Adams *et al.* (1957) (and later modified by Van Asch (1980, Appendix A1)), Imeson (1977) and Roth *et al.* (1985). However, the first one has the disadvantage of a small rained surface (6 inch in diameter), the last two have high fall heights (over 1.5 m), which is inconvenient on a steep mountain slopes.

Another wide range of rainfall simulators is of the spraying type. Light and small ones were used and / or constructed by Bork (1980), Bork & Bork (1981), Neibling *et al.* (1981), Luk & Morgan (1981), Luk (1985), Luk *et al.* (1986) and Nicolau *et al.* (1996). These are all inherited from one of the first rainfall simulators, the rainulator (Meyer & McCue 1958), but all have the disadvantage of using large amounts of water relative to the drop forming simulators. Besides, they make use of gasoline consuming pumps for the building up of the high pressures that are needed to spray the rain, resulting in total equipment yet too heavy. A last disadvantage from the spraying type simulators is the sensitivity to wind, because of the small droplets that the nozzles form. A tent may diminish the wind effect, but this means extra weight to carry.

A	*Rain shower*
B	*Wind shield*
a	*Water reservoir*
b	*Sprinkling head*
c	*Capillairs*
d	*Aeration tube*
e	*Tubing*
f	*Filling opening*
g	*Plot frame*
h	*Gutter*
I	*Sample receiver*

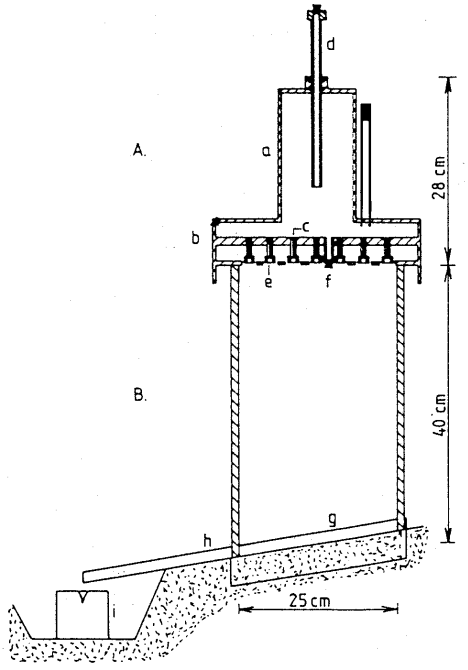

Figure 3.1. The measures of the used rainfall simulator 09.06 by Eijkelkamp Agrisearch Equipment. The gutter (h) was hardly used because of the stony soils in the area. Instead, the splash screen (not depicted here) was put in the soil, as

The rainfall simulation, which leads to the determination of the infiltration and thus *K*, is carried out in the following manner:

• First, a good and rather representative location is chosen for the plot that will be rained artificially. 'Representative' means for example that the location does not contain too many stones in the soil or has a surface stoniness grade that is abnormally high: grass is the rule rather than the exception in the study area.

Furthermore, the location has to be either in the middle of a ski run or in a naturally vegetated area. This makes the assessment of influence by skiing on the infiltration easier, because the results will be more clear-cut than when simulations are done on the fringes of natural areas or pistes. However, sometimes the simulation was

deliberately situated in a border situation, to see whether there exists a gradient in infiltration capacity across a ski run.

According to the manufacturer of the rainfall simulator, the slope of the location has to be at least 20 % or 11°. This was not always reached, but it is thought that this is not an important factor influencing the outcome of the tests.

• Vegetation (often grass or shrubs) is cut with the use of a pair of scissors, thereby reducing the influence of interception (storage) and enabling the visual observation of surface runoff phenomena during the actual test. It is tried to leave the plant roots in the soil as much as possible. Stones are left in or on the soil.

Figure 3.2. The rainfall simulator on a ski piste (rs46).

Figure 3.3. The rainfall simulator on a natural slope (rs23).

• A hole is dug in front of the plot, at the lower (down slope) side of the location. One bucket for collecting the runoff water is placed in this hole, another one is placed on top of the rainfall simulator, in reach of the person who changes the buckets every two minutes after time to runoff (t_p) is reached.

According to Eijkelkamp, a gutter has to be placed on the topsoil, enabling the runoff water to flow into the bucket. The gutter has an edge that has to be put into the soil, to prevent it from loosing its grip on the soil. Unfortunately, when stones are present in the soil, the edge often does not fit neatly in the soil and runoff water can easily infiltrate in the opening between the gutter edge and the soil. Therefore, this method was not applied during the fieldwork and it was decided to put the splash screen — that is also delivered with the apparatus — into the side of the hole as indicated on Fig. 3.3. In this way, it is ensured that runoff water does not infiltrate in the space left between the gutter edge and the soil, but simply flows over the edge of the soil and falls on the splash screen leading the water to the bucket. Another advantage of this method is the fact that it is now possible to catch both shallow

subsurface flow and overland flow. The only disadvantage is that the exposed soil directly above the splash screen can cause some lateral infiltration: water may not fall down on the splash screen, but may 'stick' to the exposed soil and may be sucked into it because of negative pore pressures. This fact is considered to be at least less problematic than the 'gutter edge effect', because the negative pore pressures which cause the lateral infiltration diminish quickly with the wetting of the soil, while the opening between the gutter edge and the soil remains a sink during the whole test.

- An aluminium plot frame is put on the location, preventing the runoff water from spreading laterally over the borders of the plot. Then the water reservoir on top of the simulator is filled, while it is upside down and resting on the metal frame outside the plot boundaries. This ensures that no spilled water falls on the plot while filling up the simulator's reservoir. After this the simulator is placed above the plot on the metal framework. The simulation begins when the cork from the aeration opening is released. It is tried to leave the air entry opening as small as possible, thereby ensuring a low infiltration intensity that is close to natural intensities. Putting the aeration tube in its lowest position helps in the achievement of low rainfall intensity. The adjustment of the rainfall intensity is avoided as much as possible. When there has not been collected any runoff after 30 minutes, the rainfall intensity is increased. Most of the time however, runoff already starts within 10 minutes.

When the influence of the wind is too large, and drops are clearly blown away from the plot, a windscreen is used. When the wind only disturbs the fall pattern of the drops, it only has a positive influence on the rainfall coverage of the plot and there is no windscreen applied.

- During the simulation test, every two minutes the water level in the reservoir is noted. Half a minute after this notation, the bucket with the runoff is emptied in a large measuring jug. This jug contains the cumulative amount of runoff. By subtraction of the amount of rainfall during two minutes by the new amount of runoff, one can assess roughly whether steady-state infiltration is reached or not. When the difference between rainfall and runoff (= the infiltration) remains constant for at least three measuring times (= six minutes), the simulation is ended because constant infiltration is supposedly reached.
- The data that are gathered during the simulation are processed in a spreadsheet and the rainfall intensity [mm / h] and K [m / d] are calculated, the last one using two methods, denoted here as 'cumulative' and 'momentary' method. These calculations are explained below.
  - To calculate the rainfall intensity in [mm / h], a graph is constructed with the time on the x axis and the cumulative rainfall on the y axis (see Fig. 3.4). A standard linear regression line is fitted through the data points (which form a nearly straight line) using ordinary least squares regression (OLS for short), as can be seen in Fig. 3.4. The slope of this line gives the amount of rainfall in unit of volume per unit of time ([mm^3 / s] in this case). When this value is divided by the surface of the sprinkled area (taken as $25.5 \times 25.5 = 650.25$ cm^2), the rainfall intensity in [mm / h] is derived after conversion.

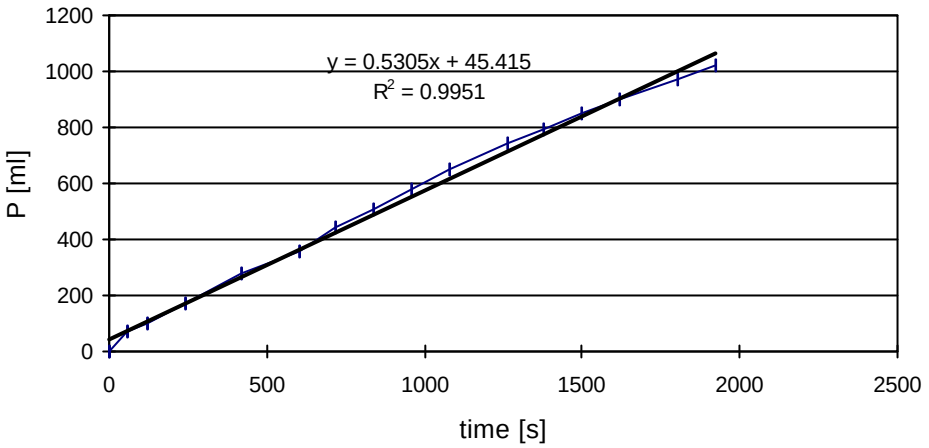

Figure 3.4. Cumulative amount of precipitation as function of time for rainfall simulation rs79

— The 'cumulative method' to determine the infiltration capacity works nearly in the same manner as the above-described method. First, the cumulative runoff is subtracted from the cumulative rainfall, to determine the cumulative infiltration until each measuring moment. One difference with the determination of the rainfall intensity is the removing of points at the beginning of the curve. This is done because at some locations steady flow was not yet reached at that time. Plotting of these points would influence the slope of the trend line, which is again used in the calculation. The slope delivers the hydraulic conductivity in [m / d] after conversion and division by plot area.

— The 'momentary method' is different from the above two methods but easy to use as well. This time a graph is made with time on the x axis but infiltration rate (=) {rainfall – runoff} /) time) on the y axis (Fig. 3.5). This graph is visually checked and the time after which steady infiltration is — more or less — reached is noted. All infiltration rate values after this moment are averaged and converted to K.

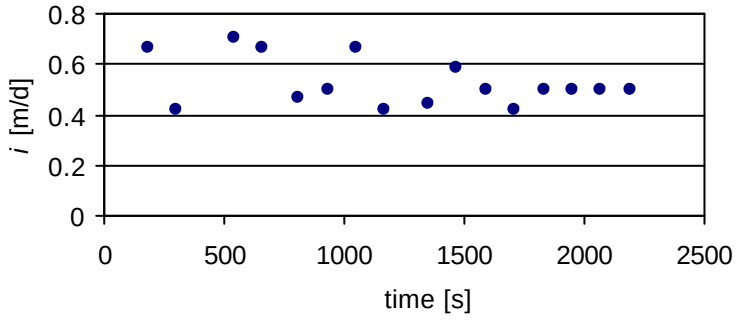

Figure 3.5. Momentary infiltration against time for rainfall simulation rs81.

3.2 Measurement of soil shear strength (J_s)

In erosion modelling, soil shear strength is widely recognised as the most important soil physical variable influencing the chance and / or amount of (rill) erosion (Cruse & Larson 1977; Govers 1985; Torri *et al.* 1987; Rauws & Govers 1988; Brunori *et al.* 1989;

Bryan *et al.* 1989; Crouch & Novruzi 1989; Govers *et al.* 1990; Bryan 2000). Therefore, this variable had to be measured for it is needed in most erosion models. With the outcomes of an erosion model, research question 2 can be answered.

There are several methods to measure soil shear strength. First of all, the classical methods such as direct or ring shear tests, and confined or unconfined triaxial compression tests are available. However, these require the taking of soil samples thereby disturbing the soil surface. Because this leads to the formation of holes in the ski tracks, it is not considered as a useful method.

Then there are the soil surface test apparatus, such as the Casagrande cup (Casagrande 1932, 1948), the pocket or laboratory vane shear tester (PVA / LVA) and the Torvane (shear tester), the pocket penetrometer and the drop-cone penetrometer (DCP, also called cone-type penetrometer or drop-cone device).

A liquid-limit test with the aid of a Casagrande cup (Fig. 3.6) gives only a derived (but reliable (Nieuwenhuis, *pers. comm.*)) measure of the soil shear strength. Besides, it is normally used with clay(ey) or other cohesive samples only (Cernica 1995) and its results are dependent upon the operator (Sherwood & Riley 1970, *op. cit.* Selby 1993). Therefore, this method was rejected as useful for measuring soil shear strength.

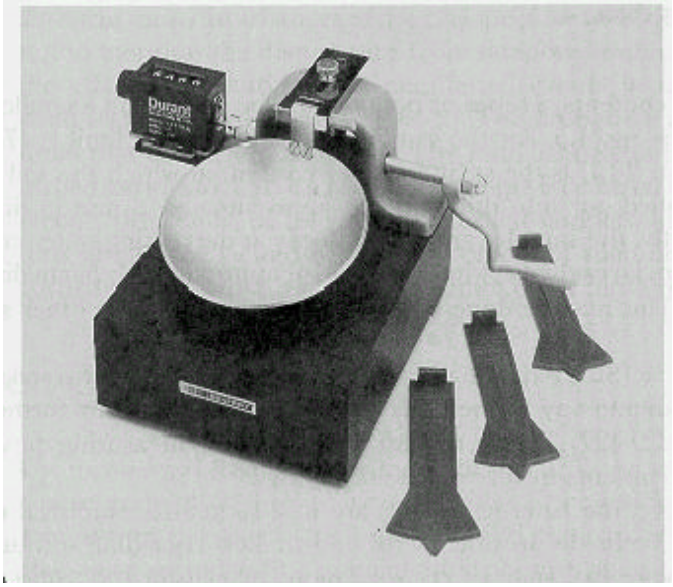

Figure 3.6. A Casagrande cup for measuring a derivative of soil shear strength. Source: Cernica (1995, Fig. 4.4)

The drop-cone penetrometer (Fig. 3.7) is widely used in Europe (Cernica 1995) but receives critical remarks from Brunori *et al.* (1989), Bradford & Grossman (1982) and Anderson *et al.* (1980): its measurements are hardly repeatable (indicated by a wide range of resulting values on a single soil) because they are highly sensitive on the positioning of the cone. Moreover, there is still a residual dependence on penetration depth, even after correction for this parameter. When a small penetration depth is used (as would be the case in the research under consideration), dial readings and cone positioning would introduce important errors (Brunori *et al.* 1989). Because of these remarks, the DCP was also rejected.

A penetrometer is also unusable on stony soils — as are present in the fieldwork area. When the penetrometer hits a stone, and the penetration is still proceeded (because the operator thinks of hitting a cohesive layer or something equivalent), the penetrometer is damaged very easily.

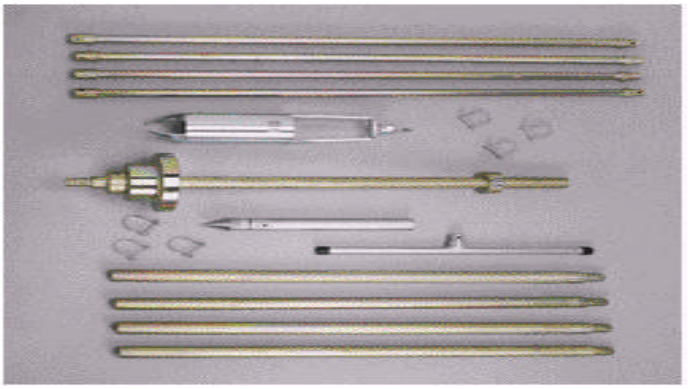

Figure 3.7. A Drop or Dynamic Cone Penetrometer. The tubes are about 76 cm in length, the cone itself is about 10 cm large. Source: ELE (2000, p. 63).

Two other potentially usable apparatus are the laboratory and pocket vane shear tester. The LVA gives fairly good results (CV's are only 10 %, according to Brunori *et al.* (1989)). The only disadvantage of the apparatus is the fact that in the calculation of J_s, the assumption is made that the sampled surface remains cylindrical during the test. This assumption is not met when using clayey soils (Brunori *et al.* 1989). Because these are not present in the fieldwork area, the apparatus could have rendered good results, if it would have been available at the department.

The pocket vane shear tester (Fig. 3.8) gives even more reliable results than its laboratory counterpart, because of its high grade of repeatability, even with different operators (Brunori *et al.* 1989), but this was not available at the time of research either.

All the above remarks leave the Torvane shear tester as the only sound and available option. Fortunately, this apparatus is small, easily manageable, simple and fast in use and light-weighted (see also Fig. 3.9). It has the advantages of the pocket vane shear tester but the sampled surface is larger (ranging from 1.9 to 4.76 cm ∅, instead of normally 1.9 cm ∅ for the PVA), rendering more reliable estimates of J_s. Moreover, since the inclusion of J_s as a rill erodibility parameter following Rauws & Govers (1988) in erosion models such as LISEM (De Roo *et al.* 1996a, 1996b) or EUROSEM (Morgan *et al.* 1998), the Torvane has become the standard test apparatus for soil shear strength.

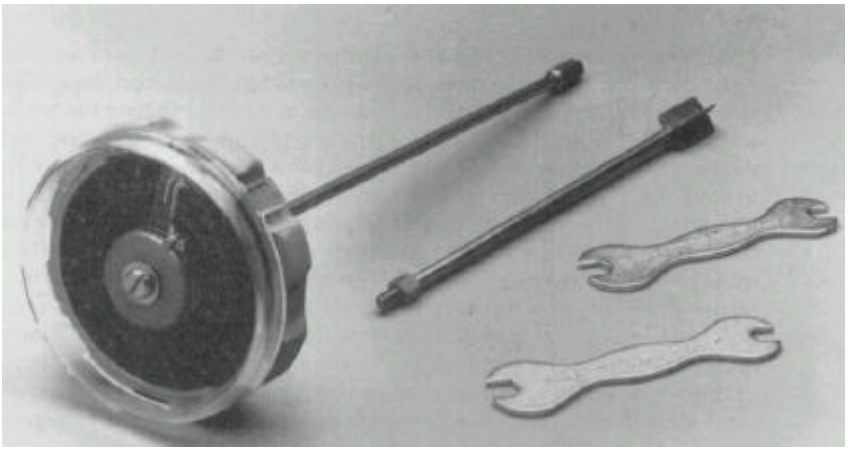

Figure 3.8. A pocket vane tester (PVA). The apparatus is about a few centimetres large. Source: Cernica (1995, Fig. 3.11).

Figure 3.9. A Torvane. A comparable apparatus was used during fieldwork. Source: ELE (2000, p. 80).

The used Torvane is slightly different from the one depicted in Fig. 3.9. It was manufactured by Eijkelkamp Agrisearch Equipment (Groesbeek, The Netherlands), but consists of the same parts as shown in Fig. 3.9. The Torvane works as follows: the apparatus is put on the ground surface, in such a way that the grooves are in the soil surface. Then a torque is applied. When the soil shears, the scale is read off and the quantity is converted to kg/cm^2 with the aid of a calibration graph; conversion from kg/cm^2 to kPa can be achieved by a multiplication with a factor 9.81 (10). When the soil is notably weak or strong, a larger or smaller vane diameter is used, respectively, and another calibration graph is used to convert the quantity. At every measuring place, the method was applied three or four times, and the noted value was the mode.

A disadvantage of the Torvane — which apparently was not noticed by Brunori *et al.* (1989) for the PVA — is its higher dependency on the operator and the operator's experience. This was also found by Luk & Morgan (1981). Bias in the measurements was avoided because only one person carried out all the J_s measurements, so the results are at least comparable within this research.

Because it was noted by Luk (1985) and Govers *et al.* (1987, *op. cit.* Bryan *et al.* 1989) and later confirmed by Govers *et al.* (1990) that the surface state of the soil has a profound influence on the shear strength, it was decided to measure J_s of both the field dry soil and the wet soil after a rainfall simulation. In the following, these two quantities will be referred to as J_{WS} or J_{DS}, which stands for wet and dry soil shear strength, respectively.

3.3 Measurements of soil physical parameters

The major soil physical parameters are — besides shear strength and infiltration capacity — bulk density, porosity and texture. Next to these three parameters, it was chosen to measure stoniness and antecedent soil moisture content (ASM for short) as well, because these may influence infiltration capacity measurement results (Bunza 1984a, 1989) and infiltration calculation, when the EUROSEM-embedded infiltration formula as proposed by Smith & Parlange (1978) is to be used. Measurements of these variables are thus necessary in the light of the first and second research questions (Section 1.4). The Smith & Parlange (1978, Eq. 33) formula is as follows:

$$f(F) = K_s \cdot \frac{e^{(F/B)}}{e^{(F/B)} - 1} \qquad \text{(Eq. 3.1a)}$$

with

$$B = G \cdot (\theta_s - \theta_i);\ B_{rock} = B \cdot (1 - R) \qquad \text{(Eqs. 3.1b \& 3.1c)}$$

and

$$G = \frac{1}{K_s} \cdot \int_{-\infty}^{0} K(\varnothing) \cdot d\varnothing \qquad \text{(Eq. 3.1d)}$$

With: f = infiltration rate [m / d]; F = cumulative infiltration [m]; K_s = the *effective* saturated hydraulic conductivity [m / d]; B = saturation deficit parameter [m]; G = effective net capillary drive [m]; 2_s = soil porosity [ ]; 2_i = ASM = antecedent moisture content [ ]; B_{rock} = B corrected for stones in the soil [m]; R = volumetric stone content of soil [ ]; $K(\varnothing)$ = hydraulic conductivity function [m / d]; $\varnothing$ = soil matrix potential [m].

For measuring ASM, a relatively new technique named Frequency or Time Domain Reflectrometry (FDR / TDR) was available. This technique is easy to use and quickly gives information about the moisture status of the soil. Descriptions of the technique can be found in Drungil *et al.* (1989) and Whalley (1993) and measurement results for an alpine area can be found in Markart *et al.* (2000). The FDR apparatus that was available has four short rods that have to be pushed into the ground in order to measure the moisture content. The bending of one of these rods renders the apparatus useless (Kutílek & Nielsen 1994). While the soils in the fieldwork area are very stony and the chance on bending is therefore rather high, the technique regrettably had to be rejected. Other ASM measurement methods, such as capacitance and neutron probes, resistance blocks and (radiation sources as summarized in general textbooks such as Kutílek & Nielsen (1994, Section 3.2) or Ward & Robinson (1990, Section 5.3.6) were not considered useful.

Considering the above stated remarks on non-gravimetric methods for measuring ASM, it was decided to use a gravimetric method for measurement of ASM. Fortunately, measurement of the other variables such as porosity and soil bulk density (BD) are only possible with gravimetric techniques, so, no double work is done in this way.

The gravimetric method makes use of soil samples, a balance and an oven. The soil sampling is most often done with pF or Kopecky rings. These rings were also used during the fieldwork. The rings have a volume of exactly 100 cm^3, a diameter of about 5 cm and are made of stainless steel. Therefore, the measurements only refer to the status of the upper 5 cm of the soil. They have to be put in the soil, if necessary helped by gently tapping on them with the aid of a rubber hammer (and covering them with a small piece of wood in order to distribute well the exerted pressure on the ring), and dug up again. This ensures that the soil sample is undisturbed. The ring sampling method suffers from the same disadvantage as the FDR apparatus: it is hard to find a place where a ring can be put totally in the ground in total if the soil is stony. Often, one has to try several times before the whole ring is filled with a soil sample. Sometimes it is impossible to fill it completely[12] or even to put in the ground. Markart *et al.* (2000) report the same problems.

The calculation of the soil physical variables after sampling is finished is carried out as follows:

- BD: the weight of the ring subtracted from the weight of the ring plus the dried soil divided by the volume of the ring (= 100 cm^3) renders the soil bulk density in [g / cm^3]. If the ring is not completely filled, the volume of the ring is measured by measuring the height of the soil in the ring. Because the diameter of the ring is known, the missing

[12] See the paragraphs on the calculation of porosity for a solution to this problem.

volume can be calculated. This value is subtracted from the 100 cm^3 in the calculation. In formula:

$$\tilde{n}_t = BD = \frac{M_s - M_r}{100 - V_m} \qquad \text{(Eq. 3.2)}$$

With: D_t = BD = soil bulk density [g/cm^3]; M_s = weight of sample + ring [g]; M_r = weight of ring [g]; 100 = volume of ring [cm^3]; V_m = missing volume of soil in ring [cm^3]. Rawls (1983) gives a method based on soil organic matter content and particle size analysis that offers a possible solution if the BD of only the fine earth fraction is to be wanted. Torri *et al.* (1994) have validated this method with the aid of several data sets and provide their own empirical formula to correct BD for rock fragment content. The analysis however proceeds with the uncorrected BD.

- ASM: this can be considered to be equal to the field capacity (FC) of the soil, because it rained regularly during the fieldwork and the soil water did not evaporate in large quantities because of foggy spells. The missing volume of soil is determined with the above mentioned method. The ring plus sample volume is weighted. Then the ring is put in the oven and dried for 24 hours at a temperature of 105 °C. The temperature is lowered to 80 °C, when large amounts of organic matter are present in the sample. After drying, the ring plus sample are weighed again. The loss of weight is due to the evaporation of moisture from the sample. When this loss of weight is divided by the density of water (which is assumed to be 1.0 g/cm^3) and the sampled volume, the ASM emerges in percent of volume. In formula:

$$\grave{e}_i = ASM = \frac{\Delta M}{1 \cdot (100 - V_m)} \qquad \text{(Eq. 3.3)}$$

With: 2_i = ASM = antecedent moisture content [%]; $)M$ = loss of water due to heating [g]; 1 = density of water [g/cm^3].

- Porosity: a possible missing volume of soil is filled up with clean sand, with a known porosity and volume. This addition of sand aids in the complete subsequent saturation of the soil sample. It was tried to fill all the rings up with more or less the same density of clean sand, but some variation in this may be present. Thereafter the ring is put in a shallow layer of water — not higher than half the height of the ring — and left for up to a few days to saturate. The end of the ring that stands in the water is covered with a nylon mesh to prevent the loss of soil when the ring is lifted out of the water. The soil is supposed to be saturated when the top side of the ring is wet. When saturated, the ring is weighted and put in the oven, using the same temperature and time as is used in determination of the ASM. After the water evaporated, the ring and sample are weighted again. It is assumed that all pores had been filled with water, therefore the volume of water lost while standing in the oven is equal to the volume of pores in the sample. This is calculated with the following formula:

$$\grave{e}_s = Por = \frac{\Delta W - \grave{e}_{s,s} \cdot (M_s/\tilde{n}_s)}{100 - (M_s/\tilde{n}_s)} \qquad \text{(Eq. 3.4)}$$

With: 2_s = Por = soil porosity [%]; $2_{s,s}$ = porosity of the possibly added sand [%]; M_s = mass of added sand [g]; D_s = density of added sand [g/cm^3].

The fourth soil physical variable is texture. This was not measured in an objective and quantifiable way as the other variables, but simply checked by hand. This was done because soil texture class is not influenced by skiing and texture class is no variable in modern soil erosion models.

Yet, another soil variable is the soil stoniness. This was also measured by eye for both the surface (considering a few square metres) and the interior of the soil, i.e. in the

hole dug for the placing of the splash screen of the rainfall simulator. This variable is also relevant when the Smith & Parlange (1978) infiltration model is to be used, namely for conversion from B to B_{rock} (Eq. 3.1c). A stone is defined here as a piece of rock that is larger than 2 cm; gravel is therefore also considered in stoniness.

3.4 Water level measurements

With the continuous measurement of the water level in three headwaters, it is tried to monitor flood peaks due to rain and snowmelt, enabling the answering to the third research question and calibration of the hydrological part of the erosion model EUROSEM.

When a non-continuous method is used, the chance of missing the important events is obviously present. Therefore all non-continuous methods (such as staff and crest gauging) that need to be read off were already rejected at forehand. The measuring devices that were left are the stilling well with a self-registering gauge, a mechanical water level recorder with either a float or a pressure transducer and the electronic pressure gauge with data logger.

The stilling well with a self-registering gauge was rejected because it needed to be built totally new at the three headwaters, which is rather expensive, not to mention the cost of maintenance after the construction. Moreover, the GETS program is only of limited extent in time, so the cost efficiency would be very low when the well would be built for only a few years of research. Besides, in a tourist area as Sölden, there is a chance of harm done to the large apparatus by tourists, either by accident or on purpose.

The water level recorder has the disadvantage of being mechanical, which means that problems can occur with paper jam or rusting. Eventually, it was chosen to use electronic pressure transducers coupled to electronic data loggers. At the time of fieldwork, the non-vented gauge and logger Explorer DC-25 from the Keller AG für Druckmesstechnik (Winterthur, Switzerland) and the vented Sewer gauge from Van Essen Instruments bv (Delft, The Netherlands) were available. To correct for the air pressure for the non-vented Keller gauge, an Explorer DC-25 BARO was also installed. Both instruments work with a membrane that is pressed by air and / or water pressure. This membrane is attached to a sensor, that converts the amount of pressure to an electric signal. With the aid of software on a notebook computer, the values that are saved by the data logger can be read out.

The installation place for the devices was chosen on basis of accessibility, non-visibility for tourists and profile stability. This last requirement is important for the validity of the stage-discharge relationship, which will be discussed later (Section 6.1). On the locations, plastic tubes about 30 cm or more in height were placed in the stratum of the headwaters. In these tubes, the Sewer and Keller pressure transducers were hung in the water, with their membranes a few centimetres above the stream bottom, preventing the membranes to be covered with sediment that settles easily in the nearly stationary water in the tube.

Because the Keller gauges are non-vented (i.e., not corrected for air pressure), this has to be subtracted in a spreadsheet operation. The following formula was used:

$$h = 100 \cdot \left[h_t - \left(\frac{p_a \cdot 100}{g \cdot \tilde{n}_w} \right) \right] \qquad \text{(Eq. 3.4)}$$

With: h = water level [cm H_2O]; 100 = conversion factor [cm / m]; h_t = total pressure on Keller gauge in the water [m H_2O]; p_a = air pressure as measured by the barometric

Keller gauge [hPa]; 100 = conversion factor [Pa / hPa]; g = gravitational acceleration = 9.81 [m / s^2]; D_w = water density = 997.2 [kg / m^3].

Because the water level as measured with the pressure transducers is not exactly the same as the real water level, the values need to be recalculated using a calibration curve or formula. An example of a calibration curve is shown in Fig. 3.10. The 'real' water level was measured by measuring the distance from the top of the stilling well tube to the bottom of the stream and the distance from the top of the tube to the water level of the stream. The difference of these two values provides the water depth. It can be seen that the offset changes slightly because of sedimentation in the tube, causing the bottom of the stream to be slightly. When sediment had settled, this was removed until rock or plant roots (providing a more reliable base level) was reached. This sediment settling is a disadvantage of the method, as is the possible loss of data due to empty data logger batteries or software / data exchange errors.

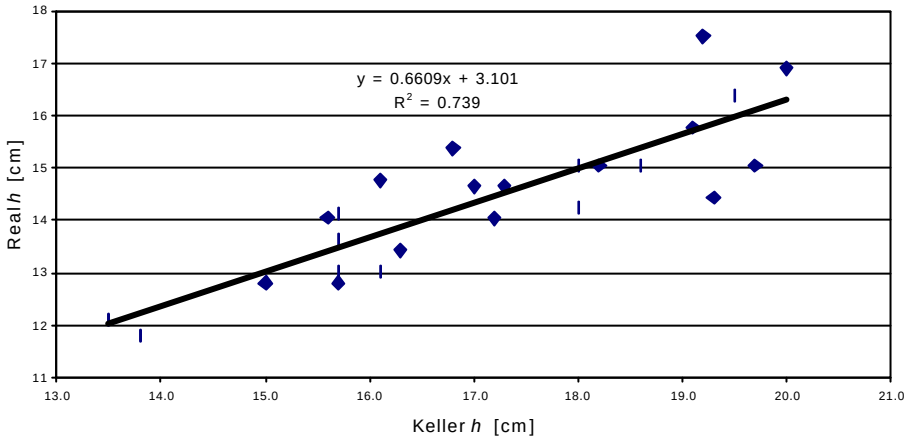

Figure 3.10. Calibration graph to convert from Keller data to real water levels.

3.5 Discharge measurements

With only water level measurements, one does not have information on the discharge of the headwaters. This has to be derived from a stage-discharge relationship, which is an exponential curve or function, which relates water level to discharge. When this relationship is known, one can recalculate the continuous water level measuring sequence to a continuous discharge sequence. With the aid of this, the third research question can be answered and the runoff / erosion model calibrated.

To calculate the stage-discharge function (rating curve / function for short), one needs a number of coupled discharge and water level measurements. There are a few methods possible with which discharge can be measured: the volumetric method, several velocity measuring methods, electromagnetic method, acoustic method, integrating-float technique and tracer methods.

For the volumetric method (direct measurement of the discharge with a bucket), the base flow — let alone the peak flow — of the three headwaters is too high to be adequately measured. Velocity measurements are not possible due to the turbulent character of the headwaters. This turbulence causes large velocity fluctuations and swirling water, which render the velocity measuring methods, the acoustic method (which needs clear water) and the integrating-float technique (which works with bubbles that float from the stream bottom to the water surface) useless. The electromagnetic device was rejected because of the same reason as the stilling well: too

expensive and not cost effective. This also holds for the construction of a measuring flume or weir.

This leaves the tracer methods or dilution gauging methods as the only possible methods for discharge measurement. The only prerequisite for the two methods, called sudden input and constant input method, is a complete mixing of the input within a distance from the input point that can be reached soon enough before the input has arrived. It is better to measure with two persons, one person adding the tracer to the stream and another person waiting downstream for the tracer to arrive.

It was chosen to use the sudden input method, because the constant input method needs a special device (a Mariotte flask for example) that assures the input of the tracer at a constant rate. This device is not needed with the sudden input method.

The sudden input method proceeds in the following way:

- Two large 25 litre buckets are filled with 20 litre of stream water. This volume is named *V*. A large amount of tracer substance, for instance 2 or 3 kilograms of cooking salt or cattle salt, is added to one bucket. Then the salt is mixed very well with a wooden stick until it is completely soluted. The other bucket is left.
- A small sample (i.e., 5 ml) from this salt water is taken and put in a third bucket. Thereafter, this sample volume is diluted with 500 ml fresh water from the bucket that was left. From this newly made solution, the electric conductivity or EC is measured. This is done every time after another 250 ml of fresh stream water from the other bucket has been added. After a total of three litres of fresh water have been added, the solution is thrown away except for a spare sample of 250 ml. This is again diluted ten times, each time after which the EC is measured. With these relative concentration (c_r) and EC data, a calibration graph can be constructed (Fig. 3.11)

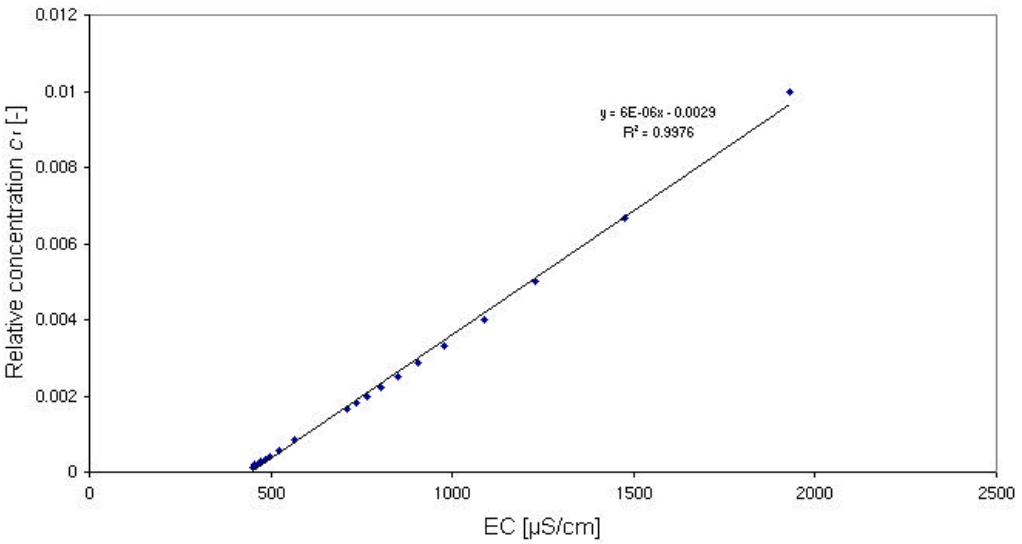

Figure 3.11. Example of a calibration graph used within the salt method. Note that the r^2 is generally very high and almost 1.

- The bucket with the 20 litres of salt water is thrown into the stream. At a down stream distance which is at least ten times the width of the stream, the EC of the stream is measured each 5 seconds for at least 5 minutes. The EC time curve will have a hydrograph-shaped character (Fig. 3.12). The area *A* under this curve can be converted to the discharge *Q* with the aid of the above mentioned calibration curve and c_r. c_r Can be derived from the following formula:

$$c_r = \frac{c_1 - c_0}{c_2} = á \cdot EC + â \qquad \text{(Eq. 3.5)}$$

With: c_r = the relative concentration of the tracer [ ]; c_1 = the absolute concentration of the tracer [mg/l]; c_0 = the background concentration of the headwater [mg/l]; c_2 = the concentration of the tracer pulse [mg/l]; " = regression coefficient derived from the calibration graph [(mg/l)/(mS/cm)]; EC = electrical conductivity [mS/cm]; $ = regression constant derived from the calibration graph c_0 [mg/l].

Next, c_r is filled in in Eq. 3.6:

$$V = Q \cdot A = Q \cdot \int_{t\text{begin}}^{t\text{end}} c_r \cdot dt \Leftrightarrow Q = \frac{V}{\int_{t\text{begin}}^{t\text{end}} c_r \cdot dt} \qquad \text{(Eq. 3.6)}$$

With: V = volume of tracer solution [l]; Q = discharge [l/s]; A = area under c_r time curve [s]. The integral is solved numerically and after deviation of the input volume by this integral, the discharge of the stream is found.

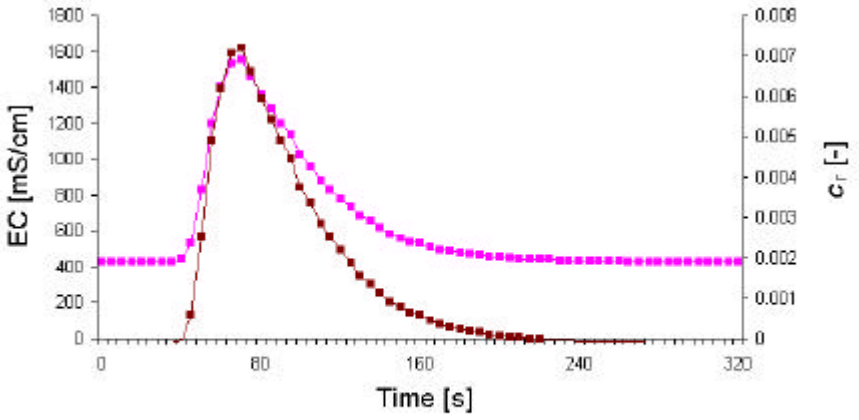

Figure 3.12. Result of the sudden input method. Note that with Fig. 3.11, c_r can be converted to discharge.

3.6 Rainfall measurements

Rainfall data serve in two ways in the present research: 1) as input in the hydrological part of the erosion model; 2) as reference data to which the runoff peaks of the streams can be related. In this manner, rainfall measurements help in answering research questions two and three.

Again, there exist several possible ways of measuring rainfall. However, all instruments bear the same basic device: a funnel or bucket in which the precipitation can be collected. They only differ in the way the rain is registered. When the rainfall is not recorded, there is no information whatsoever on the rainfall intensity; the rain is only stored until the amount is measured by pouring the accumulated rain in a measuring cup. This has to be done manually from time to time. This type of funnel, made of a plastic tube and having a height of about one metre and a catch area of 143.14 cm^2, was used on three places throughout the fieldwork area. Another two non-recording funnels were of the same height but had a diameter of 23.5 cm, rendering a catch area of 433.74 cm^2. See Fig. 4.1 for the locations of the funnels.

The registration can also be carried out automatically (mechanically or electronically), providing valuable information on the rainfall intensity. An example of such a recording instrument is the electronic tipping-bucket raingauge, which is the instrument that was used during the fieldwork. Other instruments that could have

been used are the Dines siphoning / tilting-siphon raingauge and the weighing raingauge, but these instruments have the disadvantage of being mechanical. Besides, these were unavailable since they were in use in research projects elsewhere. The tipping bucket raingauges (manufactured by Eijkelkamp Agrisearch Equipment, Groesbeek, The Netherlands) were located on two places in the fieldwork area, both accompanied by a non-recording instrument for verification. The height of the used tipping-bucket is about 50 cm and the catch area measures a few 100 cm^2. The locations of the tipping-buckets are given in Fig. 4.1 by red dots accompanied by the text 'rg' indicating '*r*ain *g*auge'.

For both recording and non-recording devices, a rule of thumb says that the gauge should be located away from the nearest object so that the distance at least equals the height of that object (Foster 1948). This was accounted when choosing the locations. Also, it is advised to have the funnel's orifice at ground level (Ward & Robinson 1990). Since the soils in the fieldwork area are very stony, it was not possible to place the funnels properly in the soil. To ensure stability and horizontality of the funnel's orifice, the devices were placed within a pile of stones, on a cemented plateau or attached to a small pole.

4 The effect of skiing on the soil

In this chapter, data on soil physical variables gathered with the previously described technique are presented. The influence of rainfall intensity on hydraulic conductivity is explored and explained. The data on ski tracks are compared to data gathered on undisturbed areas, which serve as baseline values. This is done by using common and less common statistical techniques such as descriptive and inductive statistics, correlation, regression and multivariate statistics (factor analysis, discriminant analysis and correspondence analysis).

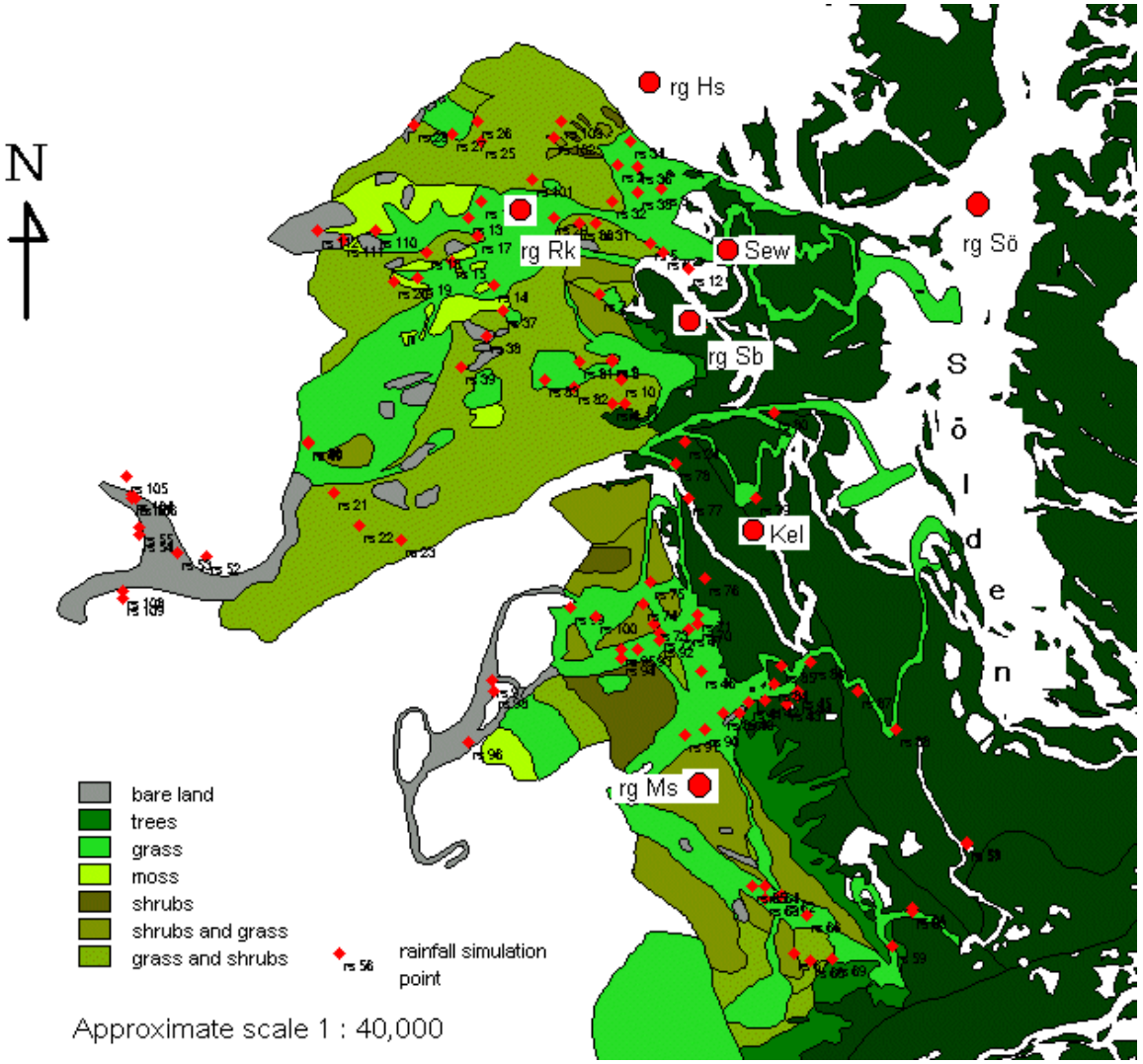

Figure 4.1. The locations of all rainfall simulations, the raingauges (Sö = Sölden, Hs = Hochsölden, Rk = Rotkogl, Sb = Seebach, Ms = Mittelstation) and the discharge measurement places (Kel = forest stream, Sb = Seebach, Sew = Hochsölden stream). 'rg' Stands for 'rain gauge', 'rs' stands for 'rainfall simulation'.

4.1 General description of the dataset

In Fig. 4.1, the locations of the 122 rainfall simulations are depicted. For all these measurements, a hydraulic conductivity could be calculated using the method described in Section 3.1. The number of measurements in Tables 4.1 and 4.2 for the variable *K* can therefore be regarded as the total number of measurements.

On the same locations as the rainfall simulations, the other measurements of wet and dry soil shear strength, BD, ASM, porosity, soil texture and stoniness were carried out. However, these measurements could not be carried out at all places due to different reasons explained below.

Regrettably, BD, ASM and porosity were determined on less than half of all these places; their values were only measured at 37, 35 and 34 percent of all visited places, respectively (see also Table 4.1). It has to be remarked that this is due to a shortage of rings from halfway the fieldwork period onwards, but at many places, it was in fact impossible to take soil samples using Kopecky rings. On places where there were no soil samples taken, the average soil surface stoniness was 31 %, while on places where it was yet possible to take soil samples this percentage on average amounted 21.5, indicating that the amount of stones indeed influenced the number of places where measurements could be undertaken.

Sometimes, it was also impossible to measure soil shear strength with the aid of the Torvane. This was mainly because of dense vegetation: on plots where the soil shear strength could be measured, a slightly lower vegetation cover (i.e., on average 8 % lower) was observed. On highly vegetated patches, the soil shear strength is rather unimportant for the onset of rilling, because the vegetation sufficiently protects the soil surface against splash and flow impact. Furthermore, the dense root mat ensures that rill erosion has little chance. The circumstances for the vegetation nevertheless need to stay well, otherwise the vegetation will suffer stress and root decay will give erosion a chance. The subject erosion will be treated later (Chapter 7).

Missing values for surface stoniness or amount of stones inside the soil are only caused by omission of the field workers to note these quantities. Fortunately, this happened only a few times (see 'number of measurements' in Table 4.1). Soil texture was noted at every location and was never omitted.

Basic statistics	Amount of stones on top of soil [%]	Amount of stones in soil [%]	Dry soil shear strength [kg/cm2]	Wet soil shear strength [kg/cm2]
Number of measurements	112	97	96	87
Mean	27.45	26.20	.44	.33
Standard Deviation	23.28	20.10	.17	.14
Skewness	1.04	.67	.64	-.30
Standard Error of Skewness	.23	.24	.25	.26

Table 4.1. Basic statistics for the eight measured soil physical variables. Skewness is a measure for the difference between the mean and the median: the larger this difference is, the more skewed the distribution and the more different the distribution from a normal/Gaussian distribution is. See also Fig. 4.2 for the histograms.

	AMC [%]	Porosity [%]	BD [g/cm3]	K [m/d]
Number of measurements	43	42	46	122
Mean	32.20	44.49	.68	1.28
Standard Deviation	12.70	10.75	.26	1.12
Skewness	.47	.17	.40	2.19
Standard Error of Skewness	.36	.37	.35	.22

Table 4.1 (continued).

In Table 4.2, the number of measurements in the four main classes (piste or non-piste, piste class, part of fieldwork area and soil texture) are given. It can be seen that no single class contains less than two values, making it possible to calculate the classical statistical measures like the mean (X), standard deviation (s), CV ($= s / X \cdot 100$) et cetera for every class for every variable. When necessary, the few measurements in the ambiguous ski affectedness classes (green / yellow and yellow / orange) could be included in the adjacent classes.

The affectedness classes as mentioned in Table 4.2 were determined in the field, with as objective to aid in the correlation of measurable quantities to visual characteristics of the ski runs in a later phase of research. The classification has therefore nothing to do with the classical classification of ski runs in degrees of difficulty (green, blue, red and black). The names were chosen to enhance the perception of how much disturbance of soil and vegetation is present on a ski run (green = safe, red = dangerous). At the same time, the names make clear that the classification is quite subjective. When the class names would have been numbers, this would have resulted in the perception of an objective classification, which it is not. The original description, as was made in the field, is as follows (see pictures in Figs. 4.2 to 4.5 for examples):

- green: the ski run has a thick, undisturbed grass cover with a dense root mat, often abundant flowers and little to no bare places (Fig. 4.2);
- yellow: rather closed grass cover with only at steeper places total absence of grass. Patches with yellow-coloured grass are clearly present (Fig. 4.3);
- orange: rather heavy harmed ski run with a non-contiguous grass cover and sods in bad condition. Shallow slopes are also affected (Fig. 4.4);
- red: strongly affected piste, virtually no vegetation present (Fig. 4.5).

Figure 4.2. Example of a green piste surface.

Figure 4.3. Example of a yellow piste surface.

Figure 4.4. Example of an orange piste surface. Note the relative large part of stones.

Figure 4.5. Example of a red piste surface. Now there is a larger percentage of the soil covered with stones than grass.

The number of measurements over the three most important skiing areas is roughly proportional with the size of these areas, except for BD, ASM and porosity, because the Schwarzsee area was sampled late during the fieldwork, when there already was a shortage of rings.

It can further be noticed from Table 4.2 that the number of measurements made on ski tracks versus the number made on natural, undisturbed slopes has the ratio 3 to 1. When Fig. 4.1 is looked at, it is also noticed that the area of undisturbed land is much larger than the area covered by ski tracks. Since the research mainly focuses on ski tracks, it was however needed to do a lot more measurements on ski tracks than non-ski areas. The measurements in the undisturbed areas are only needed to provide reference values.

Soil physical variable	Part of fieldwork area			piste or not	
	Hochsölden	Schwarzsee	Gaislach	natural conditions	ski piste
	n	n	n	n	n
AMC [%]	25	7	11	12	31
Porosity [%]	23	7	12	11	31
BD [g/cm3]	25	7	14	12	34
Kunc [m/d]	46	27	49	36	86
Surface stoniness [%]	35	28	49	30	82
Amount of stones in soil [%]	28	21	48	27	70
Dry soil shear strength [kg/cm2]	33	23	40	24	72
Wet soil shear strength [kg/cm2]	28	22	37	22	65

Table 4.2. Number of measurements carried out in the four most important classes. Kunc stands for K_{unc}, i.e., uncorrected, non-manipulated hydraulic conductivity. The difference between corrected and uncorrected *K* will be discussed later in Section 4.2.

Soil physical variable	Soil texture in five classes				
	sand	loamy sand	sandy loam	(silty) loam	clay(ey loam)
	n	n	n	n	n
AMC [%]	13	14	6	4	6
Porosity [%]	11	15	6	4	6
BD [g/cm3]	14	16	6	4	6
Kunc [m/d]	38	39	17	21	7
Surface stoniness [%]	38	36	16	18	4
Amount of stones in soil [%]	35	32	13	14	3
Dry soil shear strength [kg/cm2]	34	29	10	16	7
Wet soil shear strength [kg/cm2]	30	29	6	15	7

Table 4.2 (continued).

	Ski track damage class *)						
	no piste	green	g/y **)	yellow	y/o ***)	orange	red
Soil physical variable	n	n	n	n	n	n	n
AMC [%]	12	9	3	8	3	3	5
Porosity [%]	11	10	2	9	2	3	5
BD [g/cm3]	12	10	3	10	3	3	5
Kunc [m/d]	36	13	8	31	8	15	11
Surface stoniness [%]	30	11	8	30	7	15	11
Amount of stones in soil [%]	27	10	8	24	7	12	9
Dry soil shear strength [kg/cm2]	24	10	7	24	8	12	11
Wet soil shear strength [kg/cm2]	22	10	6	23	6	10	10

Table 4.2 (continued). *) the meaning of a affectedness class is explained in the text; **) green / yellow; ***) yellow / orange.

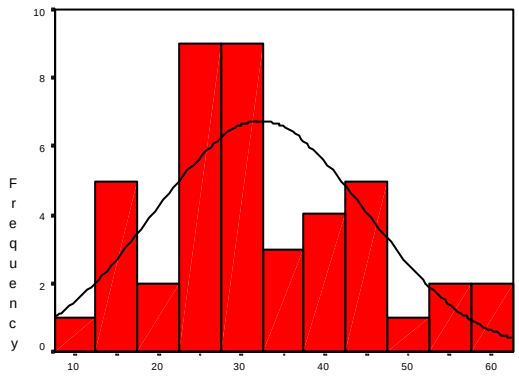

Figure 4.6a. Histogram of AMC [%].

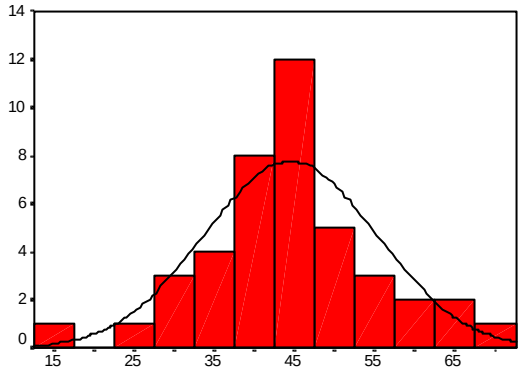

Figure 4.6b. Histogram of porosity of soil [%].

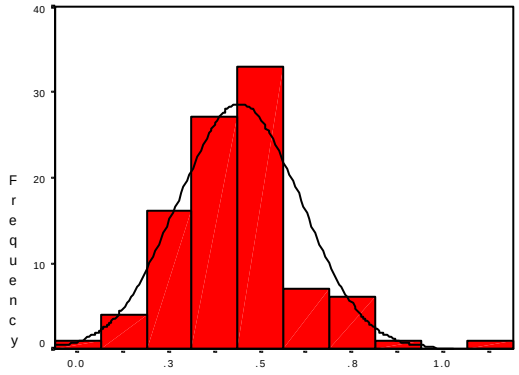

Figure 4.6c. Histogram of dry soil shear strength [kg/cm2].

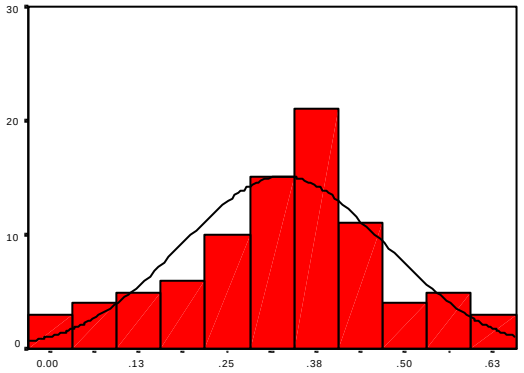

Figure 4.6d. Histogram of wet soil shear strength [kg/cm2].

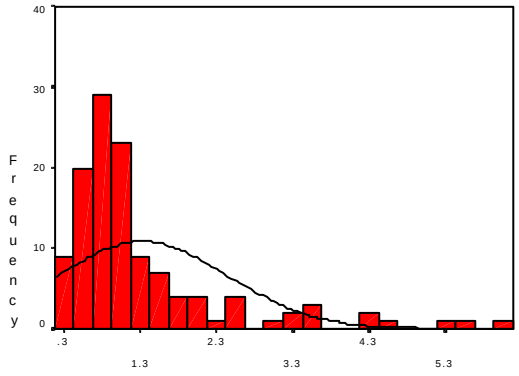

Figure 4.6e. Histogram of uncorrected K [m/d]

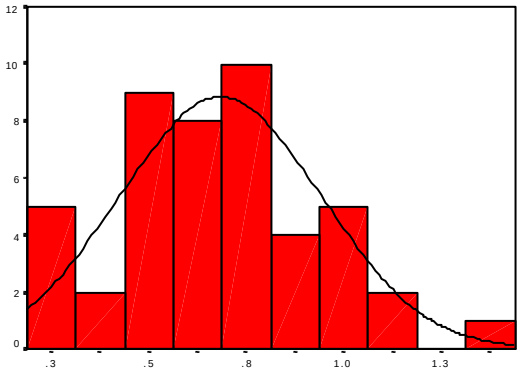

Figure 4.6f. Histogram of BD [g/cm3].

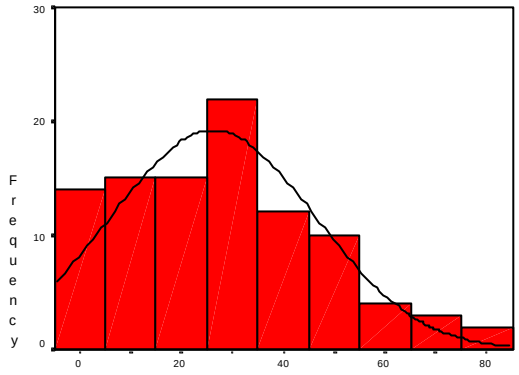

Figure 4.6g. Histogram of amount of stones in soil [%]

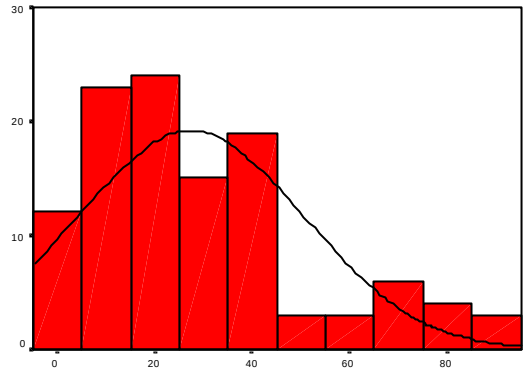

Figure 4.6h. Histogram of surface stoniness [%].

Figure 4.6. The histograms of the eight measured soil physical variables.

In Fig. 4.6, the histograms of the eight soil physical variables are depicted. The skewness values in Table 4.1 can be compared with the sample distributions and it can be concluded that they predict the global form of the distribution fairly well: a high skewness indeed means a large peak to the left side of the normal curve.

For the execution of statistical tests and analyses, it is important to know whether a distribution can be considered normal (Gaussian) or not. Therefore, this was tested using a Kolmogorov-Smirnov Z-test on normality (H_0: there is no significant difference between the normal distribution and the sample distribution; H_1: there is a significant difference between the normal distribution and the test distribution) with a significance level of 5 % (" = 0.05, two-sided). All but two variables can be considered to be normally distributed with 95 % confidence. The only two variables that do not follow a Gaussian distribution are surface stoniness and K, with *p* values[13] of 0.011 and 0.000, respectively. After transformation to a logarithmic scale, it appears as if these two variables are log-normally distributed, because with the transformed distributions, the Kolmogorov-Smirnov Z-test gives *p* values[11] that are much larger than 5 %. In the following, there will be made a difference between the non-transformed values and the logarithmic values for surface stoniness and K. For much statistics, it will be necessary to use the transformed values. However, after correction for the influence of the rainfall intensity, this will not be necessary anymore for hydraulic conductivities (see also Eq. 4.1).

4.2 The influence of the rainfall intensity on the hydraulic conductivity

As was stated in Section 1.4, it was found by Van Dijck (2000) that the rainfall intensity is positively correlated with hydraulic conductivity on sandy loam soils in Southern France. A weaker but still positive correlation was found by Blijenberg *et al.* (1996) and Blijenberg (1998) for an area in the French Alps with marl and limestone debris. Van Dijck (2000) gives references for numerous other publications in which this positive relationship is also mentioned, partly for other conditions and soils than the two mentioned above.

The relationship as was found for the Sölden ski area is depicted in Fig. 4.7. In this graph, all measurements are included. In Fig. 4.8, the logarithmic equivalent of Fig. 4.7 is shown. In both graphs, a positive relationship between conductivity and rainfall intensity is evident: in general, an increase in applied rainfall intensity leads to an increase in *K*.

[13] A *p* value can be regarded as the chance (a number lying between 0 and 1) that the H_0 hypothesis is true.

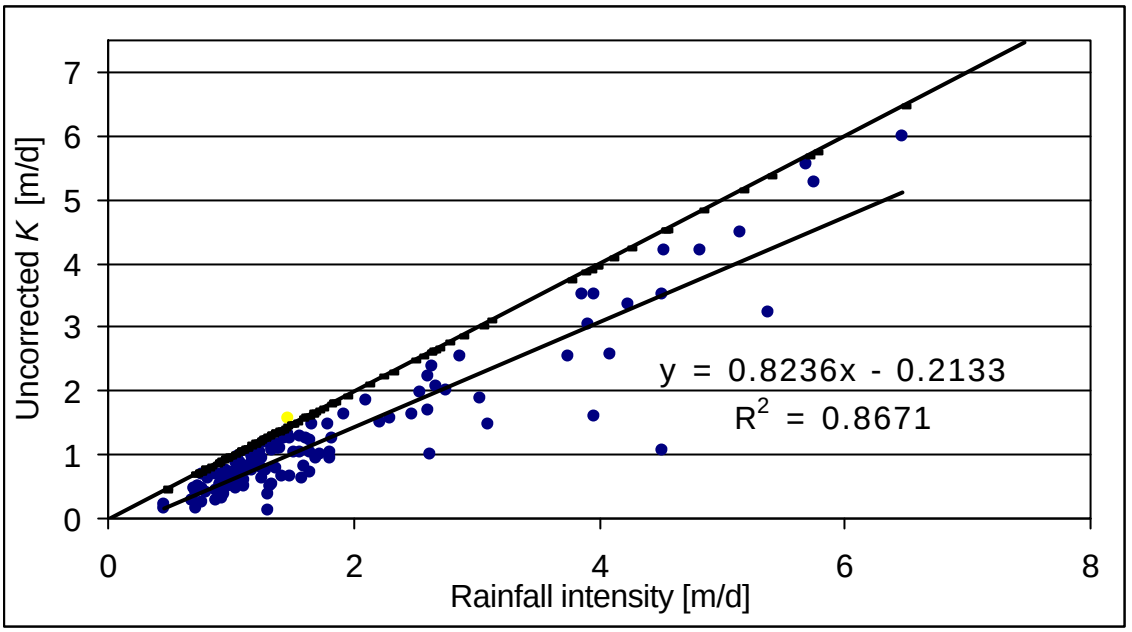

Figure 4.7. Relationship between rainfall intensity and hydraulic conductivity with the 1:1 line. Note that one point in yellow lies above the 1:1 line, which is in fact physically impossible.

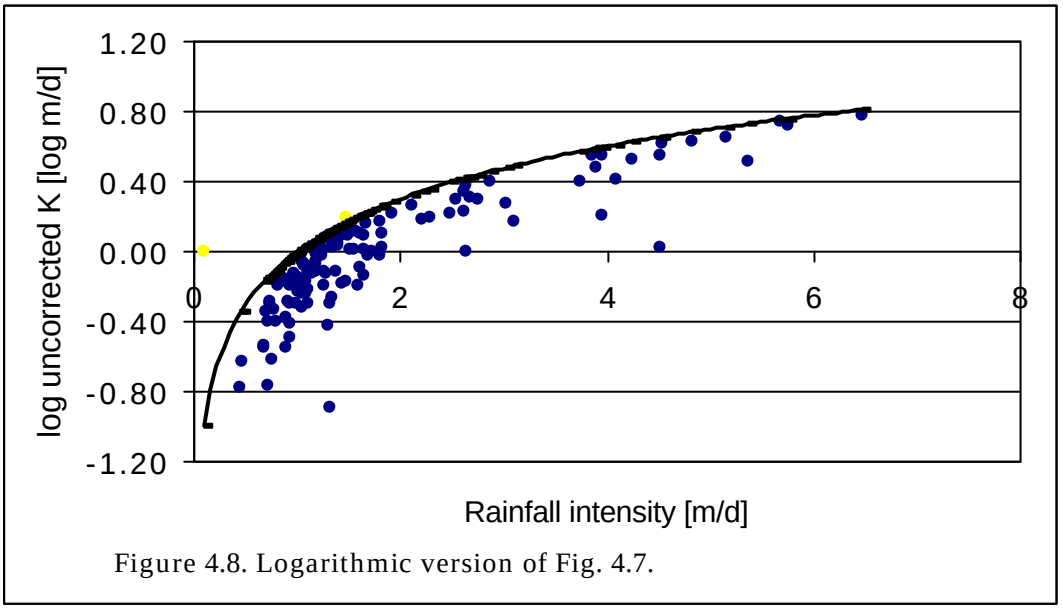

Figure 4.8. Logarithmic version of Fig. 4.7.

To verify this relationship, on some places in the field the rainfall intensity was increased after the time on which the infiltration had reached its constant value (a so called 'double run'). In all cases, the result of this action was a higher infiltration rate, showing that it is indeed possible to influence *K* by adjusting rainfall intensity, even when the infiltration rate has become constant. The results of these verification measurements are shown in Fig. 4.9: each dot type represents one double run, each dot represents one measurement. On each location, there were carried out only two measurements, thus it is not possible to fit a curve through the data points, because the exact type of relation (linear, exponential, power, et cetera) cannot be determined from only two points in a graph. However, Blijenberg (1998) used only three measurements on one location and derived a linear relationship (Fig. 4.11). It is therefore further assumed that the relationship between rainfall intensity and hydraulic conductivity is of the linear type.

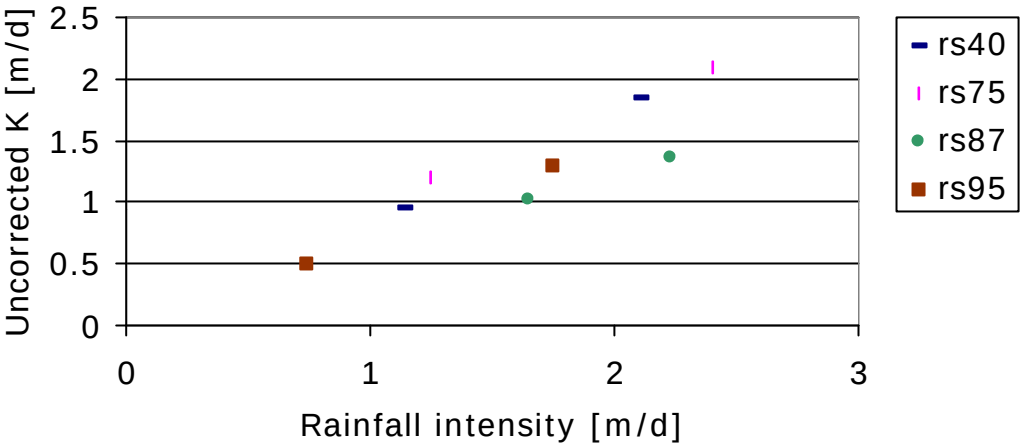

Figure 4.9. Relationship between i and K on four locations. See Table 4.3 for the slopes of the relationships

Comparison with other data

The graphs as found by Van Dijck (2000) are depicted in Figs. 4.10 (plot level) and 4.12 (parcel level, i.e. for one agricultural land unit), those by Blijenberg (1998) are shown in Fig. 4.11 for both the triple run and all measurements. It can be seen that the data in Van Dijck (2000) for field level bear an exponential relationship between K and i, while the relationship as depicted in Fig. 4.10 shows a more linear relationship.

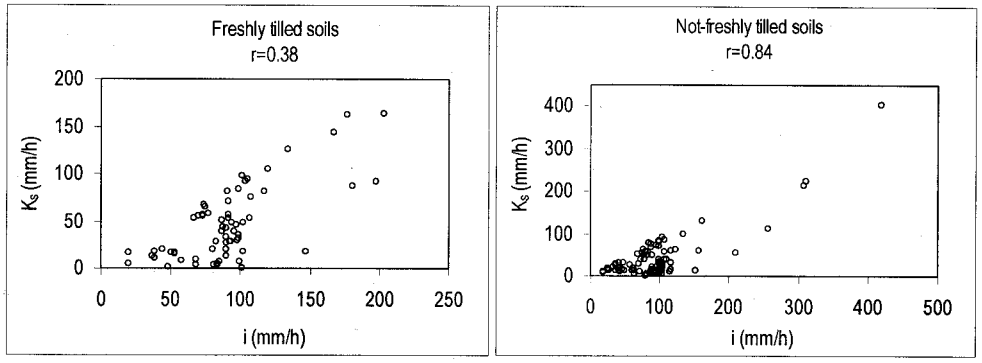

Figure 4.10. The relationship between K and i as found by Van Dijck (2000, Fig. 6.3.6) for plot level.

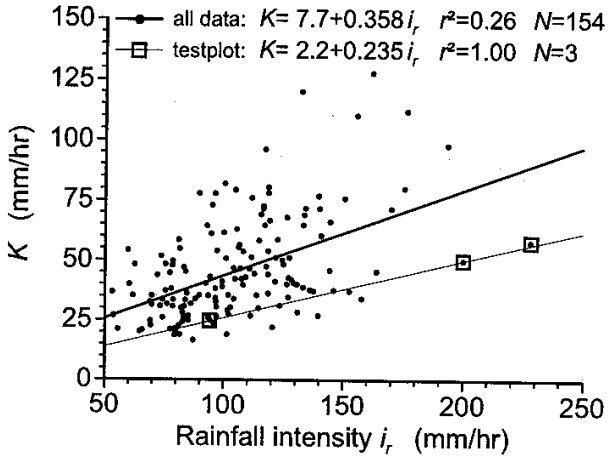

Figure 4.11. The relation between K and i as found by Blijenberg (1998, Fig. 6.3). Note the additional three point line for three simulations on one spot.

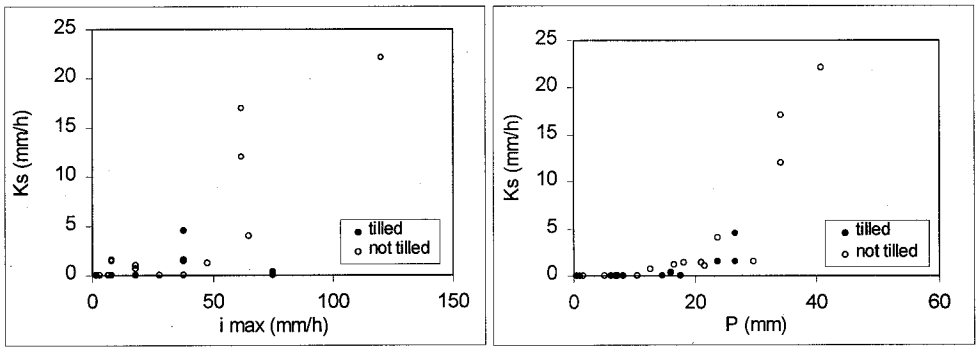

Figure 4.12. The *K–i* relationship as found by Van Dijck (2000 , Fig. 6.3.14) for parcel level

In Table 4.3, some different slopes and determination coefficients of the linear relationship between rainfall intensity and hydraulic conductivity are shown. It can be seen that both the steepest slope and the highest coefficient of determination were found in this study (i.e., 0.82 and 0.87). Comparable data provided in Sorriso-Valvo *et al.* (1995, percentage infiltration against rainfall intensity) and Lusby & Toy (1976, total amount of infiltration against rainfall intensity) show non-significant but positive relationships (" = 0.05).

Source	n	slope	r^2	p
This study, rs40	2	0.91	1.00	*
This study, rs75	2	0.77	1.00	*
This study, rs87	2	0.60	1.00	*
This study, rs95	2	0.79	1.00	*
Blijenberg (1998) **	3	0.24	1.00	0.000
Kutiel *et al.* (1995)	16	0.72	0.523	0.001
Mannaerts (1993) ***	24	0.85	0.991	0.000
Dunne *et al.* (1991)	27	0.34	0.8	n.a.
Overbeek & Wiersma (1996)	58	0.48	0.818	n.a.
Van Dijck (2000) ****	n.a.	0.54	0.62	n.a.
This study, all data	122	0.82	0.867	0.000
Blijenberg (1998)	154	0.36	0.260	n.a.

Table 4.3. The slope of the linear relationship between rainfall intensity and K, its coefficient of determination and the significance of this coefficient. *) When n < 3, p is undefinable; **) on one plot, using three different intensities (see also Fig. 4.11); ***) only two intensities used; ****) for non-freshly tilled soils.
'n.a.' Means 'not available' or 'not analyzed', 'rs' means

Explanation of the relationship

As can be noted from the above, it appears that the relation between rainfall intensity and hydraulic conductivity is indeed positive. Explanations for this can be given, some of which are stochastically; others explain the relationship from a more physical point of view.

Soil is a very heterogeneous substance, both in time and in space. Soil variables can change drastically in only a few meters or even centimetres. In time, notably moisture status can change quickly, while other variables remain fairly constant and only change under the influence of man or certain events, like flooding, mass wasting et cetera. Of all soil variables, hydraulic conductivity is one of the most variable properties in terms of coefficients of variation (CV's) (Wilding & Drees 1978, 1983):

— Babalola (1978) found CV's for *K* of 53.57 to 176.16 %for an area of 91.6 ha and each time 5 measurements. Reduction from the area to 0.34 ha did not significantly lower the calculated CV's;

— Nielsen *et al.* (1973) found CV's of *K* ranging from 88.8 to 125.9 % on a 125 ha field;

— Burden & Selim (1989) found a CV of 100.7 % on an 80 m transect with more than 250 measurements;

— Jetten *et al.* (1994) report within-class CV's of 24 to 109 %with measurements taken within 200 m from each other and n = 18 per class.

However, even within pedons or even within soil horizons in these pedons, large amounts of variation for *K* are reported by Cameron (1978).

Other soil variables show much lower variation on average. For example, mass percentage metals (such as Fe) have CV's of only 2 to 6 %in one horizon (Drees & Wilding 1973), BD normally has CV's lower than 10 % (Burden & Selim 1989; Netto *et al.* 1999), 2_i or 2_{FC} have CV's ranging around 10 % or lower (Burden & Selim 1989; Reichardt *et al.* 1993)[14].

In short, hydraulic conductivity varies considerably in a spatial context. This large spatial variation leads to a large variation in infiltration capacity and runoff production, but also in the dependency of infiltration on rainfall intensity. Let us assume a plot that is divided in nine subplots, each of which has a certain constant *K* (Fig. 4.13, plan view figure).

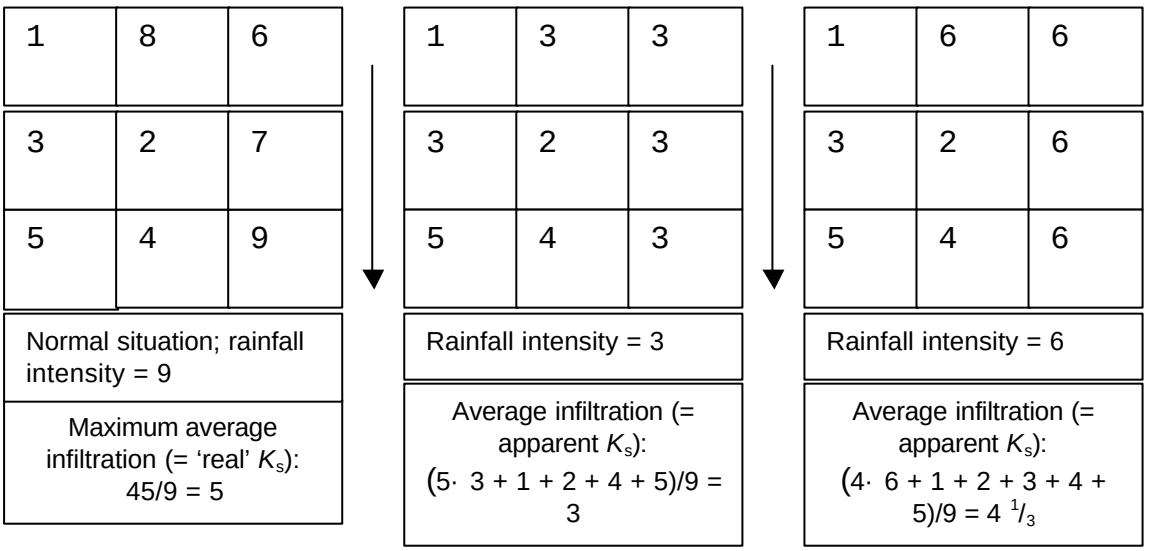

Figure 4.13. A hypothetical rainfall simulation plot with the maximal possible infiltration capacity (which would be reached when the applied rainfall intensity would be 9), the infiltration when the intensity is 3 and 6, respectively. The arrows indicate the direction of run on-run off.

Each subplot will infiltrate a certain amount of rain, dependent on its *K*, but also on the rainfall intensity *i*: when *i* is less than *K*, the amount of infiltration is equal to the rainfall intensity. When *i* is equal to or larger than *K*, the amount of infiltration is equal to *K*, the surplus runs off (this is indicated by the arrows), but may infiltrate downstream. When it is assumed that the plot is a rainfall simulation plot, the above stated situation leads to an increase in apparent infiltration rate with an increase in rainfall intensity (see captions of Fig. 4.13). Would all subplots have the same *K* (i.e., there would exist no such thing as soil hydraulic variability, so all subplots have the same average *K* of 5), then an increase in rainfall intensity would lead to the achievement of a constant infiltration rate at a lower rainfall intensity. This is illustrated in Fig. 4.14, which is based on Fig. 4.13: the more constant *K* in a plot is, the longer the trajectory in which rainfall intensity has no influence on infiltration rate. Van Dijck (2000) found that tilled soils — exhibiting a low spatial variability due to the homogenizing effect of ploughing — have a *K* that is less dependent upon rainfall

[14] From Table 4.1, it can be calculated that CV for BD and 2_i are about 38 % in this research, and CV for uncorrected K amounts to 87.5 %.

intensity (Fig. 4.12). This supports the fact the intensity has less influences on the conductivity when there is a lower spatial variability.

It can also be seen in Fig. 4.14 that when the run on-run off process is incorporated, the apparent infiltration rate can become higher then when this process is cancelled out (e.g., by means of high surface retention). Note that when lower values in the lower part of Fig. 4.13 would have been chosen, the effect would have been more pronounced. Markart *et al.* (2000) compared their results of rainfall simulations on 50 m^2 plots with the results of Bunza (1984a), who used 100 m^2 plots and the same rainfall intensity. It was shown that the latter indeed reached lower runoff values and higher infiltration rates. Markart *et al.* (2000) ascribed this to the larger area that is available for infiltration and the more efficient use of macropores. Dunne *et al.* (1991) stress the importance of plants roots in this run on-run off process: when the rainfall intensity is high, ponding occurs at a larger scale and the water layer will be thicker. In this manner, the layer can reach the protruding open fabric soil underneath plants or tussocks, where the water can readily infiltrate via the root-system.

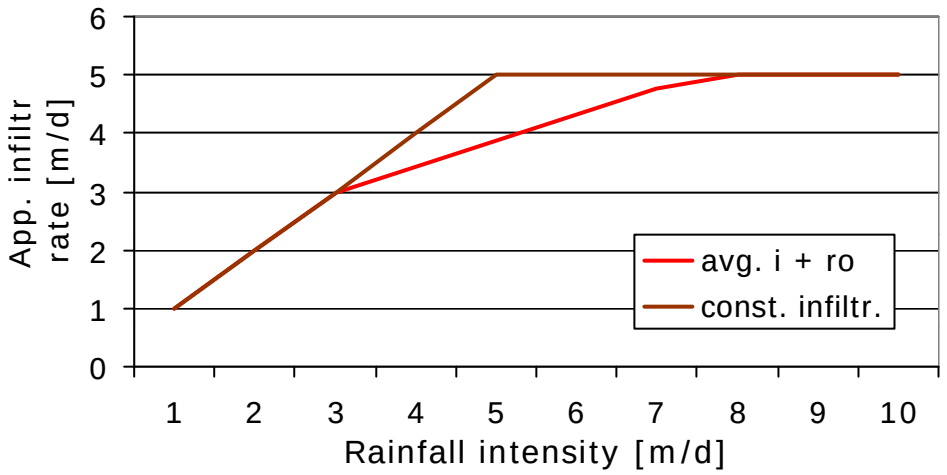

Figure 4.14. Hypothetical relationship between rainfall intensity and infiltration rate. 'avg. *i* + ro' = run on/run off incorporated, spatial variation present; 'const. infiltr.' = one infiltration rate, no spatial variation present.

The second possible explanation has a more physical background. When the rainfall intensity is low, the soil is not thoroughly wetted and the matrix suction remains high. Since only micropores can absorb water at high suctions (i.e., highly negative pressure heads), the infiltration rate will be low, for these pores cannot conduct water at a high rate. Therefore, the apparent *K* will be low. This can be seen in Fig. 4.15, where the upper left branch of the right graph indicates a low apparent *K* at high suctions, which is equivalent to low rainfall intensities. It is true that high suctions in the micropores theoretically lead to a high infiltration speed, but it is believed here that the drainage capacity of the micropores is the limiting variable.

When the rainfall intensity is high, the soil surface will be wetted fast and ponding is likely to occur. When the surface water starts to flow, it may reach a macropore and infiltrate along it. Because macropores have a large free draining area (not only at the surface, but also along the walls in the subsurface), they have a major influence on the amount of infiltration (Beven & German 1982). In this way, high rainfall intensity leads to a high apparent *K* through the action of macropores.

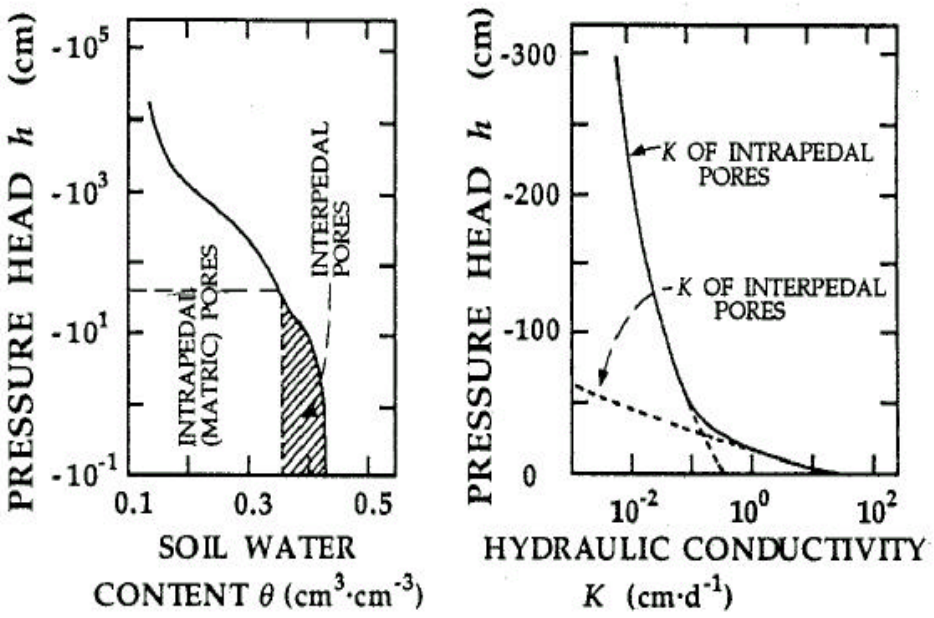

Figure 4.15. On the left, the part of the ASM that is held by macropores. On the right, the difference in the conductivity of macro- (interpedal) and micro- (intrapedal) pores. Source: Kutílek & Nielsen (1994, Fig. 5.12).

Even when the macropores are not connected to the surface, which is the case in a so called 'closed soil', they have a positive influence on the infiltration rate (Van den Berg 1989). This is because of the fact that macropores drain at low suction rates (Coles & Trudgill 1985, *op. cit.* Edwards *et al.* 1992; Kutílek & Nielsen 1994), which are reached when the soil is thoroughly wetted by a high rainfall intensity (right limb in Fig. 4.15). The infiltrated water in the matrix can enter the macropores at low suctions and forms distinct rivulets along the macropore walls. Until the moment that matrix suction increases again and forces the water to enter the soil matrix (e.g., at the level below the wetting front), the percolation speed is high relative to the percolation speed reached in micropores. This fast displacement of water away from the infiltrating surface increases the infiltration capacity.

On the other hand, Shipitalo *et al.* (1990) and Edwards *et al.* (1992) found high infiltration rates and marked preferential flow only under relatively dry (laboratory) conditions. This is due to the burrowing effect of the earthworm (*Lumbricus terrestris* L.) and hydrophobicity of organic matter. The sides of the burrow holes of this worm are also of a hydrophobic nature and therefore water repellent and only conduct water when the soil is relatively dry. The topsoil also repelles the water due to organic matter and the water runs off to micro depressions, where many burrow holes of the earthworm are present. These burrows guide the water fast to the deeper soil whilst preventing exfiltration in the matrix through their hydrophobicity. When the soil was pre-wetted before rainfall was applied, apparent *K* was lower because now the organic matter and the burrows had lost their water repellency and the water was mainly guided through the micropores, which have a lower conductivity but guide water in an earlier phase of rainfall due to their higher suction. The above case is rather exceptional, but it shows that macropores can also have a profound influence on infiltration under relative dry conditions when combined with hydrophobicity. When this hydrophobic nature is however cancelled out, the 'normal' situation is found again, in which micropores have a relatively low *K* and macropores a relatively high one. In the fieldwork area, this was also observed under dwarf shrubs with a high amount of dead and soil organic matter during a warm period: during the rainfall simulation, the infiltration capacity increased because of the wetting of the organic

matter and the decrease of its hydrophobic nature. Although this process may indeed be important in the generation of overland flow (Markart *et al.* 2000), it was not included in the modelling (Chapter 7), because of the general wetness of the soils during the summer in the Ötztaler Alps.

Correction of K for rainfall intensity

It is part of the assessment of the influence of skiing to compare infiltration capacity from ski runs with natural areas. However, when *K* is not only affected by standard variables as porosity and soil texture, but also by a non-soil variable as rainfall intensity, this comparison is not sound. To enable an objective comparison, a correction to cancel out the influence of rainfall intensity is needed. This correction (or recalculation) is done with the following formula:

$$K_{cor} = \frac{K_{uncor}}{i} \cdot 15 \qquad \text{(Eq. 4.1)}$$

With: K_{cor} = the corrected hydraulic conductivity [m / d]; K_{uncor} = the uncorrected hydraulic conductivity (as displayed in Figs. 4.6 & 4.9) [m / d]; i = rainfall intensity as used in the simulation [mm / h]; 15 = a constant [mm / h].

In this way, *K* as measured when using a rainfall intensity of only 15 mm / h is derived. This value of 15 mm / h is chosen arbitrarily, but it is a more naturally occurring value than the intensities with which the rain was applied in the experiments (ranging from 18.82 to 269.3 mm / h with 75.22 mm / h as average). When Eq. 4.1 is applied, Fig. 4.9 reduces to an unstructured scatterplot as displayed in Fig. 4.16. This shows that the effect of rainfall intensity is effectively cancelled out by the formula. Moreover, the lognormal distribution changes to a normal distribution, which favours inductive statistics since parametric tests are only allowed with normally distributed data. A disadvantage of the formula is the decrease of the range of values for K, but since this is inherent to the formula, this cannot be changed. Hereafter, all symbols *K* denote corrected hydraulic conductivity.

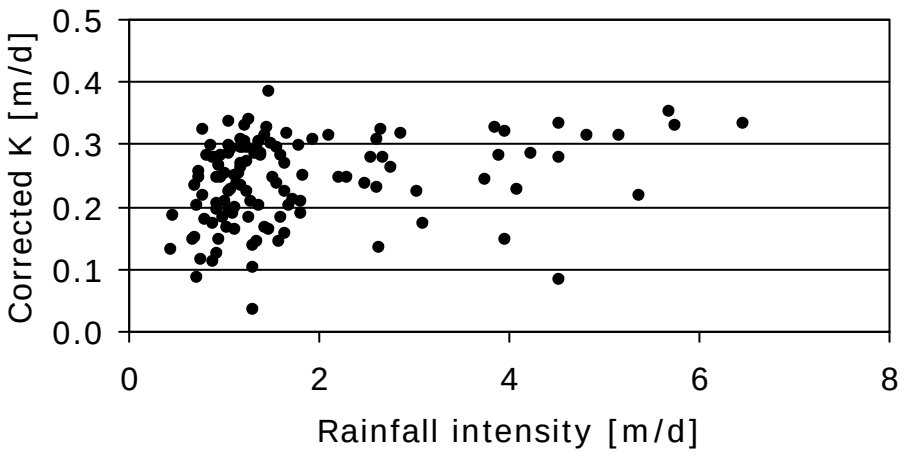

Figure 4.16. Relationship between rainfall intensity and hydraulic conductivity after correction for the influence of rainfall intensity with Eq. 4.1.

4.3 Statistical analysis of soil physical variables

In Section 1.1, it was said that skiing is expected to have a positive effect on BD and a negative effect on porosity (and ASM), resulting in a negative effect on *K*. In Fig. 4.17,

the box-and-whisker plots (box plots for short) for BD, porosity and ASM show that there is in general little difference in porosity between ski tracks and natural slopes, in spite of the higher BD under ski tracks. This may be caused by a higher degree of gravel in the soil under ski tracks. This is supported by a Student t test (one-sided " = 0.05), which shows the amount of stones in a piste soil is significantly higher than in an undisturbed soil. This is probably caused by the selective erosion of fines on the ski tracks, leaving a coarser residue with a larger degree of gravel. A high grade of gravel may provoke a higher bulk density, but does not lead to a drastically lower porosity for the matrix.

For BD and ASM, the differences between pistes and non-pistes are actually quite large and both variables exhibit the expected characteristics: BD values for pistes are about 0.25 g / cm³ or 58 % higher than for non-pistes, ASM values are on average 15 percent point or 35 % lower. Note that the values for porosity and ASM lie in a rather normal range, but the values for BD are rather low for both classes. Normal BD values are approximately 1.4 1.6 g / cm³ for most of the soils, with 0.88 g / cm³ as minimum (Kutílek & Nielsen 1994, Table 2.1). For example, Jetten *et al.* (1994) report 0.71 g / cm³ as lowest value for tropical sands, Bunza (1989) gives values from 0.9 to 1.0 g / cm³ with a lowest value of 0.78 g / cm³ for alpine morainic and solifluction material under alpine grasses and sedges and Bunza (1984a) gives 1.2 g / cm³ for alpine moraine under *Juniperus* shrubs. The BD values may be too low because of measuring the bulk density in a stony soil with the Kopecky rings (Section 3.3), a method that is not optimal for the measurement of BD in stony soils. However, porosity was measured using the same rings and the porosity values (with a mean of 44 %) are not too high when compared to the range of 35 55 % in Kutílek & Nielsen (1994, Table 2.1). On the other hand, the values may however be too low, because the rings were often pushed or hammered in the soil, i.e. there was exerted pressure on the soil. This was needed because of the high degree of stones in the soil. This pressure might have damaged the macropore system, leading to a lower measured porosity than is present in the undisturbed soil. This again shows the relative inapplicability of the Kopecky rings in a stony soil.

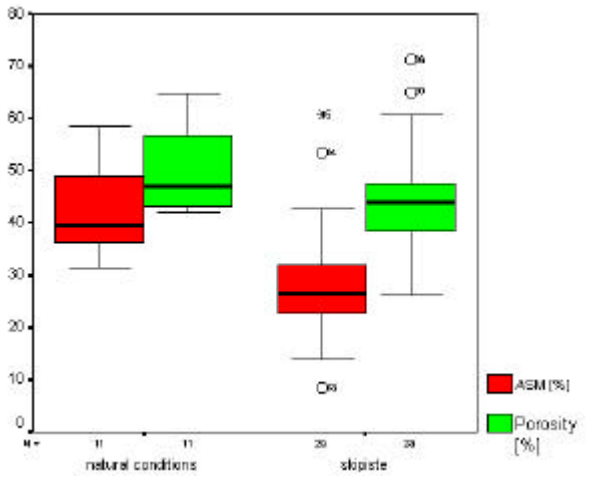

Figure 4.17a. The difference between porosity and soil moisture content between piste and non-piste. Note the little difference for porosity between the two units.

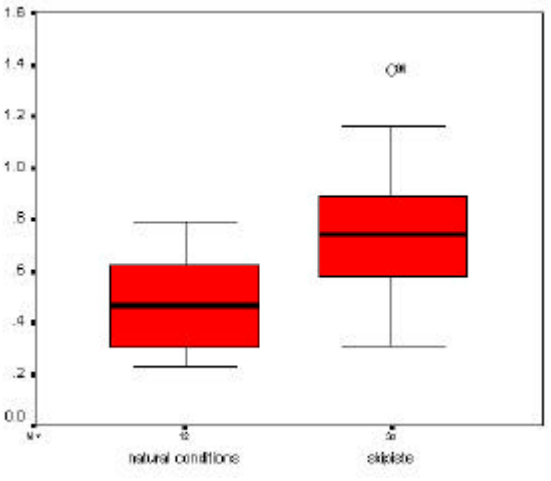

Figure 4.17b. Soil bulk density for piste and non-piste. The units are in g / cm³.

A Student-Newman-Keuls t test (Student t test for short) was carried out to see whether the values for ski pistes are significantly lower than for non-ski pistes. With "

= 0.05 (one-tailed[15]), it was found that the BD under natural vegetation is significantly lower than under ski tracks (p = 0.001, n = 46, df = 45). When an ANOVA test is carried out on the four piste classes (green, yellow, orange & red), no significant difference is indicated (p = 0.489). However, when the green / yellow and yellow / orange classes (g / y and y / o in Table 4.2) are also used in this test (without reallocation of the values from these classes to green, yellow or orange), there emerges a statistically significant difference in BD between pistes and non-pistes (p = 0.003).

Before testing on the ASM was carried out, it was visually ensured that there was no bias due to different rainfall amounts between pistes and non-pistes, for instance because the pistes were visited on dry days and the non-pistes on wet days. This was done by putting the ASM values with the daily rain amounts in one graph. No bias was found in this graph (not depicted here).

The tests on ASM as on BD show the same results: the Students t test returns a highly significant difference (p = 0.000, df = 42, n = 43), the subsequent ANOVA tests without the mixed classes returns a non-significant difference (p = 0.554), whereas the ANOVA test with mixed classes results in a significant difference again (p = 0.002). When the Spearman correlation coefficients are calculated for the ASM and BD with or without mixed piste affectedness classes, the results are again strikingly different. With mixed classes, the variables ASM and BD are significantly negatively (r_s[16] = 0.501, p = 0.000) and positively (r_s = +0.544, p = 0.000) correlated with the status of the pistes. With the mixed classes split up, these correlation coefficients drop to 0.042 and +0.165 and become highly insignificant. Therefore, it can be put forward that the delineation of mixed classes or not influences the outcome of the statistics. This renders the classification of the pistes for these two variables useless. However, the significant differences as indicated by the Students t test of the two soil variables ASM and BD between pistes and non-pistes remain statistically sound. Even if the BD values are too low because of systematic measurement errors, the difference can still be interpreted on a relative basis instead of an absolute basis.

A third soil variable that may be related to skiing is surface stoniness. Skiing and piste preparation damage the soil plant cover, thereby exposing the soil to action of flowing water and the washing out of fine material (sheet erosion). This may lead to a higher grade of stones and gravel on the soil. This hypothesis was tested with the aid of a non-parametric test (Mann-Whitney U test, because of lognormal distribution of the test variable) between piste and non-piste. On pistes, the average surface stoniness is 12.5 % higher than on non-pistes, and this difference is statistically significant (p = 0.007, n = 112). Furthermore, the correlation with piste affectedness class is significant but rather weak: r_s = 0.315 (p = 0.001, n = 103 because of log transformation).

Before drawing conclusions about the influence of skiing on ASM, BD and surface stoniness — the only three variables that appear to be influenced by damage due to skiing, although the classification also influences the statistical analysis —, it has to be checked whether the above tests and analyses are not biased. The most important variable that was used in the piste classification is vegetation cover [%] (see Section 4.1). Discriminant Analysis confirms this: when discriminating the piste affectedness classes in a statistical manner, the only variable that is considered to be good enough for classification is total vegetation cover (67.8 % was classified correctly). It is possible

[15] All tests are done on basis of a one-sided or one-tailed ", unless reported otherwise.

[16] A subscript s denotes the Spearmann correlation coefficient for interval / ratio variables with ordinal classes, a subscript p denotes the Pearson product-moment correlation coefficient for interval / ratio variables.

that the statistical relationships between the three soil variables on the one side and piste classes on the other side is influenced by the vegetation cover percentage. When there exists a notable correlation between a variable and the vegetation cover, it can be deduced that the variable is only indirectly related with the ski piste classes, because vegetation cover also influences the ski piste classification. In order to investigate this, the correlation between ASM, BD and surface stoniness against vegetation cover was checked.

This check led to the following:

— r_p = 0.463 between BD and vegetation cover percentage is significant (p = 0.001);

— r_p = 0.242 between ASM and vegetation cover percentage is weak and insignificant (p = 0.059);

— r_p = 0.163 between *log* surface stoniness and vegetation cover is weak but significant (p = 0.050).

This leads to the conclusion that BD is not largely influenced by piste type (i.e., the direct action of skiing and piste preparation) but more by vegetation cover: more vegetation means a lower soil bulk density, probably because of protection against compaction of soil, a higher faunal activity and a higher humus content. For surface stoniness, it may have been that on the more scarcely vegetated pistes stones were detected more easily than under the more dense shrub vegetation of the natural slopes. But the cause that was mentioned earlier (damage of vegetation through skiing leads to the washing out of fine material and a stony surface) may also be possible. In other words, for surface stoniness the relation is too weak to draw a clear conclusion.

The only parameter left that is directly effected by skiing action is ASM: the more affected a ski track is, the lower its moisture content will be, provided that the classification with mixed classes is more sound than the one with unmixed classes. This is supported by Cernusca (1977), who compared the field capacity of ski tracks with bordering forests and meadows. The data show that the ski track soil has a moisture content at field capacity in the upper humic horizon that is up to ten times as low as that of the adjacent natural areas. For the total soil, Cernusca (1977) reports a FC that is 14 percent point lower under ski tracks, which is about the same as the here reported value of 15 for the upper soil layer only. Giessübel (1988) reports that the piste soil under alpine meadow in Super-Dévoluy (Southern French Alps) has a FC that is about half of the capacity of the native forest. Mosimann (1983) reports a FC under ski tracks that is about one third to one half lower than for undisturbed soils in the ski area of Crap Sogn Gion (Swiss Alps).

The main reason for this loss of moisture retention capacity is the loss of humus on ski pistes due to erosion of the artificially added humus (Bunza & Porzelt 1991) and the levelling of the ski pistes that destroys the soil profile (Mosimann 1981, 1986; Löhmannsröben & Cernusca 1990). The destruction of the soil structure leads to the loss of water-stable aggregates and therefore to the loss of water binding capacity of the soil. Furthermore, the loss of these bindings may lead to the selective erosion of the finest earth fraction, which is the most active fraction in the binding of soil water. It is probably the levelling that causes the soil moisture content to be lower under ski tracks. Mosimann (1985) indicates that the first aspect (loss of humus) only plays a role on some spots when caused by skiing and piste preparation itself. Mosimann (1983) also gives sheet erosion on pistes as a possible reason for the lower ASM under pistes: this selective process removes the finer material in the topsoil, which causes the water retention capacity to drop because the finer pores are lost as well (see also left part of Fig. 4.15). A last reason for the low moisture status under pistes is the fact that pistes

have more overland flow than subsurface flow, although this is not expected to explain the whole difference. That this is the case will be demonstrated in Fig. 4.19 and Section 4.4.

All other soil parameters are non-significantly different between either piste and non-piste or the piste affectedness classes. In addition, the correlation coefficients between these variables and the piste affectedness classes are low: the highest value is 0.275. Results of Discriminant Analysis (a multivariate technique) show that there is not one single variable or a small group of variables related to piste class and piste / non-piste. This is supported by results of Factor Analysis, which indicate a high intrinsic dimensionality in the data, i.e. there is not one variable that is highly correlated with another one, piste class for example. It is therefore expected that soil variables such as porosity, J_w and J_D do not bear any relation with skiing and that skiing does not notably influence these soil variables in the research area.

4.4 Statistical analysis of soil hydrological variables

It was shown by Mason *et al.* (1957) that both bulk density and porosity have a certain effect on soil hydraulic conductivity. The correlation coefficient between BD and *K* is reported to be 0.324; r_p between 2_s and *K* +0.736 (values for sandy texture). The values found in this research are: between BD and K, significant r_p of 0.346 ($p = 0.009$) and between 2_s and K, insignificant r_p = 0.196 ($p = 0.106$) (values for all texture classes). Mason *et al.* (1957) report that the relationship between BD and *K* is indirect and via soil texture. This will probably also hold for the present case: *K* is slightly negatively correlated with soil texture class (r_s = 0.247, i.e. the 'heavier' the texture, the lower *K* will be).

Bunza (1984a, 1989) reports effects of ASM on the infiltration capacity. With rainfall simulations during moist soil conditions, saturation of the soil occurred in an earlier phase and overland flow was initiated earlier as well. In the formula of Smith & Parlange (1978), the parameter 2_i influences the infiltration capacity directly through the action of *G*. It may thus be that ASM influences *K* negatively, because *K* is an overall infiltration variable here, incorporating *G* (the infiltration due to unsaturation of the soil) as well. This effect was not found, however: the correlation coefficient between *K* and ASM is near zero. In summary, it can be said that there are no clear relationships expected for *K* with BD, 2_s or 2_i: the possible relation between *K* and skiing cannot be blurred by other relationships.

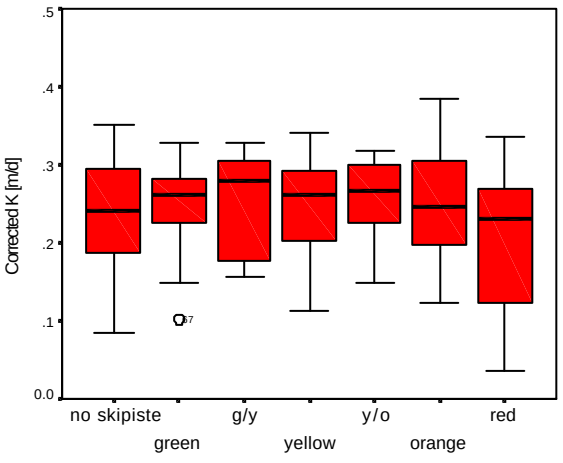

Figure 4.18a. The lack of relationship between ski track affectedness and corrected

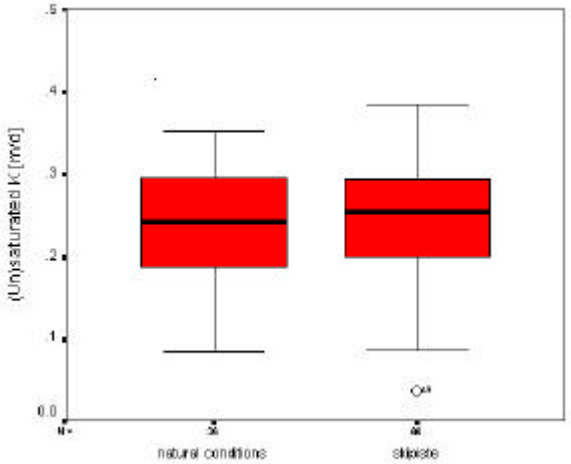

Figure 4.18b. The complete lack of difference between piste and non-piste con-

hydraulic conductivity (K_{cor}). sidering corrected *K*.

When Fig. 4.18a is studied, there is however no relationship observable between piste affectedness class and *K*. This is supported by a very low and insignificant r_s = 0.008. Even when the classes are aggregated in two classes (piste and non-piste), no influence of skiing can be noticed (Fig. 4.18b). This is supported by results in Strik (2000), who measured *K* in the fieldwork area with the method of Kessler & Oosterbaan (1974). Strik (2000, Table 3) also gives slightly (but statistically insignificant) higher values for *K* under piste than non-piste, as is the case in Fig. 4.18b. This lack of relationship may have two reasons:

- In general, the infiltration capacity from morainic soils is relatively high. Even when there is a moderate compaction (as indicated by a higher BD, the most important indicator of compaction according to Van Dijck (2000)) or a higher grade of stones (as is the case on the ski tracks in comparison to the natural soils), the hydraulic conductivity remains rather high. This is due to a high amount of sand in this type of moraine (close to the glacier source): more than half of the fieldwork area has a sandy, loamy sandy or sandy loamy texture. It may even be that the higher degree of stones (which can provoke a higher infiltration capacity) more than outweighs the compaction due to piste preparation and skiing. This is dependent upon the position (Poesen 1986), cover (Poesen & Lavee 1994) and size of the rock fragments (Brakensiek & Rawls 1994) and the terrain slope (Jean *et al.* 2000).
- Both shallow subsurface flow and Hortonian overland flow were considered a loss during the rainfall simulations (see also Section 3.1). Therefore, *K* as measured with a rainfall simulation is a vertical conductivity, which is rather the same for both units (Fig. 4.18b). However, on ski tracks drainage is mainly by the action of overland flow and in natural areas by subsurface flow, so the pistes can still be considered to be affected in a hydrological sense. Subsurface flow cannot harm the soil through the action of erosion (pipe erosion and roof collapse were not observed), but overland flow indeed can.

This last reason will be supported with results of Correspondence Analysis (CA for short[17]). CA is a multivariate statistical technique with which relationships between variables measured on a nominal, ordinal and / or Boolean scale can be revealed. In this case, the drainage is a Boolean variable: there is overland flow (1) or not (0, subsurface flow). Besides, the piste classification is an ordinal classification. Neither normal correlation and regression analysis, nor P^2 tests can reveal possible one-to-one relationships.

CA results in a plot of values, called loadings, when using more than two possible original values. In this case, only one axis, called dimension, results from the analysis. The values which are extracted by the CA can be easily interpreted: values close to each other indicate a strong relationship, values far apart a weak relationship; values with different sign indicate that there exists no relationship at all. The results for CA on kind of runoff versus piste class are shown in Fig. 4.19.

[17] Further information on the calculation procedure, which involves matrix algebra, can be found in Davis (1986) and other textbooks on advanced statistics.

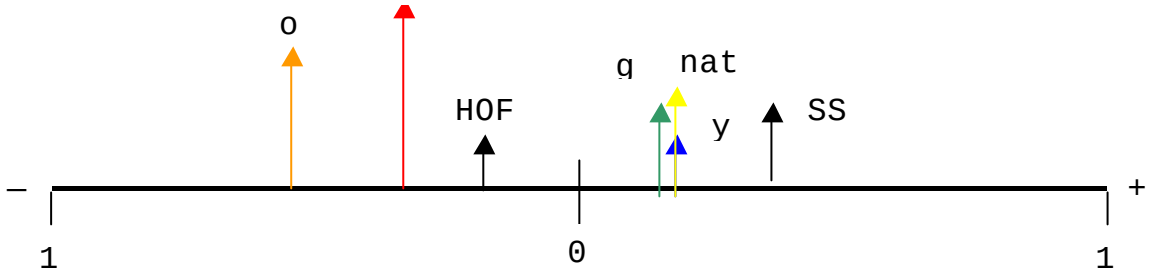

Figure 4.19. Results of the Correspondence Analysis on kind of runoff (HOF = Hortonian Overland flow; SSF = shallow subsurface flow) and kind of piste (nat. = natural, g = green, y = yellow, o = orange, r = red) (with n = 104, principal normalization, P^2 distance measure).

These results show that the two most affected classes have a higher than average chance of overland flow, the least and not affected classes have a higher than average chance of subsurface flow. Unfortunately, CA cannot attach an absolute value to the qualification 'higher than average chance'; plots such as Fig. 4.19 can only be interpreted qualitatively. Still, it illustrates that pistes, especially the more affected ones, have in general more overland flow and natural areas more subsurface flow.

The same analysis was carried out for different soil textures and the four different vegetation classes. Fig. 4.20 summarizes the results for the vegetation types. The results for the soil textures show that there is no clear discrimination possible between the classes, as was already noted for the hydraulic conductivity data. Only clayey soil has a distinct loading that points to high Hortonian overland flow risk (clay(ey loam): 0.618; overland flow: 0.134). This is not surprising, since all plots on clay and clayey loam Hortonian overland flow was observed.

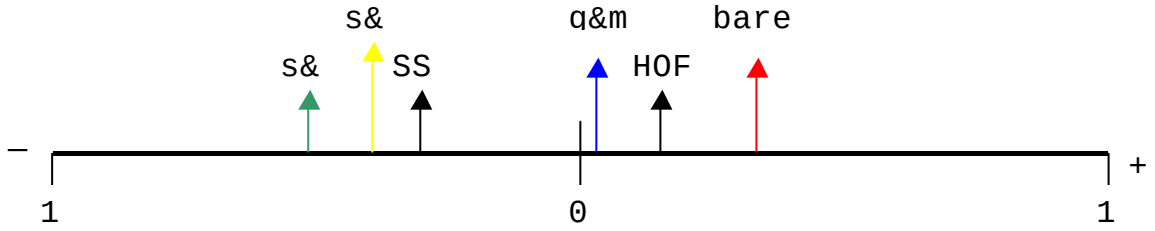

Fig. 4.20. Results of Correspondence Analysis on kind of runoff (HOF = Hortonian overland flow; SSF = shallow subsurface flow) and vegetation type (bare = bare soil; g&m = grass and moss; s&g = shrubs and grass; s&f = shrubs and / or forest) (with n = 123, principal normalization, P^2 distance measure).

The above can be summarized as follows: on orange and yellow pistes that are bare or under mixed grass / moss vegetation with a clayey topsoil, Hortonian overland flow is very likely to occur. For natural slopes and green pistes under shrubs (and grass) with a more sandy texture, shallow subsurface flow is the most likely drainage type. The relevance of this for the stream discharge will be discussed in Section 6.5.

The fact that there is a large chance of overland flow on ski tracks may have led to the lower average moisture content under ski pistes: subsurface flow contributes to the ASM, but overland flow does not. In this sense, overland flow does not only have a harmful effect on the topsoil through the action of erosion, but also on the health of the vegetation via the shortage of moisture (Dikau 1986), which indirectly lowers the resistance against erosion.

5 Interpolation of hydraulic conductivity data

For modelling purposes (as described in Chapter 7), an interpolated map of the hydrological conductivities of the study area is needed. The making of this map and the used methods are described. The chapter starts with a non-exhaustive description of the underlying theory of the interpolation methods used here. Following this, the results from the actual interpolations are presented and subsequently discussed.

5.1 Theory behind interpolation techniques

In general, two classifications of interpolation methods can be made. One can classify the methods in local and global interpolators — whereby 'local' refers to the use of data points in the locality of the point under consideration and 'global' to the use of all available data points —, or in geostatistical and non-geostatistical interpolators. Here, the last classification will be used to stress the different approaches adopted by these methods. The explanation of the underlying theory starts with the simpler non-geostatistical interpolators.

Theory behind non-geostatistical interpolation techniques

The following kinds of non-geostatistical interpolation are the most well-known:

- Thiessen / Voronoi / Dirichlet polygon interpolation;
- Trend surface analysis (TSA);
- Inverse / linear distance weighted interpolation (IDW).

The simplest method is Thiessen interpolation (Thiessen 1911) (see Fig. 5.1). In this local interpolation method, the first step taken is the calculation of the distances between data points (thick fuzzy lines in Fig. 5.1a). Halfway these distances, boundaries can be drawn between the different polygons of influence of the data points (Fig. 5.1b). The value of each data point is assumed representative for its immediate surroundings (= the polygon(s) around the data point(s) in Fig. 5.1a & b) and each polygon is assigned the value of its data point. It is obvious that the distances between the data points and their distribution influence the resulting interpolation. For instance, interpolation of data points on a regular grid results in a gridded representation. Another artefact of Thiessen interpolation is the unknown amount of variation within each polygon, because statistics cannot be computed with only one data value per polygon.

Trend surface analysis is a rather simple (global) method but is often used to remove spatial trends in data sets before there is made use of geostatistical techniques. In general, trend surface analysis resembles normal linear regression analysis: it tries to predict attribute values at unsampled points with the aid of a regression formula. In the case of trend surface analysis, the attribute is the dependent variable and (combinations of) the x and y coordinates of the sample area are the independent variables in the regression formula. The regression formula is found by a least squares fitting procedure, which means that the residuals (the sum of squared differences between the expected / interpolated and the measured values) are minimized through fitting of the trend surface. The trend surface can be of any order. However, with increasing order, the amount of regression coefficients increases drastically, because the combination of x and y coordinates that can be made increases fast as well. For instance, a first order trend surface is described with the following three-parameter formula:

$$z(x, y) = b_1 \cdot x + b_2 \cdot y + b_0 \qquad \text{(Eq. 5.1)}$$

with b_n denoting a regression coefficient. In contrast, a third order regression formula already contains ten regression coefficients and ten combinations of x and y (e.g. $x^2 \cdot y$ or y^3). This method is not used here, because preliminary research showed the inapplicability of this interpolation method with hydraulic conductivity data due to the extreme smooth interpolated surface and a bad fit of the trend surface (Thonon 2000).

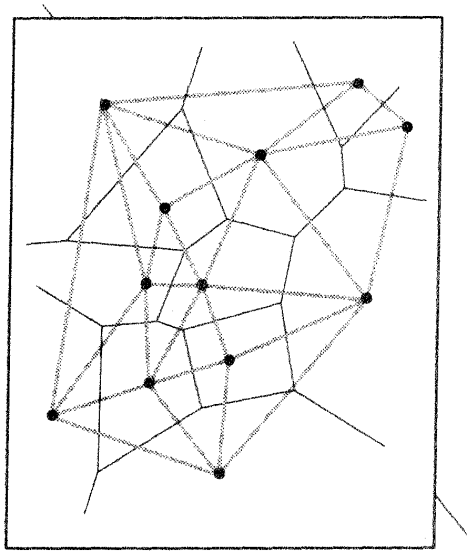

Figure 5.1a. The dark spots denote the data points, the narrow black lines the Thiessen polygons them selves and the wide vague lines the Delauney triangulation. Source: Kraak & Ormeling (1996, Fig. 5.29(c)).

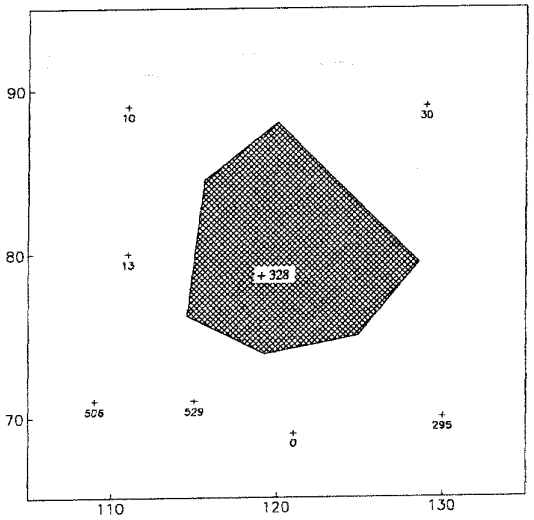

Figure 5.1b. The black zone indicates the polygon of influence around a fictitious point 328. Source: Isaaks & Srivastava (1989, Fig. 10.1).

The third interpolation method, inverse or linear distance weighting interpolation, is local. In this method, the following rather intuitive approach is adopted: data points further away from the point under consideration have less influence on interpolation than points nearby. In order to incorporate this approach in the actual interpolation, the weights of data points in interpolation are made distance dependent: the larger the distance between an unvisited point and a data point, the less the weight of that data point in the interpolation routine will be. Because distance and weight are inversely correlated, the method is called inverse distance interpolation. The inverse distance interpolation formula is as follows (Burrough & McDonnell 1998):

$$z(x_j) = \left[\sum z(x_i) \cdot d_{ij}^{-r}\right] \Big/ \sum d_{ij}^{-r} \qquad \text{(Eq. 5.2)}$$

with: $z(x_j)$ = the value at the point to be interpolated; $z(x_i)$ = the value at a data point; d_{ij}^{-r} = the interpolation weight. Within the interpolation weight, r = the inverse distance power and d_{ij} = the distance between data and unvisited point.

It can be seen that the larger the distance, the smaller the interpolation weight will be. Besides this, the larger the inverse distance power, the faster the interpolation weight will decrease with distance and the more local the interpolation will be. The most generally used inverse distance power (idp) is two; when r =1, the interpolation is said to be linear. idp's Can be of any real positive value.

This method was not used here either, because kriging, a similar but more statistical sound technique was available. The technique was however used in earlier research on

the *K* data set as described in Section 4.1. These interpolations are not used here in further analysis — although the results are fairly well and the methods is fast and easy. Reference is made to Thonon (2000) for the results of the IDW interpolations.

Theory behind geostatistical interpolation techniques

Geostatistical interpolation[18] is a special form of inverse distance interpolation, in which the interpolation weights are not only dependent upon distance but also on the amount of spatial association (called covariation or correlation) between data points. Spatial or geostatistical correlation / covariation is alike normal bivariate correlation / covariation in that it refers to the existence of association between groups of points or data values. However, in geostatistics, covariation does not denote association between *variables* – although this can be added – but association between values measured at different *locations* at a certain distance apart from each other. In this so called regionalized variable theory, the separation distance is called 'lag' and is denoted with the symbol h; the amount of association is called (auto)covariance and is denoted with C(h). Also the correlation coefficient D(h), which is merely C(h) divided by F^2 (the data set variance), is dependent upon the lag. A graph in which C(h) is a function of h is called a (auto)covariogram (Fig. 5.2a), a graph of D(h) against h is called a correlogram (Fig. 5.2b). In these examples, the amount of correlation or association between points at a small distance from each other is large, whereas points at larger distances from each other do not resemble each other very much. Many natural variables have a correlation structure that more or less resembles the one in Fig. 5.2c.

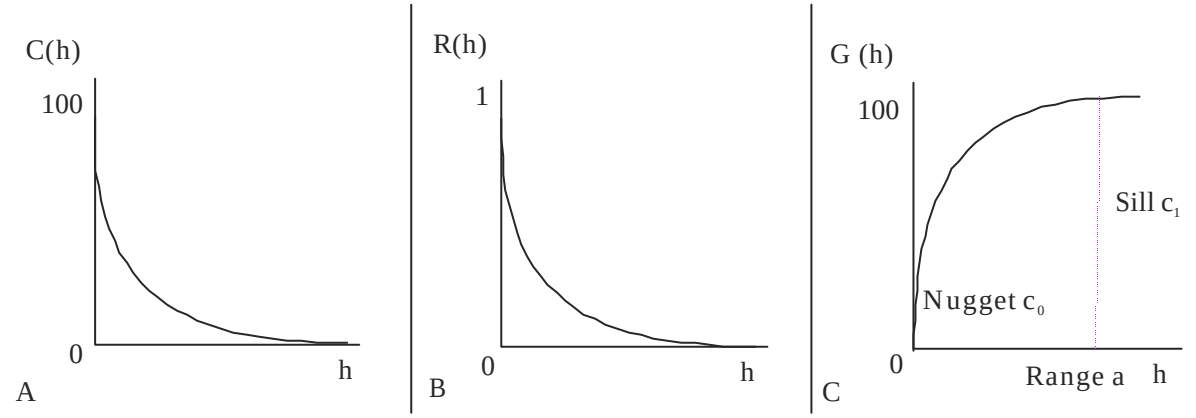

Figure 5.2. In a, an autocovariogram is depicted, with the covariance on the *y*-axis. In b, the correlogram is shown, with the correlation on the *y*-axis. c Contains the semi-variogram with the description of its properties.

Kriging makes use of another, yet comparable, geostatistical quantity in the calculation of the interpolation weights: the semivariance ((h)[19]. In Fig. 5.2c, a (semi)variogram is given. As can be seen, this is just the mirror image of the

[18] Another name for geostatistical interpolation is 'kriging', after the South African engineer Danie G. Krige, who carried out the first experiments with geostatistics (Krige 1966), together with Herbert Sichel (Armstrong 1998). However, the concepts of spatial dependency, range, nugget etc. were already found by Mercer & Hall (1911) (Webster 1994) and the first theoretical considerations were already recognized by Kolmogorov (1941) (Kutílek & Nielsen 1994), but these publications are not well known due to circumstances. More on the history of geostatistics can be found in Cressie (1990).

[19] Goovaerts (1992) states that the variogram is more useful in kriging because it requires fewer assumptions to be fulfilled than the covariogram (i.e. only the intrinsic hypothesis). Oliver & Webster (1986) also prefer the use of the semi-variogram in lieu of the covariogram.

correlogram and the (auto)covariogram. (This is not always the case, as will be seen later.) The definition of the semivariance and covariance are as follows (Armstrong 1998):

$$(\gamma(h) = \sigma^2 - C(h), \qquad \text{(Eq. 5.3a)}$$

$$(\gamma(h) = 1 / n \sum [z(x) - z(x + h)]^2, \qquad \text{(Eq. 5.3b)}$$

$$C(h) = 1 / n \sum [\{z(x) - m\} \cdot \{z(x + h) - m\}] \qquad \text{(Eq. 5.3c)}$$

with: $z(x)$ = an attribute value z at a certain point x in the area; m = the general mean of the attribute in the area.

Because points at large lags exhibit hardly any association (covariance and correlation approach zero when the lag goes to infinity, see also Fig. 5.2a & b), it results from Eq. 5.2a that the semivariance mounts up to the data set variance for large lags (Fig. 5.2c): there is no more spatial correlation between data points at large distances from each other. The lag after which the spatial correlation becomes negligible is called the range a. The semivariance accompanied with the range or large lags is called the sill (c_1), whereas the semivariance at h = 0 is called nugget (variance), c_0 (see also Fig. 5.2c). The nugget is made up of uncorrelated ('white') noise in the measurements due to measuring errors or other reasons. The larger the sill is in comparison to the nugget, the more structured the semivariogram is called and the more spatial association is present in the area. When both sill and range are relatively large, the variogram is called structured. A structured variogram can help in optimising the interpolation weights in kriging, thereby enlarging the chance to get a well-interpolated map.

Before kriging can start, it is first necessary to check whether the requirements for kriging are fulfilled. These are the conditions of second order stationarity (or the less restrictive intrinsic hypothesis) and the admissibility of the variogram model.

- The definition of stationarity is the invariance of statistical moments (e.g. mean and variance) in a certain area. First order stationarity is only present when all statistical moments are invariant throughout the whole area. In kriging, only second order or weak stationarity needs to be present: the random function of the attribute[20] needs to have an equal expectation value for the mean throughout the whole area (Armstrong 1998):

$$E[Z(x)] = m(x) = m \qquad \text{(Eq. 5.4)}$$

with: $Z(x)$ = the random function of the attribute at point x; $m(x)$ = the mean of the attribute at point x; m = the general mean of the attribute in the area.

Besides this, the covariance between values at points at a distance h separated from each other has to be independent on the position of the point in the area and only dependent on the lag (Armstrong 1998):

$$E[Z(x) - Z(x + h)] - m^2 = C(h) \qquad \text{(Eq. 5.5)}$$

It is easy to check whether the attribute exhibits second order stationarity or not: only second order stationary attributes have a covariogram and a semivariogram that is mirror like to the covariogram, as for example in Fig. 3.

- The intrinsic hypothesis calls for a weaker version of second order stationarity (Fig. 5.3). For instance, C(h) is allowed to be non-existent (Armstrong 1998). Besides, it only calls for local stationarity (Isaaks & Srivastava 1989) for it assumes only the increments of the area to be weakly stationary (Armstrong 1998):

$$E[Z(x + h) - Z(x)] = 0 \qquad \text{(Eq. 5.6)}$$

However, *the variance of the data set needs to change in a structured way*, being only lag-dependent and not point-dependent at the same time (Armstrong 1998):

$$Var[Z(x + h) - Z(x)] = 2\gamma(h) \qquad \text{(Eq. 5.7)}$$

Especially when Eqs. 5.6 & 5.7 do not hold, kriging cannot be applied with confidence. In that case, heteroscedacity may be present in the area, which means that parts of the area exhibit smaller or larger variation in data values than other parts (Isaaks & Srivastava 1989). These variation anomalies restrict the use of geostatistics by causing the change of the variance to be *unstructured*. Applying a moving search window that calculates the variance within the window can check the homoscedacity of the area. When the resulting variances are equal, the area can be considered homoscedastic. When the area is heteroscedastic, it can be split up in parts with an equal amount of variance, each of which can still obey to the intrinsic hypothesis. The implication of the split-up action is the calculation of a separate variogram for each sub area.

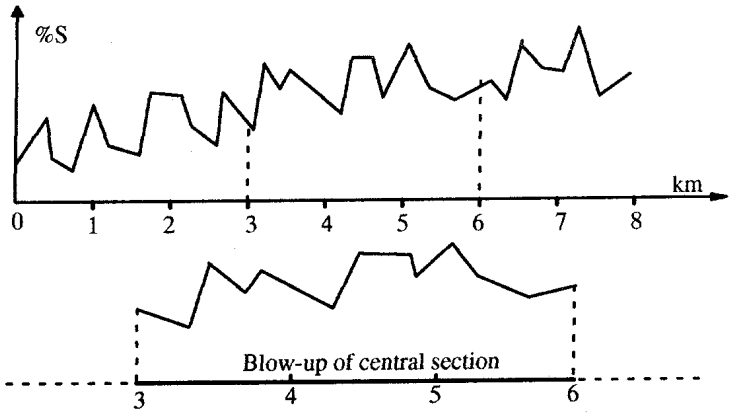

Figure 5.3. The intrinsic hypothesis means that only *increments* of an area (= the blow-up in the figure) have to exhibit second-order stationarity. Source: Armstrong (1998, Fig. 2.1).

• An admissible (semi)variogram model is a variogram model which is said to be 'positive definite' (Isaaks & Srivastava 1989)[21]. A variogram model itself is nothing but a certain formula that describes the change of γ as function of h. In practice, the positive definiteness condition means that when a certain variogram model is used in kriging, the resulting estimation error must have a positive variance.

Unfortunately, positive definiteness cannot be tested beforehand. It is therefore common practice to use only variogram models of which it is already known that they are positive definite (Armstrong 1998). The most well known functions are listed in standard textbooks such as Burrough & McDonnell (1998) and Isaaks & Srivastava (1989), some less well known can be found in Karssenberg (1997) and Armstrong (1998). In Fig. 5.4, the three most common models are depicted. It is always allowed to add different models, but distraction or piecewise combination is not allowed (Fig. 5.5) (Armstrong 1998).

[20] More information on random functions, random variables and probability density functions can be found in Russo & Bresler (1981) and Tietje (1993).

[21] According to the definition given in Armstrong (1998), the requirement is a 'conditionally *negative* definite' variogram. In fact, *co*variograms have to be positive definite. But since the error variance is required to be positive, the term 'negative' causes confusion and is therefore less used.

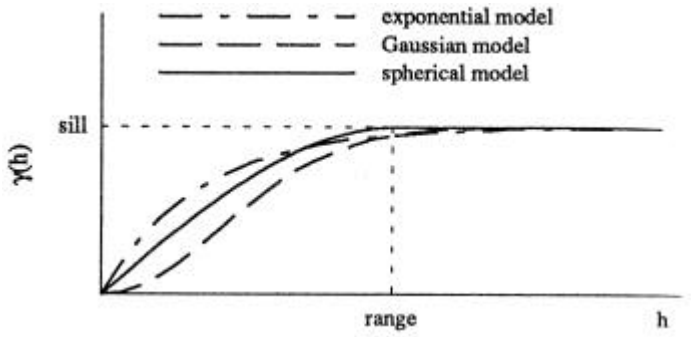

Figure 5.4. The three most widely used variogram models. Source: Isaaks & Srivastava (1989, Fig. 16.2).

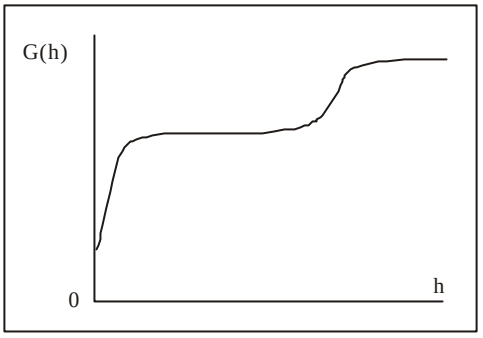

Figure 5.5. Example of an *in*admissible variogram model constructed by piecewise combination.

When it can be adhered to the at least the intrinsic hypothesis and the positive definiteness condition, kriging can start. With the help of the variogram, it is tried to find the best linear unbiased estimate (BLUE) of the attribute. This means that

$$E[Z' - Z] = 0, \qquad \text{(Eq. 5.8a)}$$

$$\text{Var}[Z' - Z] = \min \qquad \text{(Eq. 5.8b)}$$

with Z' = random function of estimates of the attribute. In words, Eq. 5.8a means that the average expected deviation from the random function of the data values is zero. Eq. 5.8b means that the variance between the interpolated values and the original values has to be as small as possible.

In order to obey to the above equations, there is made use of matrix calculation and general algebraic rules. Because the interpolation weights can hardly be calculated by hand, the calculations are implemented in computer programs like, for example, Gstat. For it is not the purpose of this report to explain the intricacies involved in matrix calculus or the derivation of the actual kriging equations, it is referred here to Armstrong (1998, Chapter 7) for the derivation of the ordinary and block kriging equations and to Burrough & McDonnell (1998, 139-141) or Isaaks & Srivastava (1989, 290-296) for a worked example on the complete ordinary kriging routine.

5.2 Results of non-geostatistical interpolations

First of all, it has to be said that K_{uncor} will probably follow the lognormal distribution, inferred from the test outcomes for the log-transformed values in Section 4.1 and Sisson & Wieringa (1981), Mason *et al.* (1957) and Coelho (1974). The other two values, log K_{uncor} and K, can be considered normally distributed with 95 % confidence[22]. A Gaussian distribution is not required for the application of kriging or other interpolation methods, but for correlation & regression, it is. It only helps to get better results from (geo)statistical methods, such as kriging (Isaaks & Srivastava 1989; Gotway *et al.* 1996).

Thiessen polygon interpolation results

The Thiessen polygon interpolation (Thiessen 1911) can serve as a reference interpolation, because it is the most simple interpolation possible. It is often used to judge the quality of other forms of interpolation (e.g. by Goovaerts & Journel (1995)

[22] If it would not be able to carry out a test on normality, it could be inferred from the Sk values in Table 4.1 how close the distribution is to the Gaussian. Commonly, Sk values in the range of -0.5 to +0.5 are considered to indicate a normal distribution.

and Isaaks & Srivastava (1989)), because a map of only data points with their respective values is hard to interpret and difficult to read.

The results of the Thiessen interpolation can be seen in Fig. 5.6. They were calculated with the aid of a PCRaster model. Because there is in general little difference between the interpolation results for the whole study area and the ski tracks only (Fig. 5.6d), the results for the ski track are not shown here.

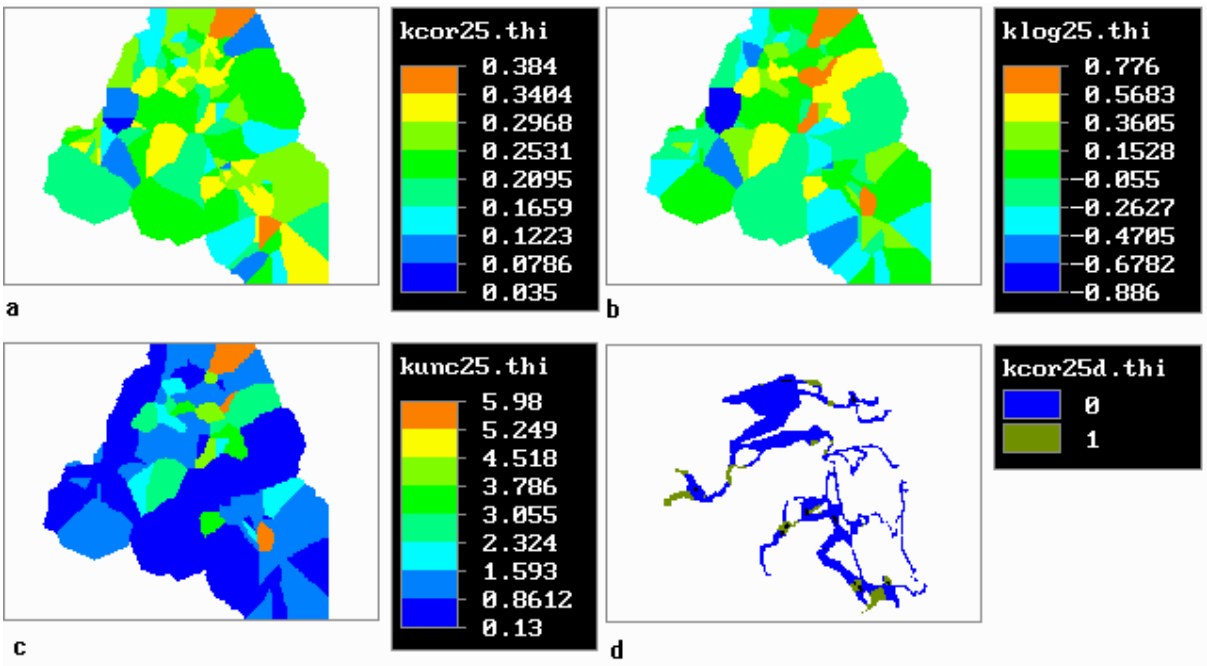

Figure 5.6. Results of Thiessen polygon interpolation for Kunsat,c (a), log Kunsat (b), uncorrected Kunsat (c). In d, it is depicted whether there exists difference between the polygons for ski tracks only and the total area; 1 indicates difference and 0 indicates no difference.

A major disadvantage of the Thiessen interpolation is the unnatural triangular appearance of the polygons. Besides this, the interpolated patches are totally unrelated to the structure of the area; the interpolation does not take the pattern of the ski tracks into account. However, this cannot be expected from a rather simple method like Thiessen interpolation. On the other hand, when a PCRaster model or a Gstat command file is used, the interpolation method is rather fast and gives a good overview of conductivities in the study area. The differences between the area weighted averages of the Thiessen interpolated maps and the arithmetic averages of original values were found to be of minor importance and non-significant with 95 % confidence. For global overview purposes, the Thiessen interpolation can be considered to be a better method than for example trend surface interpolation: the whole range of values is present and, at the same time, negative values and an unnaturally smooth interpolation surface are absent.

It can be concluded that Thiessen interpolation serves well as a local interpolator. The same was found by Isaaks & Srivastava (1989), who compared ordinary point kriging to polygon interpolation. They also found the Thiessen polygon interpolation method to do “(…) a very good job in terms of global bias”. An improvement can be made by pycnophylactic interpolation (Tobler 1979), which transforms the stepwise Thiessen polygon surface into a smooth and undulating surface. This method is however difficult to implement in PCRaster.

5.3 Variograms and variogram surfaces

The first step in kriging is the check on homoscedacity, with the method suggested by Isaaks & Srivastava (1989), i.e. application of a variance calculating moving window. The method is rather laborious, so this was only done for the *K* data. The map of local variances (for 500 by 500 m windows), which is not shown here, consists of generally low variances with a few positive outliers. A structural pattern of outliers could however not be detected. At least the *K* data set is therefore considered to be homoscedastic, thereby allowing variogram modelling and kriging. It is expected that the log *K* and K_{uncor} values are homoscedastic as well.

The second step in kriging is the formation of an experimental variogram, which is subsequently fitted by one of the various variogram models. The formation of an experimental variogram is done semi-automatically by programs such as Gstat; the only input from the user is the definition of the so called 'cutoff' and 'width'. The cutoff is the maximum lag for which semivariances are calculated, the width is the extension zone around each lag (see Fig. 5.7). The definition of cutoff and width influence the experimental variogram. For instance, if the experimental variogram increases or decreases drastically after the cutoff, this will not be fitted by the variogram model, because this part of the variogram is literally cut off. The width mainly influences the amount of detail in the experimental variogram: a small width means a large amount of detail, which may be important for fitting the variogram model in the nugget region. On the other hand, choosing a large width can prevent the experimental variogram from pollution by outliers.

Variograms are either isotropic or anisotropic. Isotropic means that all the points within the radius around a data point are included in the semivariance calculation. Anisotropic means that only points in a certain wind direction are included in the calculation, for example only points which are located north or south from the data point in the middle of the radius (see Fig. 5.7). From variogram surfaces, which are actually maps of the semivariances in all wind directions (see Fig. 5.8 for an example for the height in the study area), one can judge whether a variable is isotropic or anisotropic. When it is anisotropic, it is very useful in kriging to use more than one variogram at a time, for each direction one distinct variogram.

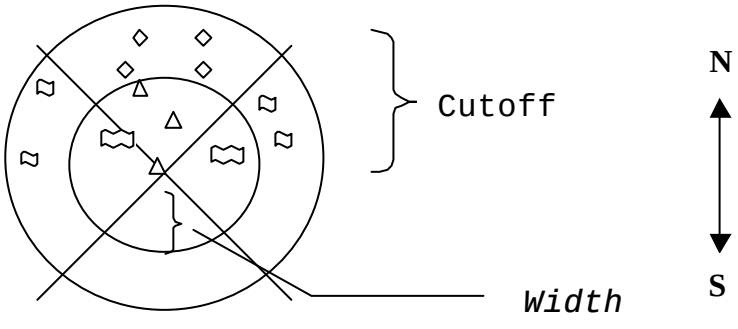

Figure 5.7. The outer ring denotes the zone in which points are used to calculate the semivariance. In the isotropic case, both the waves and the rectangles are used in the calculation. In the anisotropic case, only the rectangles are used, for the search direction is NS. The double waves and the triangles are not used in both the isotropic and

There can be made a distinction between zonal and geometric anisotropy. In zonal anisotropy, the height of the sill is dependent upon direction (Fig 5.8). In geometric anisotropy, the range is dependent upon direction (Fig. 5.9).

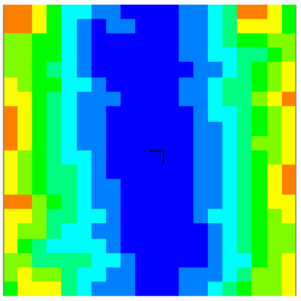

Figure 5.8 Variogram map for the variable height in the study area. Note the low semivariance in NS direction and the large semivariance in EW direction (zonal anisotropy).

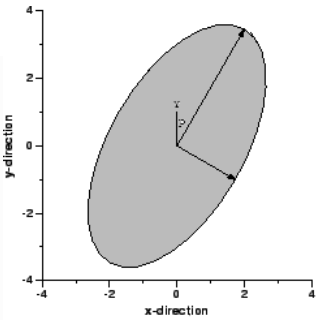

Figure 5.9 Example of geometric anisotropy. In the SSW-NNE direction (called major axis), the range is much longer - two times as long - than in the direction perpendicular to this (called minor axis).

Source: http://www.geog.uu.nl/gstat/manual/gstat.html

Isotropic variograms for 'total area' case

Four different isotropic variograms were calculated: for *K*, log *K*, uncorrected *K* and rainfall intensity. These are shown in Fig. 5.10. The automatic fitting procedure used by Gstat (version 2.0b) was weighted least squares (wls). Only the rainfall intensity variogram model was fitted by hand. All variogram models show a rather good fit before the range and a rather bad fit after the range. This is admissible, because a variable does not exhibit correlation for lags larger than the range. Besides, interpolation is only carried out within a search radius that is only a little larger than the range of the variogram model, so the fit of the model after the range hardly influences the kriging interpolation. Unfortunately, Gstat gives no measures such as r^2 that indicate the goodness-of-fit. However, in these cases it is easily discernible by eye how well a model is fitted. A possible solution for this bad fit is a method provided in Bardossy *et al.* (1990a, 1990b), which involves the fitting of a variogram model with a band of confidence instead of only a line. This can be used in subsequent interpolation to assure the incorporation of the uncertainty. This method was however not available in Gstat at the time of research and was therefore not used here.

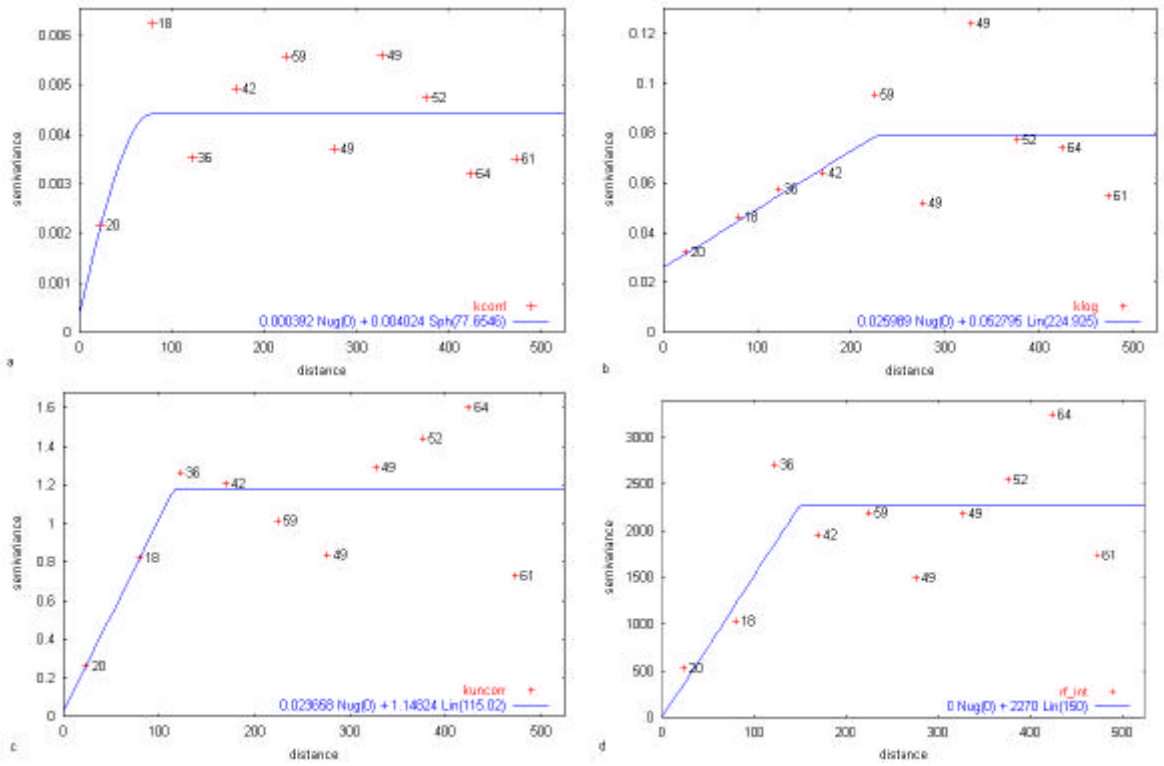

Figure 5.10. The isotropic variograms calculated with all the points in the study area incorporated (n = 117). In a, the spherical variogram for *K*, in b the linear for log *K*, in c the linear for original *K* and in d the linear

model for applied rainfall intensity is shown. All variograms were calculated with a cutoff of 500 m and a width of 50 m.

It can be noted that the range of the *K* variogram (Fig. 5.10a) is rather short in comparison to the uncorrected *K* and the rainfall intensity variograms (Fig. 5.10c & d) (see also Table 5.2). A short range (as well as a high nugget) is generally seen as an indication of an unstructured variable, i.e. a variable that does not have a large spatial correlation. Moreover, a short range limits the extent around data points for which interpolations are made[23].

Because the correction of *K* only involves a division by rainfall intensity and a multiplication by 15, the interpolated area for *K* can be extended by nearly fifty metres when *K* is calculated *after* interpolation from uncorrected *K* and rainfall intensity, thereby benefiting from the larger ranges from the respective variables. However, even interpolation of the variable with the largest range (log *K*) does not cover the total study area with values, because the distances between the data points are often larger than the range of the variograms in Fig. 5.10 (see Figs. 5.13 & 5.14).

The variograms all have a relatively small nugget variance. This is important, because it causes the interpolation variances to be small as well, thereby ascertaining a small uncertainty in interpolated values. All variograms have a sill variance that is equal to or a little less than the sample variance, thereby adhering to the theoretical considerations in the Section 5.1.

Variogram maps for 'total area' case

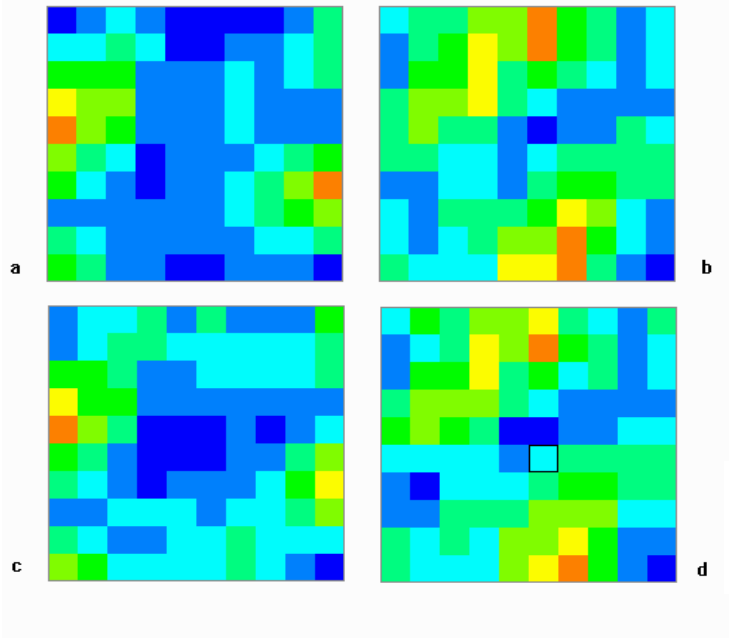

Figure 5.11. Variogram surfaces for *K* (a), uncorrected *K* (b), log *K* (c) and rainfall intensity (d).

In Fig. 5.11, the variogram surfaces for the three states of *K* and for the rainfall intensity can be seen. Note the large amount of alikeness between the uncorrected *K* and the rainfall intensity variogram maps (Fig. 5.11b & d): in both maps, a major axis with WSW–ENE trend can be spotted. The major axis for log *K* is SWS–NEN and for *K* it trends north–south (Fig. 5.11a). All four variables were found to be anisotropic. The three *K*'s all exhibit both zonal and geometric anisotropy (uncorrected *K* only little geometric), the rainfall intensity exhibits only zonal anisotropy. For instance, the major

[23] It is, strictly spoken, allowed to interpolate with a radius that is larger than the range (Isaaks & Srivastava 1989), but for the part larger than the range the predicted values are simply the average of all points within the search radius.

axis of the *K* variogram map is 377 m, whereas the minor axis measures about 78 m. Incorporation of these anisotropies in kriging can lead to a serious drop of interpolation errors, because the variogram model can be defined more precisely.

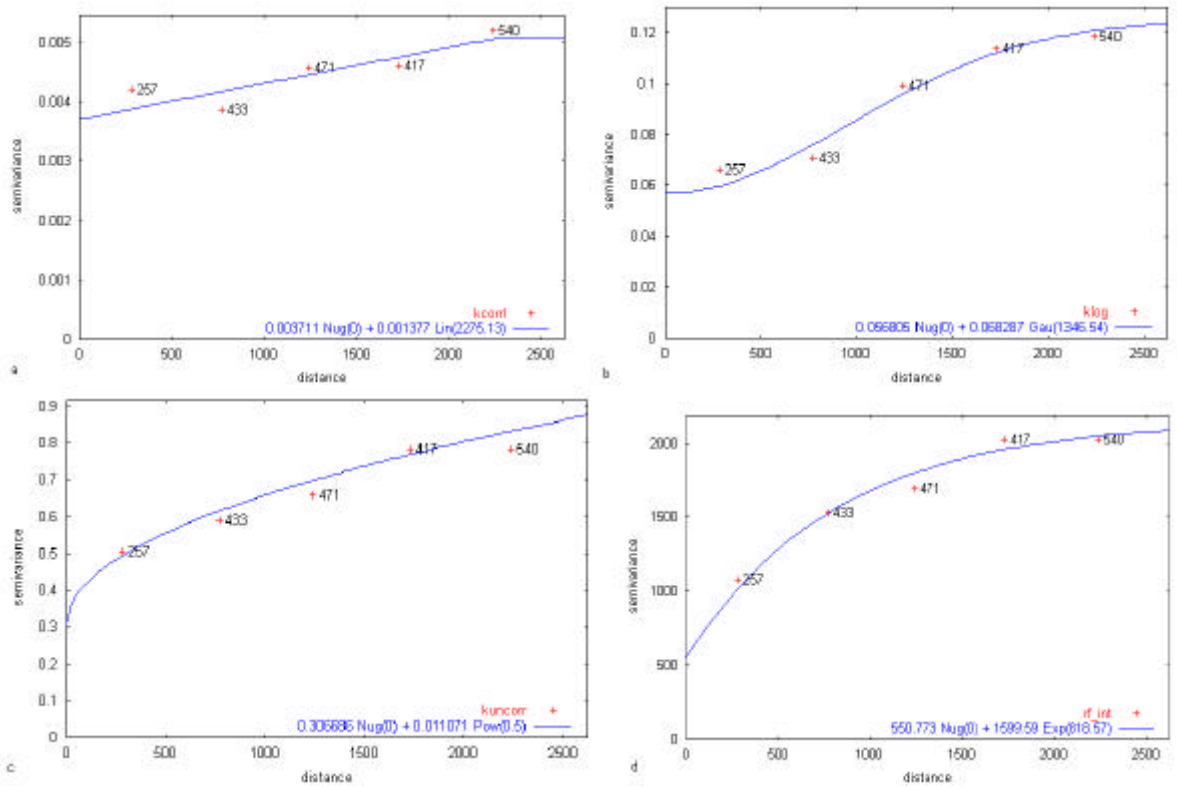

Figure 5.12. The isotropic variograms calculated with only the points at ski tracks incorporated (n = 84). In a, the linear variogram for *K* is displayed, in b the Gaussian for log *K*, in c the square root model for original *K* and in d the exponential for applied rainfall intensity. All variograms were calculated with a cutoff of 2500 m and a width of 100 m. Note that the model for original *K* could also be linear, but when a smaller width was used, it was noted that the nugget is smaller than a linear model would indicate. Even the now fitted power model has a nugget that is too large.

Isotropic variograms for 'only ski tracks' case

Because the main purpose of the study was to assess the hydrological impact of skiing, the variograms for the above named four variables were also calculated with only data points at ski tracks (n = 84). The results, as depicted in Fig. 5.12, are strikingly different from the variograms in Fig. 5.10 (see also Table 5.1): the ranges are much longer and the fitted models are different, although the same fitting procedure (wls) and the same program (Gstat 2.0b) were used.

Fig. 5.12a is a good example of a weakly structured variogram: the nugget is very large compared to the sill. Fortunately, the range is rather large; if it would be 78 m as in the 'total area' case, it would be unwise to use it in kriging. The other three variograms are better structured, well defined and well fitted, so this time the reason for calculation of *K after* interpolation is the higher amount of spatial correlation for both uncorrected *K* and rainfall intensity.

Since the ranges are much longer for the variograms in Fig. 5.12 (see Table 5.1), the interpolation can now cover the whole network of ski tracks. It is also possible that the kriging variance will be smaller than in the 'total area' case, because the 'only ski tracks' variogram models exhibit better fits, although the nugget variances are larger (Table 5.1). Again, the sill variances are approximately equal to the sample variances.

variable	n	model	c_0 *	c_1 **	c_0 / c_1 ***	a5 [m] ****
K	total	Spherical	$3.9 \cdot 10^{-4}$	$4.4 \cdot 10^{-3}$	0.089	78
”	*ski*	*Linear*	*$3.7 \cdot 10^{-3}$*	*$5.1 \cdot 10^{-3}$*	*0.72*	*2275*
log *K*	total	Linear	$2.6 \cdot 10^{-2}$	$7.9 \cdot 10^{-2}$	0.32	225
”	*ski*	*Gaussian*	*$5.7 \cdot 10^{-2}$*	*0.13*	*0.45*	*2332*
unc. *K*	total	Linear	$2.4 \cdot 10^{-2}$	1.17	0.021	115
”	*ski*	*Power*	*0.31*	–	–	?
rf. int.	total	Linear	0	2270	0	150
”	*ski*	*Exponential*	*551*	*2150*	*0.26*	*2457*

Table 5.1. Parameters for the eight different variogram models for both ‘only ski tracks’ and ‘total area’ cases. *) c_0 denotes nugget variance [(m / d)²]; **): c_1 denotes sill semivariance [(m / d)²]. Some authors define this as the *gain* of semivariance *above* the nugget variance; here it *includes* the nugget variance; ***) because of **), the nugget-sill ratio c_0 / c_1 lies between 0 (no nugget) and 1 (pure nugget model). ****) a5 denotes practical range, which is the physical distance (lag) to where spatial correlation exists.

The four variables for the ‘only ski tracks’ case were not found to be largely anisotropic. It may be possible that the anisotropy could not be detected because of lack of data points in most wind directions. It was therefore decided not to use anisotropic variograms in subsequent kriging interpolation on only ski tracks.

5.4 Kriging results

In Figs. 5.13 to 5.17, the results of ordinary point kriging are depicted. The support (the area of measurement) of the *K* measurements was 650 cm²; the interpolated values are only valid for this support area. The following terminology is used in the legends: the first letter is always a k (from K for conductivity), followed by cor (*K*), log (log *K*), unc (uncorrected *K*), int (rainfall intensity) or co2 (*K* corrected *after* kriging of uncorrected *K* and rainfall intensity). 25 Denotes the resolution in metres, i stands for the use of isotropic variograms and a for the use of anisotropic variograms. See Thonon (2000) for the different Gstat command files used in interpolation.

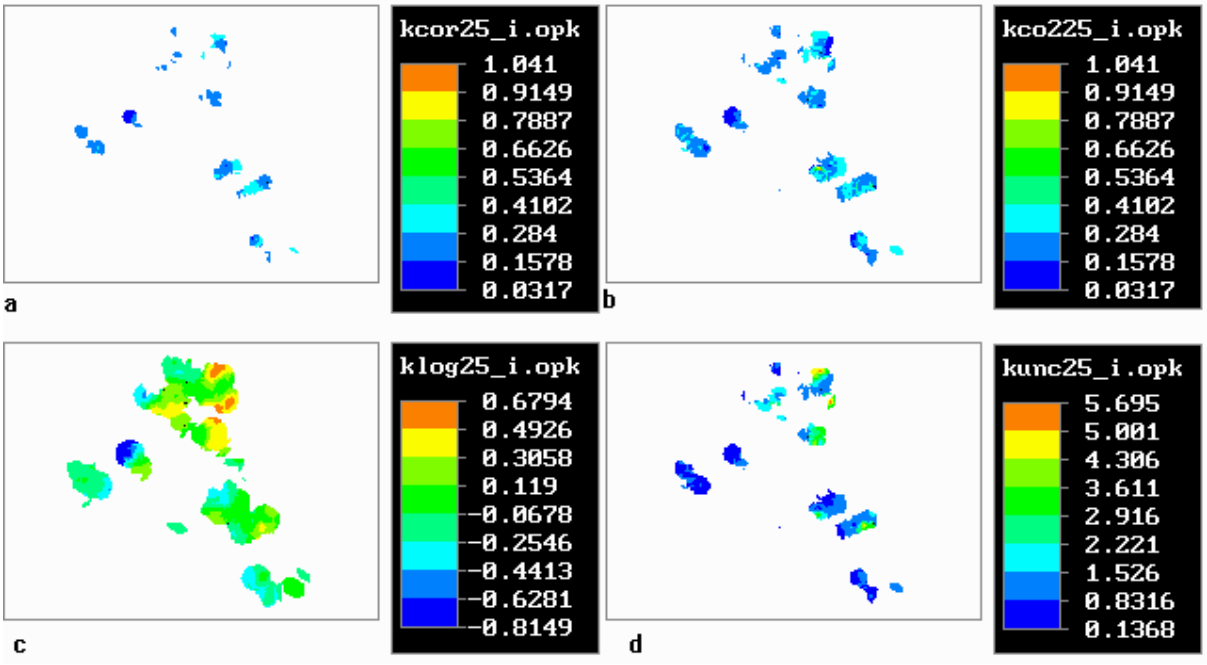

Figure 5.13. Results of ordinary kriging interpolation (opk) for the ‘total area’ case with isotropic variograms.

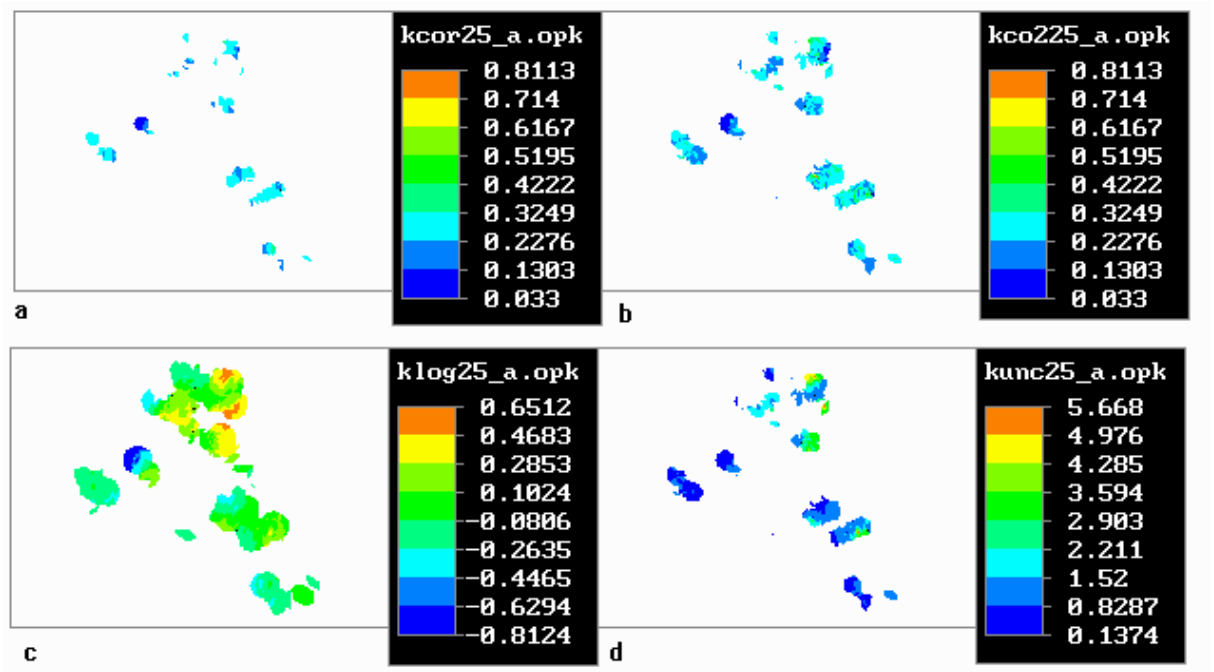

Figure 5.14. Results of ordinary kriging interpolation (opk) for the 'total area' case with anisotropic variograms.

When the results of the anisotropic and isotropic kriging are compared visually, it is obvious that the differences between both results are not large. Yet, the results differ significantly according to the standardized Euclidian distances in Table 5.2. On the other hand, the correlations between the anisotropic and isotropic results are high. In addition, the kriging variances (F_e^2) or kriging standard deviations (F_e) are not highly different (Table 5.3). It was expected that the F_e and F_e^2 for the anisotropic interpolations would be lower. This is however only true for log *K*. For all the other variables, the CV_e's and F_e's are even higher for the anisotropic than for the isotropic interpolations. This is possibly due to the relatively strange variogram surface (Fig. 5.11) for the variables rainfall intensity and uncorrected *K*: a steady increase in semivariance from the midpoint to the borders of the variogram maps, as is the case in the example of Fig. 5.8, cannot be detected. Instead, a relatively 'hummocky' variogram surface is present, which cannot be modelled accurate enough to benefit from the inclusion of anisotropy in the kriging. The log *K* and *K* variogram surfaces (Fig. 5.11a & c) can be modelled better, which resulted in relatively equal isotropic and anisotropic F_e's & CV_e's (Table 5.3).

Table 5.2. Correlation and difference measures for the anisotropic and isotropic results. All values are found to be significant with 95 % confidence (n = number of pixels on map). *) *after* denotes that correction for applied rainfall intensity took place after kriging. **) d^2 = standardized Euclidian distance, see Thonon (2000, Appendix 3) for calculation procedure.

variable	r	r^2	d^2 **
K	0.973	0.946	8.213
K after *	0.881	0.776	26.76
unc. *K*	0.981	0.963	10.66
log *K*	0.980	0.960	18.37
rf. int.	0.993	0.986	8.78

variable	avg. CV_e i [%]	avg. CV_e a [%]	avg. CV_e p [%]	avg. F_e i *	avg. F_e a *	avg. F_e p *
K	54.8	37.2	27.3	0.073	0.080	0.065
K after	12.3	14.3	7.13	0.025	0.029	0.018
unc. *K*	138	163	72.1	1.1	1.3	0.74
log *K*	–	–	–	0.28	0.28	0.26
rf. int.	74.9	85.8	55.1	46	53	34

Table 5.3. Average coefficients of variation and kriging standard deviations for the isotropic (i), anisotropic (a) and isotropic 'only ski tracks' (p) interpolation results. *) units in [m / d] for *K* and unc. *K*, [mm / h] for rainfall intensity, in logarithmic units for log *K*.

The calculation of *K after* (= *K* values corrected after kriging) led to very low estimation errors (Table 5.3). Because the estimation errors of *K after* could not be calculated directly, error propagation rules stated in Burrough & McDonnell (1998, Eq. 10.5) were used to calculate them indirectly. Because the calculation of both F_e and the *K after* value itself consist of division, the calculation resulted in fairly low F_e's and CV_e's for *K after*. Validation of the *K after* values with the original *K* values is again impossible, because of the lack of an independent validation data set. When it is assumed that the *K after* values found are correct, the method of correction afterwards can serve as an alternative for correction on beforehand. Besides, the interpolation area can then safely be extended, using the larger ranges of the variograms of both rainfall intensity and uncorrected *K*.

Two more methods to lower estimation errors were tested: simple kriging (kriging with the sample mean as an extra input) and ordinary block kriging (kriging on blocks of land). Block kriging on 50×50 m blocks was carried out on both 10 m and 25 m resolution grids. Again, no large differences in kriging results, F_e's or CV_e's between the two grids were found. Both methods indeed lower the F_e, but both methods smooth the interpolation surface even more than ordinary point kriging. When a smoothened map is used in modelling, the spatial variation is not represented adequately: it is unnaturally low. This low spatial variation is due to the subtraction of the within-block semivariance from the total semivariance in block kriging and the assignment of a kriging weight to the average in simple kriging. Therefore, these two methods are rejected for interpolation because a low amount of spatial variation in input maps may cause errors in distributed hydrological model outcomes (Beven 1989; De Roo & Riezebos 1992).

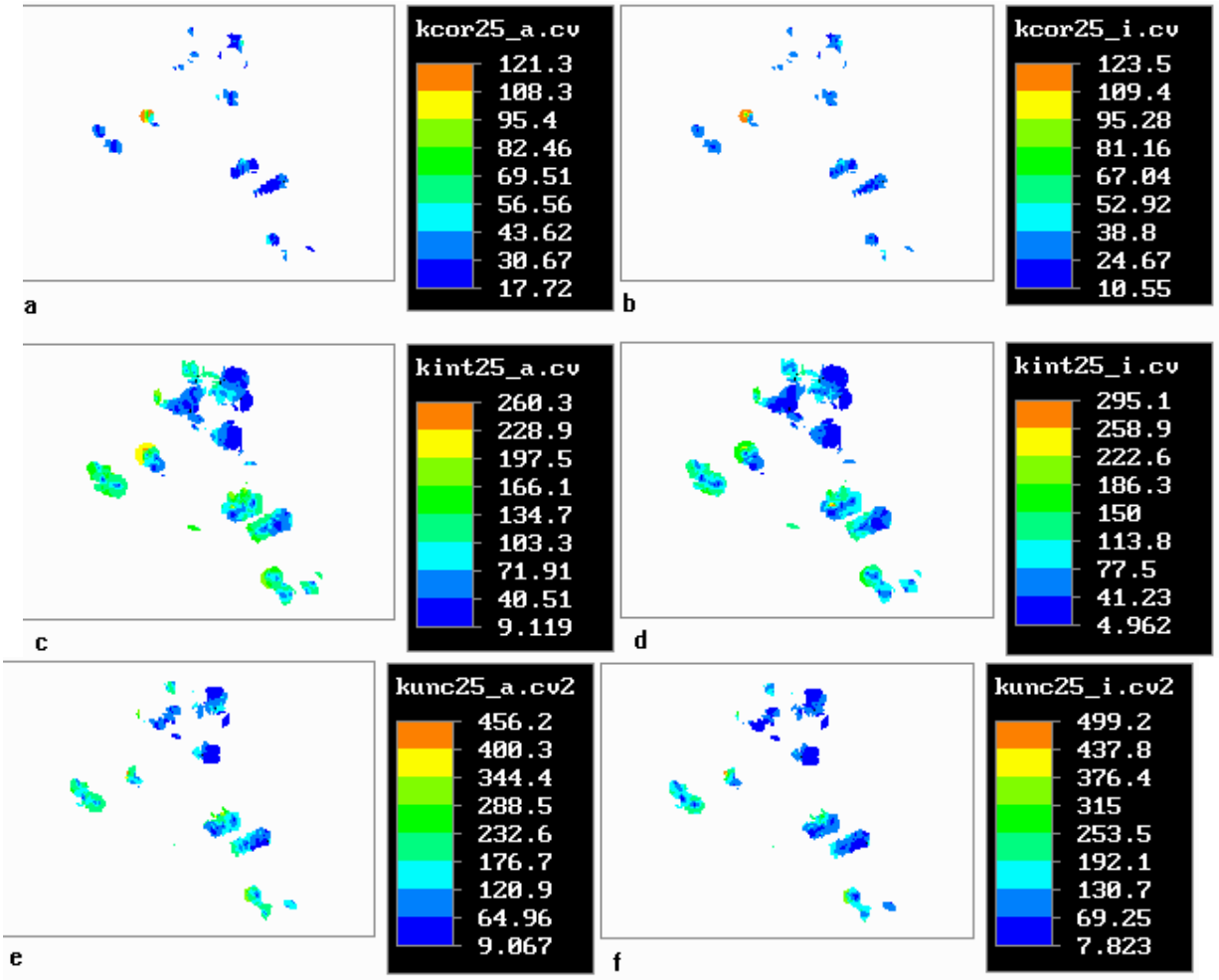

Figure 5.15. Coefficients of variation for both 'only ski tracks' and 'total area' cases. Note that the range of the CV_e's is always larger in the isotropic than in the anisotropic case. For uncorrected *K* (e & f) the range has been cut off by 500; the highest CV_e's are originally above 1000 %.

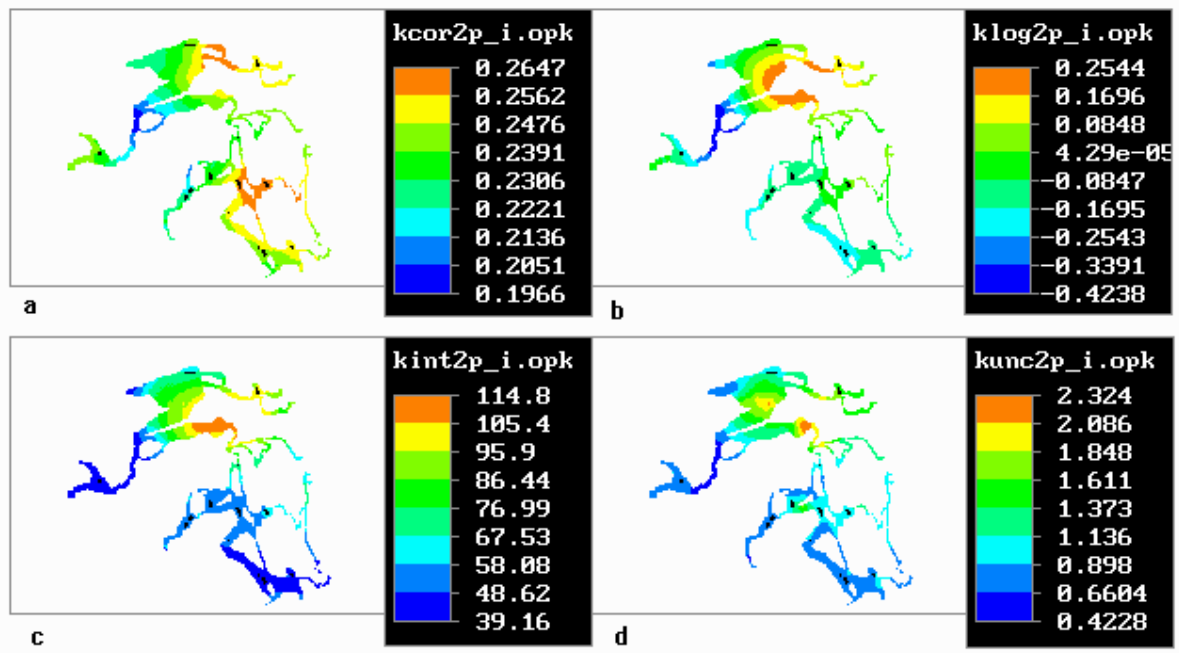

Figure 5.16. Results for ordinary kriging interpolation (opk) for the 'only ski tracks' case. Note that the total area of ski tracks is covered with interpolated values.

A last comparison can be made between the results of the isotropic kriging for the 'total area' and the 'only ski tracks' case. From the maps with CV_e's (Figs. 5.15 & 5.17), it is already obvious that the estimation errors for the 'only ski tracks' interpolation are much smaller than the errors for the 'total area' interpolation. The lower average values for ski tracks in Table 5.3 confirm this observation. Moreover, the 'only ski tracks' interpolation covers a much wider area.

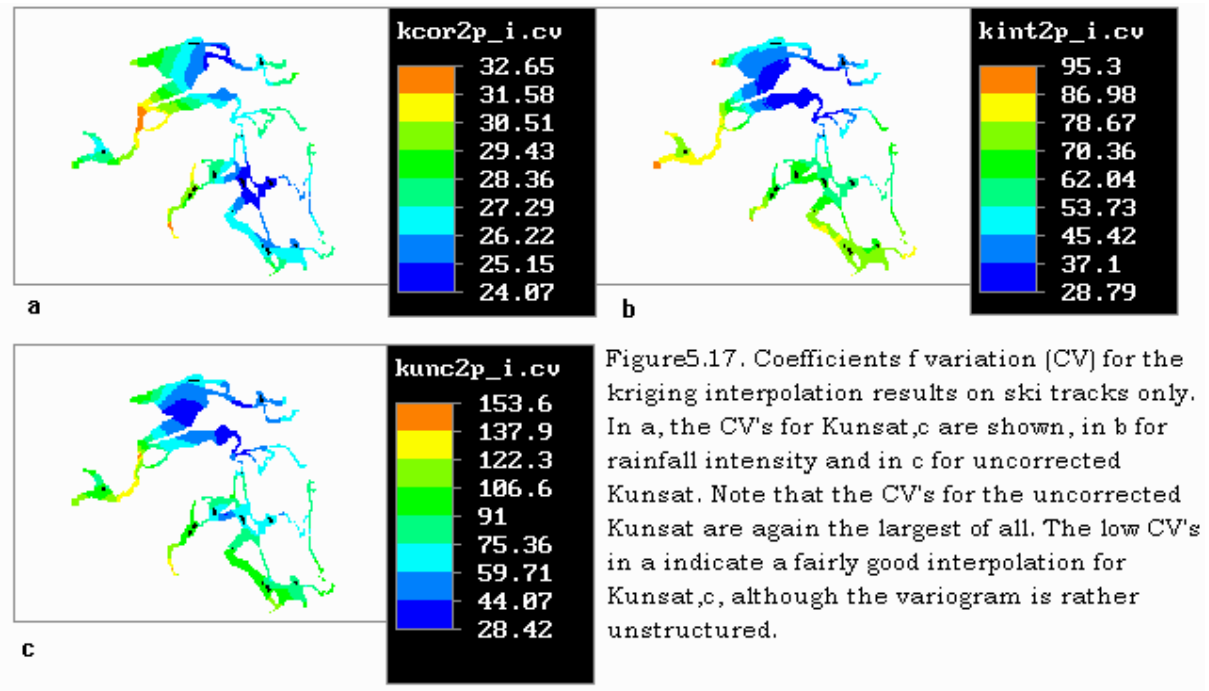

Figure5.17. Coefficients f variation (CV) for the kriging interpolation results on ski tracks only. In a, the CV's for Kunsat,c are shown, in b for rainfall intensity and in c for uncorrected Kunsat. Note that the CV's for the uncorrected Kunsat are again the largest of all. The low CV's in a indicate a fairly good interpolation for Kunsat,c, although the variogram is rather unstructured.

Both the low estimation errors and the large interpolation area are a direct consequence of the long ranges for the 'only ski tracks' variograms. Because the search radius for interpolation is almost equal to the range of the variogram used and interpolation only makes use of data points within the search radius, the amount of data points used in interpolation can be larger in the 'only ski tracks' case than in the 'total area' case. As in ordinary statistics, a higher number of observations included in calculation lower the variance and standard deviation (central limit theorem).

Cross validation results for kriging

As a surrogate validation, cross validation is often used to validate both the variogram model and the method used in kriging. Isaaks & Srivastava (1989) recommend the use of cross validation *before* interpolation, to see which method (isotropic or anisotropic kriging) and model (e.g., spherical or linear?) will probably perform the best. Here cross or x validation is used afterwards, to check whether other possible models could have performed better[24]. Sometimes there were other models available that could fit the experimental variogram as good as — or even better than — the model used for interpolation. This was the case for both the 'total area' and 'only ski tracks' isotropic rainfall intensity variograms and the 'only ski tracks' isotropic log *K* variogram. The x validation results indicated that only for the 'total area' isotropic variogram a more

[24] In fact, all models were checked with cross validation afterwards. Fortunately, no model used for interpolation was rejected because of improper validation results. All Gaussian Z values were found to be close to zero and all F_z were found to be close to one, as is required (Burrough & McDonnell 1998; Isaaks & Srivastava 1989).

suitable variogram model might exist. When a Cressie variogram estimator[25] besides a spherical model would have been used, the γ would be minimized from –5.016 to –4.019 [mm / h] and the F_e would be lowered from 41.27 to 30.65 [mm / h]. Note that these values are not exactly the same as in Table 5.3, because only 83 points were used. Besides, cross validation involves a different procedure than real interpolation. This makes it hard to use x validation results in changing the variogram model (Isaaks & Srivastava 1989). The rainfall intensity variogram was therefore left unchanged and no new interpolation was carried out.

5.5 Discussion of the variograms and kriging results

As already noted, the variograms for the 'total area' case all have a rather short range in comparison to the 'only ski tracks' case. Nevertheless, variograms found in literature have a rather small range as well. For example, Vieira *et al.* (1981) found a more or less exponential variogram model[26] (r^2 = 0.858; n = 1280) with a practical range of about 70 to 80 m for infiltration rate measurements with point support. In a much smaller experiment (n = 30), a well fitted spherical variogram with a nugget variance of zero and a range of 52.5 m was found for a support of 2.2 × 2.2 m (Russo & Bresler 1982). Beven (1989) constructed a linear variogram model with a range of nearly 100 m for point infiltration data gathered by Sharma *et al.* (1980). Jetten *et al.* (1993) carried out a nested sampling on infiltration rate and sorptivity in French Guyana on an area similar in magnitude as the one investigated here. Their nested analysis of variance indicated that the range for the infiltration rate of the three tropical soils under their consideration probably lies around 100 to 200 m.

No variograms with ranges as long as those in the 'only ski tracks' case were found in literature. This is not surprising, as hydraulic conductivity is a very heterogeneous variable as compared to other soil variables (Wilding & Drees 1978, 1983; Section 4.2). For instance, variograms of conductivities in ground water typically have a range of only a few tens of centimetres in the *z* direction to a few metres in the *x* direction (Sudicky 1986, *op. cit.* Domenico & Schwartz 1990). Tietje (1993) used a range of 0.5 m (Gaussian model, practical range = 0.867 m) in Monte Carlo simulations of unsaturated infiltration, while De Roo & Riezebos (1992) found a pure nugget effect for infiltration values measured on 735 cm^2 supports, sampled within 4 m distance from each other.

The long distance variation dominates over the above quoted short distance variation in both the 'ski tracks only' and the 'total area' case. In the 'only ski tracks' case extra short distance variation was removed, since the pseudo cross-semivariance between natural area and ski track values for the different states of *K* can be described by a pure nugget model. In other words: there is no spatial correlation between ski tracks and natural areas at any scale, therefore separate variogram models describe the semivariance of each area more adequately. The short-range variation is incorporated in the nugget variance for both cases.

Still, it is remarkable that the high variability of hydraulic conductivity on adjacent soil plots or soils in the same soil grouping as can be found in literature (Babalola 1978; Mason *et al.* 1957; Reichardt *et al.* 1993) does not blur the long range correlation as found here by introducing a considerable nugget effect. An even higher variability (= semivariance) between conductivities at large lags than at very short lags may be

[25] This estimator yields a robust estimate of the semivariance, since it is less sensitive to outliers than the classical semivariance estimator (Hawkins & Cressie 1984, *op. cit.* Karssenberg 1996).

[26] Vieira *et al.* (1981) classified their model as spherical, despite the following hyperbolic semivariance formula: $\gamma(h) = h / (1.207 + 0.105 \cdot h)$.

possible, thereby ‘overruling’ the high short-range variability when the area is extensive enough (the study area is 10 to 15 km^2 large). If the short-range variance is considered to be important — as may be the case when one wants to use a model —, Monte Carlo simulation serves in the interpolation of a realistic, non-smoothed surface with a relatively more important short-range variability but at the same time incorporating the variogram when conditional simulation is used. This simulation procedure can be carried out as an alternative for kriging in later research, thereby delivering a surface that serves as an even better input for modelling.

The kriging interpolation results itself cannot be compared to literature values, because of different supports and measurement methods used. Anyhow, the main indicators of interpolation quality (F_e and CV_e) are found to be rather low and of a magnitude comparable to the F and CV of the sampled values in the ‘only ski tracks’ case. The F_e and CV_e for the ‘total area’ case are however rather large. Improvement of interpolation by application of stratified kriging and Universal kriging are shown to be impossible (Thonon 2000), and the models used in interpolation seem to be validated. Enlargement of the study area to include more variation is not necessary in the ‘total area’ case, since the estimation error due to finiteness of the area (g_f, Russo & Bresler (1982)) is only a few percent of the CV_e. For the ‘only ski tracks’ case, half of the CV_e consists of g_f because of the large ranges, but enlargement of the measurement area is nearly impossible. Therefore, the only way to improve the results of the interpolation is to add data points. With the aid of the F_e map, this can be done purposively (Russo & Bresler 1982): the higher F_e in a region, the more influence the addition of a data point in the respective region has.

Probably the most useful interpolation for modelling is the interpolation for ski tracks only with an isotropic variogram. This is because then the total covering of all ski pistes (which are the areas of interest) is assured, no useless anisotropic variograms are used in interpolation and the interpolation is (geo)statistically sound. Therefore, this `kcor2p_i.map` is used in the modelling as described in Chapter 7.

6 The effect of skiing on the hydrology

This chapter covers the effect of skiing (i.e., the use of the soil as a ski track instead of natural land such as forest or scrubland) on catchment hydrology. An important remark has to be made considering the available data: only the reference values are available. This is because of malfunctioning from the Sewer gauges, which were described in Section 3.4. These were used in the measurements of the headwaters that drain the (partly) piste covered catchments. See Fig. 6.1 for the location of the three catchments and Table 6.1 for the land cover data. The Keller gauges functioned well most of the time and these provided the discharge data for the 'forest' catchment. Only these reference data are presented here.

Two normalization methods have been used in order to compare the three catchments with each other in a later phase of research: the Unit Hydrograph (UH) and the Dimensionless Hydrograph (DH). Both methods are discussed later on. The chapter starts with the stage-discharge relationships for the three streams. The water height was measured manually when conducting the discharge measurements, therefore this relationship is available for all three headwaters.

Name	'forest stream'		Seebach		'Hochsölden stream'	
Land use class	Area [m²]	Area [%]	Area [m²]	Area [%]	Area [m²]	Area [%]
Bare	46,875	10.7	144,375	6.7	5625	1.3
Grass, piste, moss	161,875	36.8	1,433,125	66.6	204,375	46.1
Shrubs and grass	96,875	22.0	536,250	24.9	233,125	52.6
Scrubland	14,375	3.3	0	0	0	0
Woodland	120,000	27.3	37,500	1.7	0	0
Total	440,000	100.1	2,150,750	99.9	443,125	100

Table 6.1. Absolute area and percentage of area per land cover class in the three gauged catchments. Note that the 'forest' catchment is for only slightly more than one fourth covered by woodland.

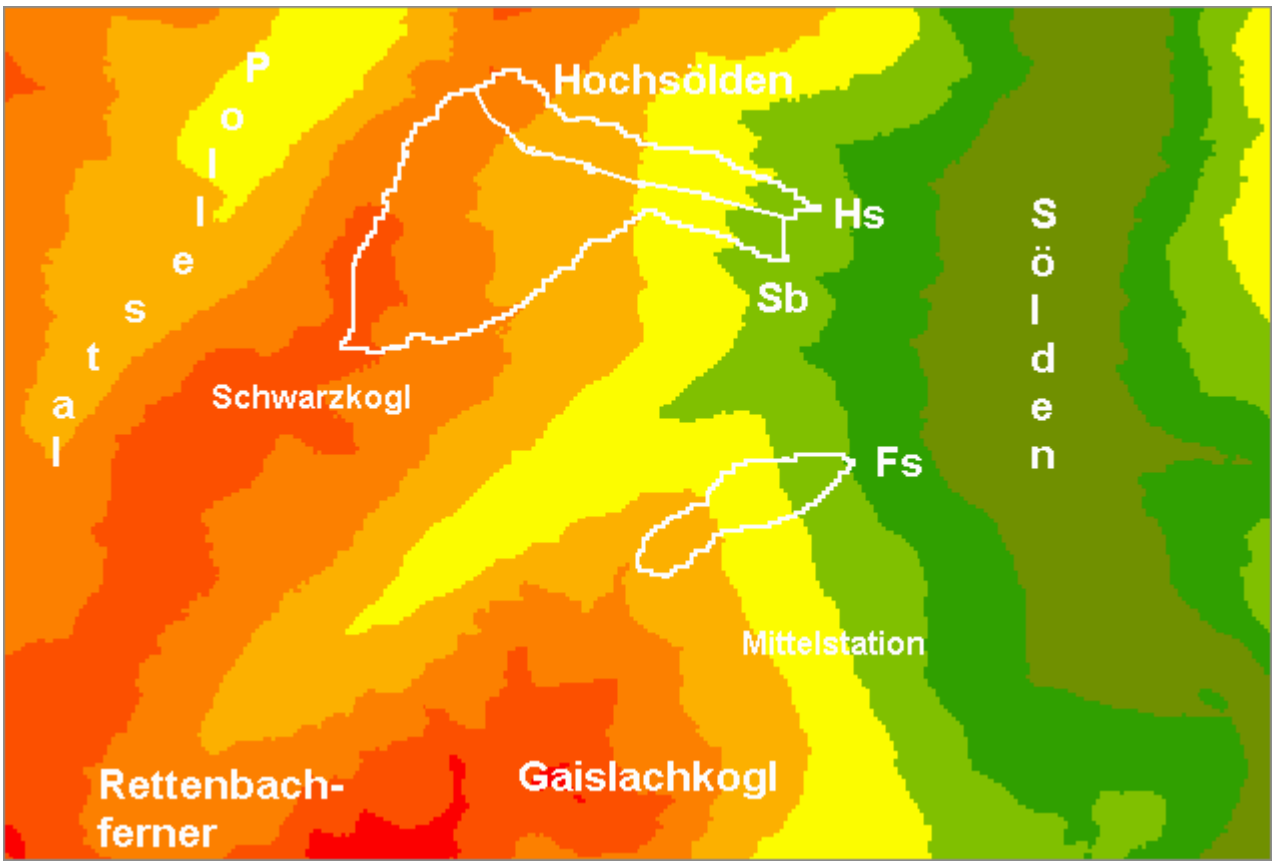

Figure 6.1. Location of the three gauged catchments and the main features in the area. Hs = 'Hochsölden stream'; Sb = Seebach; Fs = 'forest stream'. Approximate scale 1 : 50,000.

6.1 Stage-discharge relationships

A stage-discharge relationship (also called a rating curve or Q-h relation) is the quantitative relation between a water height and discharge for a certain channel. This relation can be in the form of a curve, an equation or a table. Here only the first two will be provided. The relationship is widely used to transfer water height measurements to discharge data, because water height itself is rather useless in a hydrological sense (except for flooding problems). Discharge is needed to calculate the UH and DH for a stream as well as the time to peak, time to concentration etcetera.

A Q-h relation can be constructed with the aid of the discharge measurements (Section 3.5): Q is provided by means of Eq. 3.6, h is measured directly with a ruler. When these two quantities are put in a graph, a stage-discharge relationship emerges. Most of the time, this relationship is of an exponential, power or logarithmic form. For each stream, the discharge was measured six times. A rule of thumb says that five is the absolute minimum amount of points to get a reliable rating curve (Hendriks, *pers. comm.*). The graphs are depicted in Figs. 6.2, 6.3 and 6.4, with the rating curve for the forest stream in Fig. 6.2.

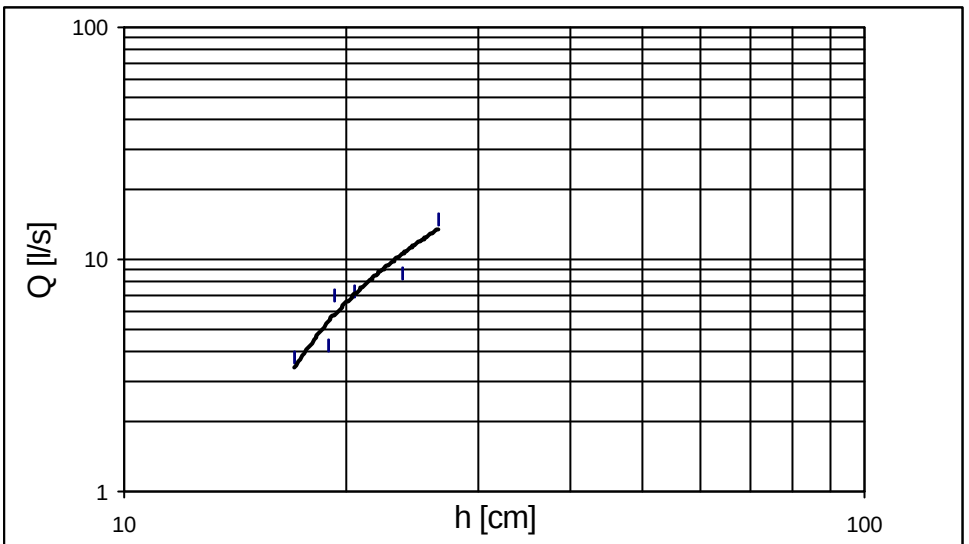

Figure 6.2. Stage-discharge relationship for the 'forest stream'. See Eq. 6.1 for the relation in the form of formulae.

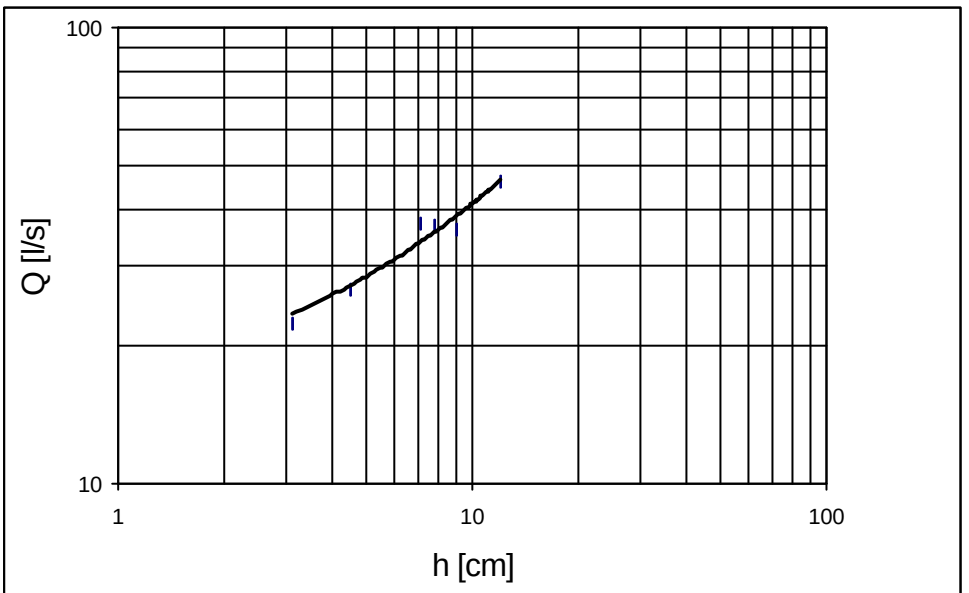

Fig. 6.3. Stage discharge relationship for the Seebach. See Eq. 6.2 for the relation in the form of formulae.

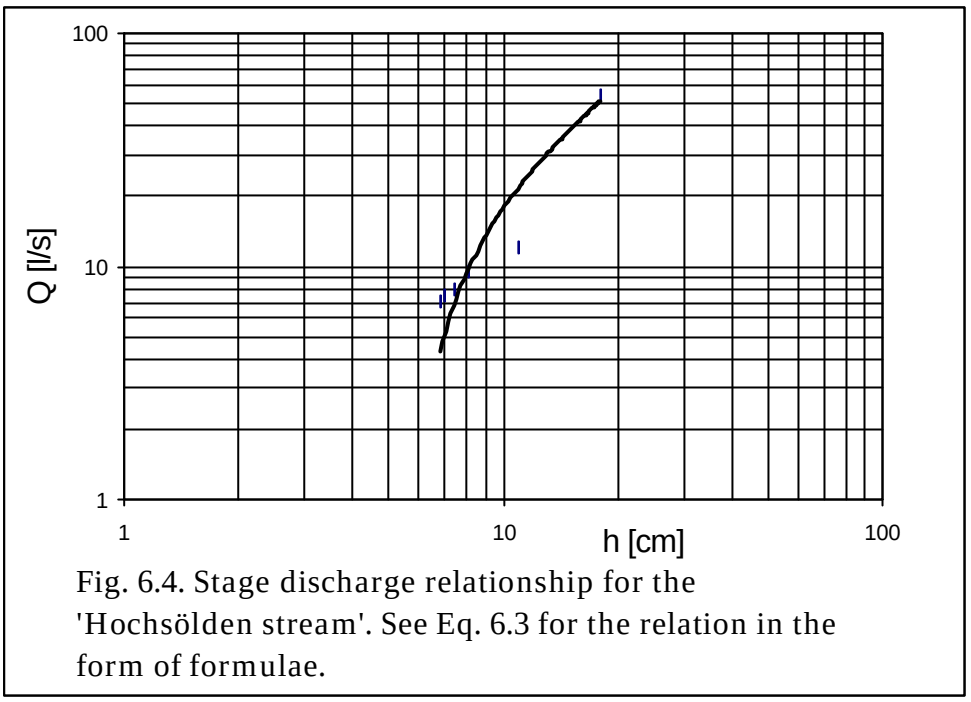

Fig. 6.4. Stage discharge relationship for the 'Hochsölden stream'. See Eq. 6.3 for the relation in the form of formulae.

The formulas of the rating curves are as follows:

- for the forest stream:

$$\log Q = 1.5083 \cdot \log h - 14.577 \ (r^2 = 0.897), \qquad \text{(Eq. 6.1a)}$$

$$Q = 0.0013 \cdot h^{2.8389} \ (r^2 = 0.885) \text{ or} \qquad \text{(Eq. 6.1b)}$$

$$Q = 0.4395 \cdot e^{0.131 \cdot h} \ (r2 = 0.880); \qquad \text{(Eq. 6.1c)}$$

- for the Seebach:

$$\log Q = 2.5434 \cdot \log h - 15.71 \ (r^2 = 0.937), \qquad \text{(Eq. 6.2a)}$$

$$Q = 12.46 \cdot h^{2.5195} \ (r^2 = 0.962) \text{ or} \qquad \text{(Eq. 6.2b)}$$

$$Q = 18.895 \cdot e^{0.0779 \cdot h} \ (r^2 = 0.911); \qquad \text{(Eq. 6.2c)}$$

- and for the stream near Hochsölden:

$$\log Q = 4.1843 \cdot \log h - 24.141 \ (r^2 = 0.936), \qquad \text{(Eq. 6.3a)}$$

$$Q = 0.1388 \cdot h^{2.0126} \ (r^2 = 0.951) \text{ or} \qquad \text{(Eq. 6.3b)}$$

$$Q = 2.0939 \cdot e^{0.1779 \cdot h} \ (r^2 = 0.986); \qquad \text{(Eq. 6.3c)}$$

with: Q = discharge [l/s]; h = water height [cm].

Note that all determination coefficients (r^2's) are about 0.9 or higher. This indicates that the fitting of the rating equations and curves was done adequately. However, for the third stream (close to Hochsölden), the uppermost point in the curve (Fig. 6.4) can be considered to be an outlier when the present data are examined. This point determines the rating curve and equation largely on its own. When more data would be present, a proper decision could be made to include or exclude it from the curve fitting procedure. Now it was included, but there is no information available about the error that is made by this inclusion.

Eq. 6.1b was used in the transition from stage to discharge for the forest stream, because it passes through the origin, which is the most feasible: when the water level is zero, no discharge is expected. The other two rating equations (Eqs. 6.1a & c) do not pass exactly through the origin. This also holds for Eqs. 6.2 and 6.3: Eqs. 6.2b and 6.3b are thought to be the more sound ones. These are not used here because hardly any continuous water level measurements for the Seebach and Hochsölden stream are available.

6.2 Discharge for the 'forest stream' and precipitation data

With the Q-h relation as indicated by Eq. 6.1b, it was possible to convert the water height data (as measured with the Keller pressure transducers) to discharge data. The discharge data was measured from 10 07 1999 to 29 08 1999, with data from 15 07 to 20 07 and from 06 08 to 15 08 lacking because of reading-out errors. Furthermore, the data from 22 07 to 27 07 are not corrected for air pressure because of a reading-out error of the barometric Keller. These uncorrected data were not used in further data processing.

The precipitation and discharge data for the month July are presented in Fig. 6.5, whilst the data on August are presented in Fig. 6.6. It can be noted from these graphs that the base flow diminishes very slowly from about 4 l/s at the beginning of July to some 3 l/s at the end of August. This is rather unexpected, because the summer is the rainy season in the Ötztaler Alps. The daily precipitation data from the non-recording gauge in Sölden are shown in Fig. 6.7. These however indicate that the summer in 1999 is rather dry. In two months, about 150 mm of precipitation fell in Sölden. This is normally almost 200 mm (in July and August, according to Fig. 2.12). The slow recession of the base flow may thus be explained by a lower than normal precipitation.

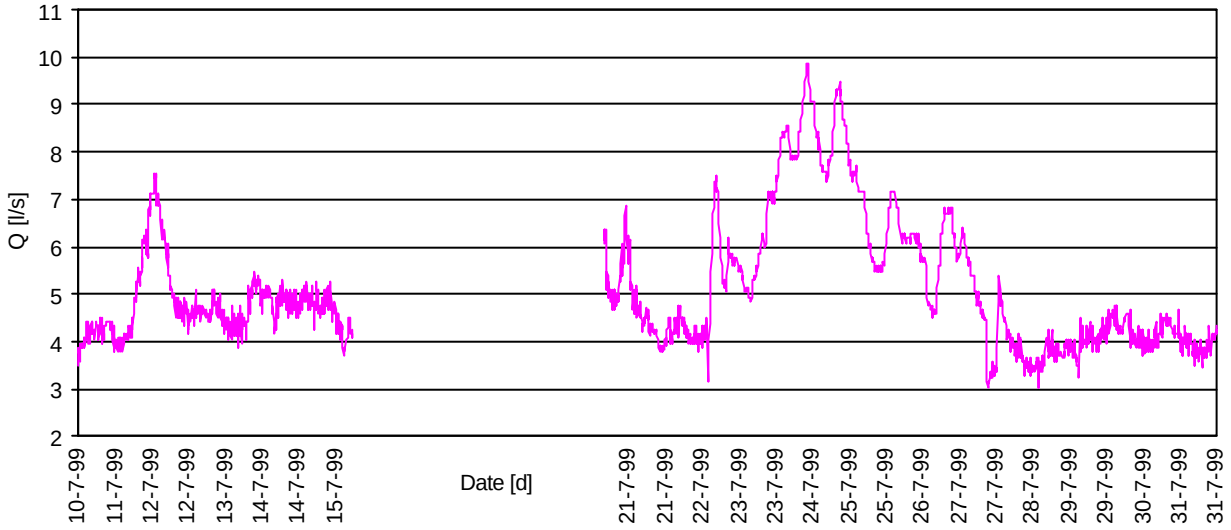

FIgure 6.5. Discharge of the forest stream in July 1999. Note the loss of data between 15-07 and 20-07.

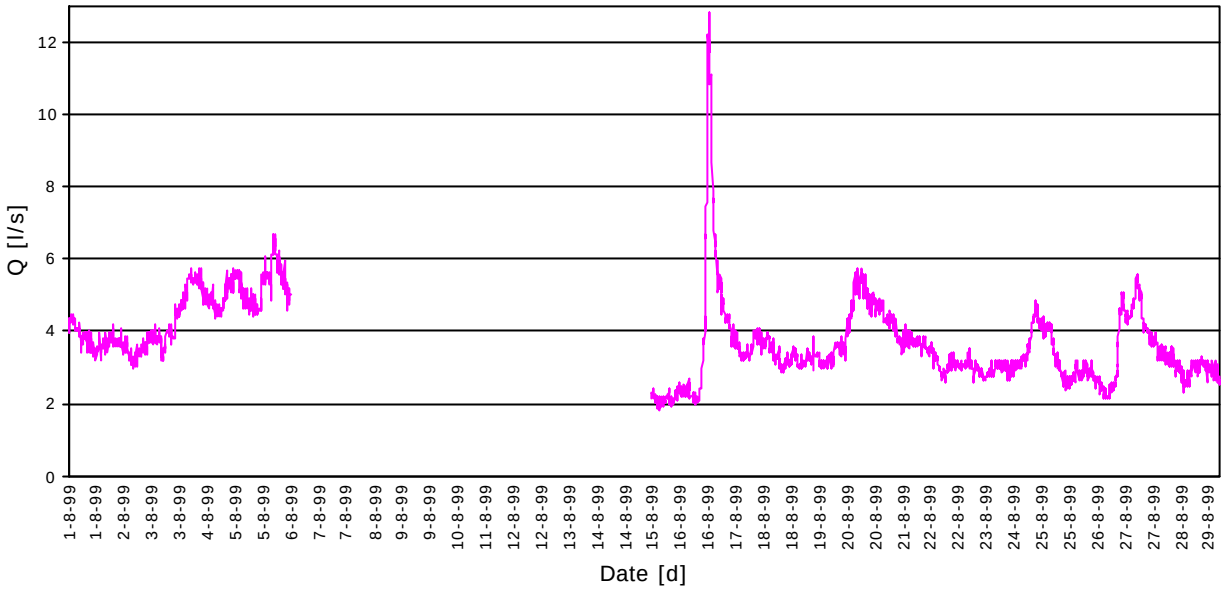

Figure 6.6 Discharge of the forest stream in August 1999. Note the loss of data between 07-08 and 15-08.

The data in Fig. 6.7 are only valid for the lower regions of the Ötztal. At the upper rims of the valley, there is a larger amount of precipitation. See Table 6.2 for average daily precipitation values on five locations. According to the general trend in the data, the amount of precipitation increases with height, which is normal for a mountainous area. Obviously, the values for the Seebach gauges (close to the water level measurement point in the stream) are too low. This is caused by the location of the gauges, which was chosen too close to the surrounding trees in the valley. These

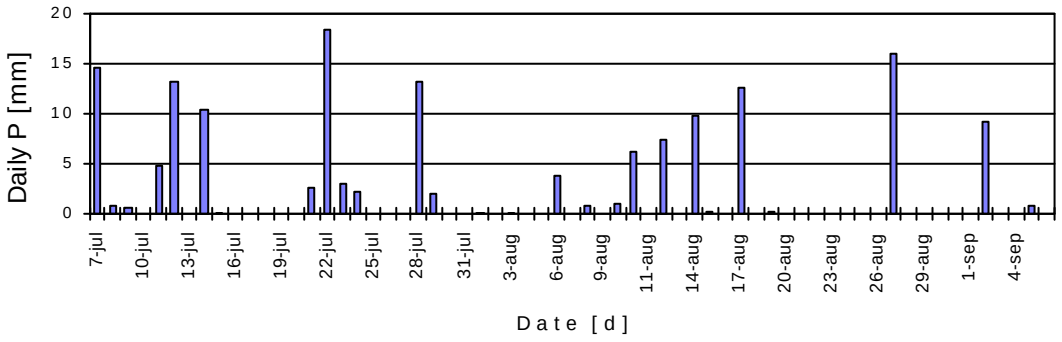

Figure 6.7. Precipitation in Sölden (Ötztal) during July, August and the beginning of September in 1999.

values were not used in the analyses.

Another remark can be made about the large difference between the non-recording and recording rain gauges: the latter recorded about 18 % (in the case of the Seebach) to 83 % (in the case of Hochsölden) more precipitation than the former. The tipping bucket meter works with a mechanical device that may also be set in motion by wind action or even insects, which may induce extra tippings and thus a higher than expected amount of precipitation. Moreover, the tipping buckets are lower than the cumulative rain gauges and therefore less sensitive to turbulence around the rim,

which causes the catch of rain to be higher than the cumulative rain gauges. Because of these reasons, the values for Hochsölden were corrected downwards. This was done by multiplying by the ratio between 3.17 and 5.81 (values in Table 6.2), which is 0.555. These corrected data were used in further processing: the delineation of UH's and DH's.

Sevruk (1996), however, states that tipping buckets in general record too little precipitation instead of too much, as was found here. It was found that in the summer half year, the tipping bucket gauge that was used in the experiment measured 11 % less precipitation than a Hellmann non-recording rain gauge that was 1.5 m next to it. The Hellmann gauge also measured more rain days than the non-recording gauge. The wind speed, which also influences the catch deficit, was 1.5 to 2 m/s on average. The average wind speed in the fieldwork area during the period from 26 07 to 19 08 was about 1.4 m/s. This value was measured on the windy ski piste of Rotkogl and is representative for the rain gauges at Hochsölden. Therefore, the wind speeds are comparable. Notwithstanding this contradicting difference as found by Sevruk (1996), the tipping-bucket data were still reduced with the factor 0.555. This was done because the non-recording data show a lower than average amount of rainfall in the summer months, as was indicated in the first paragraphs in this section, and are therefore believed to provide more reliable data than the tipping bucket rain gauges in this case.

Station name	Height [m. asl]	P_{avg} non-recording gauge [mm/d]	P_{avg} recording gauge [mm/d]
Sölden	1368	2.45	
Seebach *	2130	2.25	2.65
Hochsölden	2140	3.17	5.81
Mittelstation	2300	3.34	
Rotkogl	2350	3.95	

Table 6.2. Average daily precipitation for five different locations in the fieldwork area. A non-recording gauge denotes a cumulative gauge, a recording gauge a tipping bucket. *) These values are too low due to nearby trees shielding off the rain.

Foster (1948) indicates that wind may induce a precipitation catch that is too low. Foster (1948) presents data on the percentage deficit of standard US rain gauges that is caused by turbulence. This turbulence is positively correlated with wind speed and causes the rain drops to be blown over the funnel orifice. The deficit increases exponentially: for a wind speed of 2 m/s, 4 % of the rain is undetected, with 8 m/s 29 % is not caught and with 16 m/s even 71 % of the rain is not registered. If it is assumed that these values also hold for the here used rain gauges, an estimation can be made of the percentage error due to wind influence. When the relationship of Foster (1948) is used, an underestimation of rainfall of 2.6 % on average emerges. This is probably within the range of the measuring error and can therefore be considered negligible.

6.3 Unit Hydrographs for the 'forest stream'

Sherman (1932) invented the concept of the Unit Hydrograph. A Unit Hydrograph, UH for short, is defined as: the discharge curve (Q_d) caused by a spatially and temporally uniform unit amount of effective rain (P_{eff}) in a unit amount of time. This unit amount of effective rain (snow does not give a UH, because it is stored on the ground) can be chosen to be 1 mm or 1 cm, the unit of time 1 or more hours. P_{eff} is defined as the amount of rain that runs off directly (and as such does not contribute to ground water

storage or evapotranspiration). The concept of the here used conventional UH[27] uses several underlying assumptions, which can be summarized in one principal assumption: there is a linear relation between P_{eff} and Q_d and this relation does not change in time, neither does the spatial distribution of P_{eff}.

A UH is constructed in the following way (Chapman 1996a):

1. Separation of the base flow (Q_b) to obtain the direct runoff hydrograph (Q_d);
2. Processing of the hyetograph of catchment rainfall (P);
3. Application of a loss model to P to obtain P_{eff}, which by definition has the same volume as Q_d.
4. Data processing in order to get a UH.

The different steps were carried out in the following ways:

Ad 1. It was noticed that the onset of rain always resulted in an immediate but that it is hard to exactly determine the onset of increase in discharge (Q). This is because channel precipitation directly leads to Q_d. It was therefore decided that the time on which it starts to rain denotes the first point of the line that separates Q_b and Q_d. This method has the advantage of being fully objective. The decision where to put the start of rise of Q is highly subjective because the increase in Q at the onset of the rain is hard to detect.

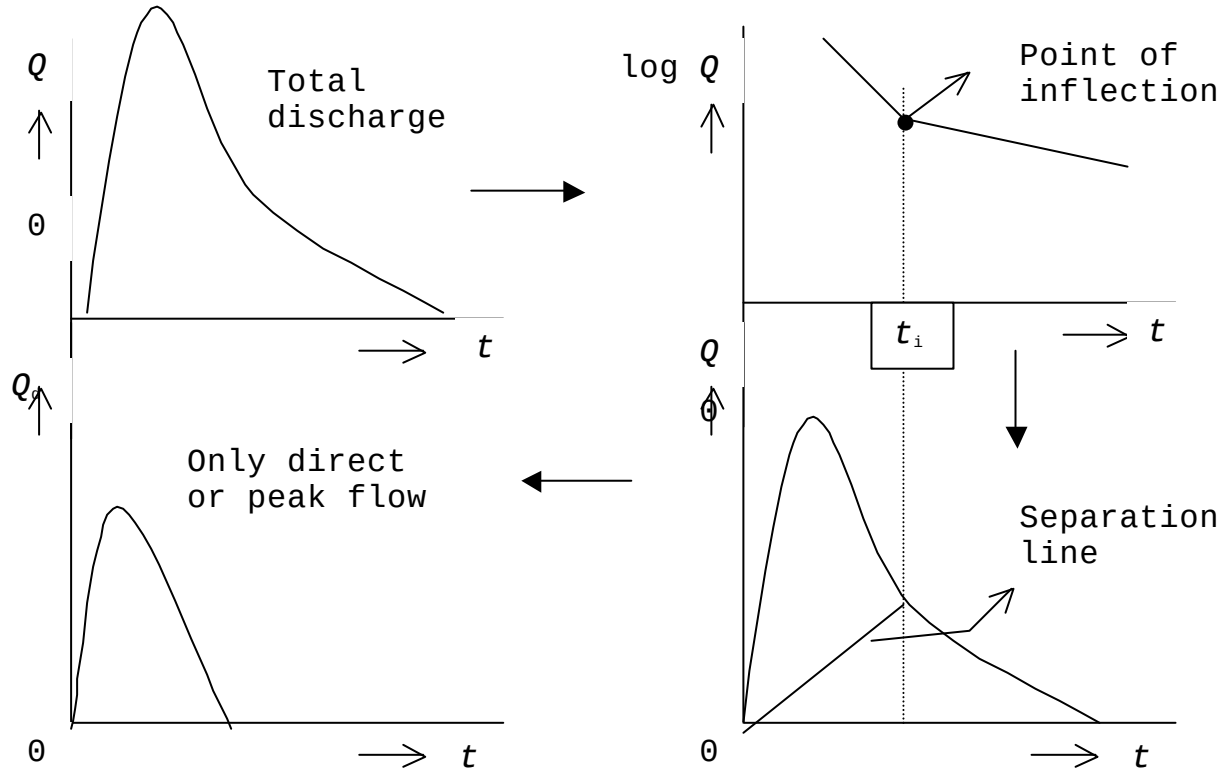

Figure 6.8. Procedure to find the amount of direct discharge in four steps.

It was chosen to locate the end of the separation line on the time of the knick point of the log Q time curve of the falling limb of the hydrograph (see also Fig. 6.8). This is a well-known and widely applied method, but has the disadvantage of being subjective, because it is sometimes difficult to delimit the knick point, especially when the falling limb does not have a logarithmic recession but a more linear one.

[27] In literature, there also exists a common UH (Chapman 1996a, 1996b) and an instantaneous UH (IUH) (Rodriguez-Iturbe & Valdes 1979; Gupta *et al.* 1980; Corradini *et al.* 1986).

When these two points are found, a straight line is constructed that connects the two points. All discharge above the line denotes Q_d, all discharge below the line denotes Q_b. Q_b is subtracted from Q to get Q_d, which is used in the subsequent steps.

Ad 2. This part consists of the multiplication of the 10-minute tipping bucket data by 0.555. No other data manipulations were carried out.

Ad 3. In most cases, there was no loss model applied to convert from P to P_{eff}, because the ASM and *K* of the forest soil are rather constant in time. The forest soil was observed to remain humid during the whole fieldwork period. Only in some cases, a simple empirical loss model (initial abstraction) was used when a relatively dry period proceeded the discharge peak and the rain. Instead, this conversion was done with the aid of the runoff coefficient. This coefficient denotes the fraction of P that runs off as Q_d; the remaining rain is lost by infiltration, evapotranspiration etcetera:

$$RC = \frac{Q_d}{P} \Rightarrow P_{eff} = RC \cdot P \qquad \text{(Eq. 6.4)}$$

with: *RC* = runoff coefficient [ ]. In other words, this is by definition the fraction P_{eff} within P. When every 10-minute data value is multiplied by this runoff coefficient, which lies between 0 and 1, P_{eff} results. This value is used in the next step.

Ad 4. When the UH has been finished, it is checked whether the amount of Q_d in the UH sums up to the unit amount of rain (1 mm) that was used in the construction. A UH with a too large discrepancy (above 30 %) is rejected.

The above-mentioned procedure was used to construct a UH for each clear runoff peak that was present in the data set (see Figs. 6.5 & 6.6). It can be seen in Fig. 6.9 that the hydrographs, which in theory have to be all the same, are in reality quite different. Not only the peak discharges differ, but also the time bases. This is a well-know disadvantage of the conventional UH method and is mainly determined by the rainfall duration: the longer the rainfall, the longer the time base. Besides, the determination of the initial abstraction is rather subjective. Since the first rainfall is a very important parameter in the calculation of the UH with the here used method, this influences the outcome of the analysis to a great extent.

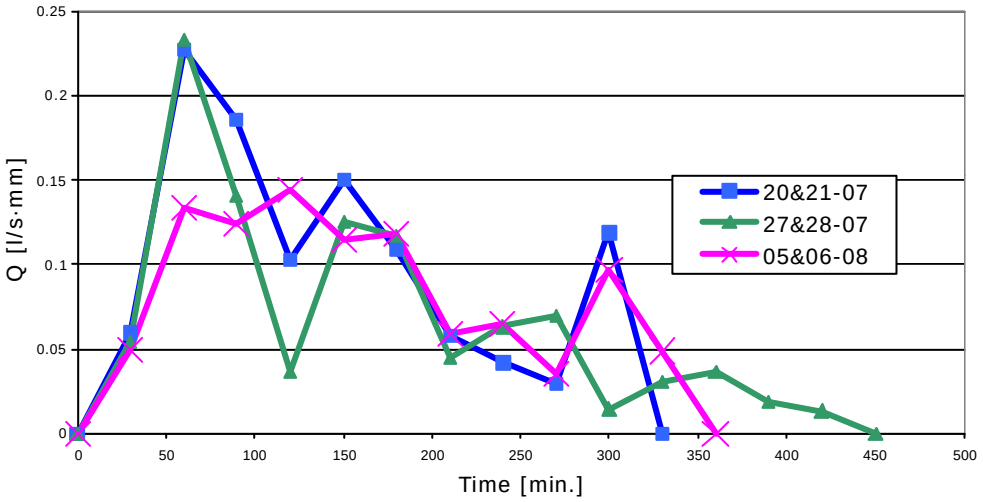

Figure 6.9a. UH's with a unit time of half an hour. Note the sharp rise at the beginning and the slow recession afterwards.

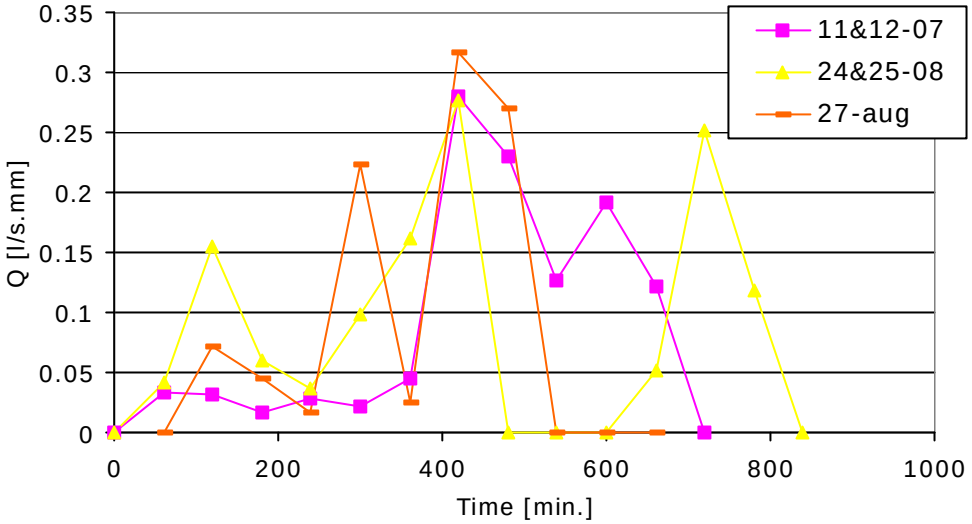

Figure 6.9b. UH's with unit time of one hour. Note the large fluctuations in discharge with respect to time and other UH's (such as in Fig. 6.9a).

6.4 Dimensionless Hydrographs for the 'forest stream'

Langbein (1940) originally developed the concept of the Dimensionless Hydrograph. A Dimensionless Hydrograph (DH) is defined as: a dimensionless discharge curve that shows the percentage of total direct runoff (Q_d) per time step as function of time that is divided by centroid lag time (*L*). *L* is defined by Leopold (1991) as the time between the center of mass of rainfall (P) and the center of mass of direct runoff (Q_d). The center of mass can be defined as the time at which half of a certain total amount (e.g., rain or direct runoff) is reached. The DH assumes the same as the UH: a linear association between effective rainfall and runoff.

The delineation of the DH proceeds in the following way:

1. Separate Q_d from Q_b;
2. Calculate the center of mass for Q_d and P;
3. Calculate *L* and divide the time base by *L*;
4. Split the dimensionless time base in time steps;
5. Calculate the fraction or percentage of Q_d that runs off per dimensionless time step.

Here, this procedure was carried out as follows:

Ad 1. The same procedure as mentioned in Section 6.3 (ad 1) was used.

Ad 2. The cumulative amount of rain per time step of 10 minutes was set out against the total rain duration. Then this cumulative rain amount was divided by the total amount of rain to get the fraction of rain fallen in a certain time interval. The time where half of the rain had fallen was read off and noted. The same was done for direct runoff. See Fig. 6.10 for a graphical example.

Ad 3. *L* can easily be calculated by determining the difference between the centers of mass for rain and direct runoff. The time in minutes from the onset of rain is divided by this period *L* in minutes and this renders dimensionless time. This dimensionless time is expressed as a percentage of centroid lag time.

Ad 4. The dimensionless time is divided in parts of 20 % *L*.

Ad 5. The length of a dimensionless time step in minutes is calculated. For each time step, the amount of runoff is determined. This amount is divided by the total amount of Q_d and expressed as a fraction. It is checked whether the sum of fractions is close to one. This was always found to be the case.

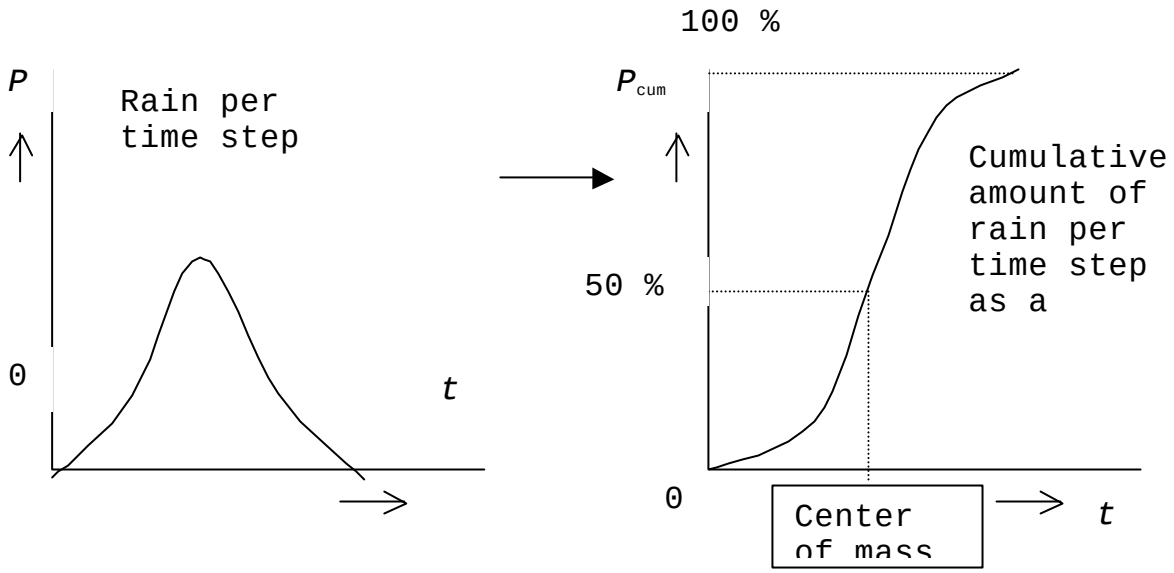

Figure 6.10. Graphical explanation of the delimitation of the center of mass for rain. The same procedure applies to direct runoff.

For every discharge peak for which a UH was constructed, a DH was constructed as well. The Dimensionless Hydrographs are depicted in Fig. 6.11. Because they have a different time axis, they cannot be depicted in the same figure with their counterpart UH.

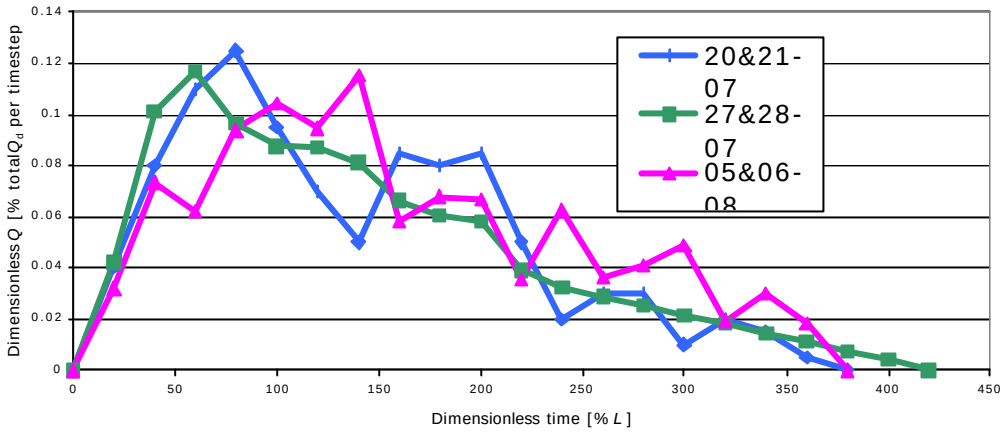

Figure 6.11a. DH's of the same rainstorms as in Fig. 6.9a. Note the large amount of equality in both base time and recession between the three DH's and the lack of this for the UH's in Fig. 6.9a.

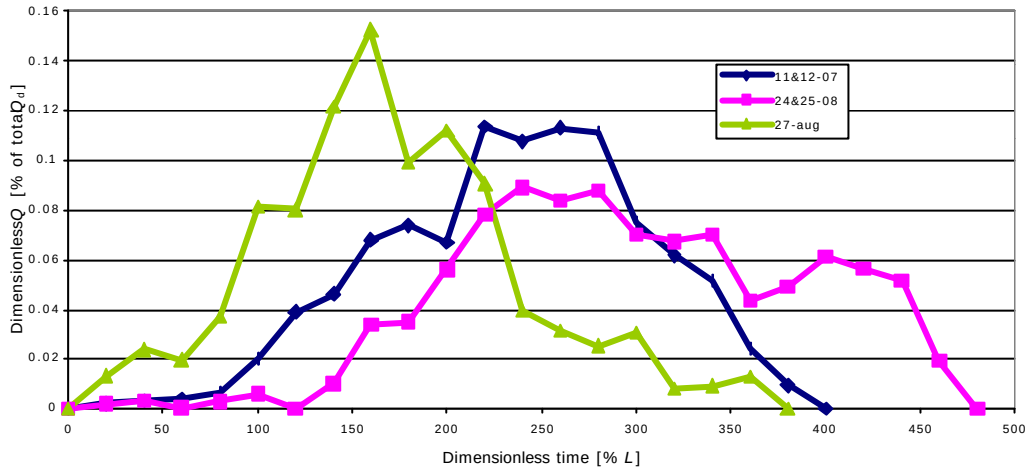

Figure 6.11b. DH's of the rainstorms that were added to Fig. 6.9a to get Fig. 6.9b. The form equality is less for these three DH's, but still larger than for the UH's for the same rainstorms.

Comparison of UH's with DH's

It can be noted immediately that the DH's better resemble a discharge peak than the UH's (cf. Figs. 6.9a & 6.11a). Furthermore, the DH's hardly exhibit intermittent rising and falling of the curves. A third difference that can easily be spotted is the closer resemblance between the time bases for the distinct DH's than the UH's: notably in Fig. 6.9b, it can be seen that the time base differs largely between the different UH's.

A difference that cannot be noticed from the figures themselves is the amount of time used to construct the Hydrographs. This labour time is far less for the DH's than for the UH's. The method that is normally used to construct UH's is far more complicated and time-consuming than for the DH's. Especially the spreadsheet operations involved in UH delineation are laborious.

A second difference in the concepts themselves is the ability to predict flood waves with a method: this is only possible with Unit Hydrographs and not with Dimensionless Hydrographs. This is inherent to the determination of both Hydrographs: an UH still has dimensions and, when the ordinates are multiplied with a certain amount of rain, the discharge can be predicted. A DH is, however, dimensionless and can therefore not be used for prediction. It is however not needed in this research to predict peak discharges. It is only needed to compare the three catchments for runoff peaks and relate the size and form of these (manipulated) peaks

to land use / skiing. This can more easily be done with DH's than UH's. Leopold (1991) gives an example of a method to calculate the new DH when land use is changed.

It can be deduced from the above that the concept of the Dimensionless Hydrograph method has more pro's than contra's when compared to the Unit Hydrograph method, at least in this research and with these research questions. It is therefore advised to use the concept of the DH instead of the UH concept in order to compare the effect of skiing on the three catchments when enough discharge data are gathered.

6.5 Basic hydrological parameters for the 'forest stream'

With the aid of the basic data, some hydrological parameters can be calculated, such as *L*, time to peak (t_p, time from beginning of rainfall to the peak discharge), time base (t_b, duration of direct runoff) and RC (runoff coefficient, that part of *P* that becomes Q_d). These are summarized in Table 6.3, which covers the same discharge peaks from which UH's and DH's were determined. A parameter such as " is rather stable, but a parameter such as *L* is rather dependent upon the amount of rain, because the rain has a profound influence on the parameter; the same holds for t_p and t_b. So, the lower four measures in the table are relatively useless to characterize a stream because they exhibit a large amount of variation.

Rain storm	11 / 12 07	20 / 21 07	27 / 28 07	05 / 06 08	24 / 25 08	27 08	16 / 17 08
P [mm]	18.8	1.4	8.1	3.4	10.2	13.3	15.7
D [h:m] *	15:40	0:50	1:40 ***	2:20	11:10	12:30	6:10
i_{max} [mm / h]	4.0	2.6	13.3	3.3	2.0	6.0	6.7
i_{avg} [mm / h]	1.2	1.7	4.0 ***	2.1 ***	1.4 ***	1.7 ***	2.6 ***
RC [%]	1.42	1.80	0.84	1.67	1.61	1.94	3.00
L [h:m]	6:06	1:23	2:05	1:59	4:53	4:25	3:44
$t_{p,W}$ [h:m] **	15:36	0:50	1:13	1:43	6:12	6:22	6:23
$t_{p,L}$ [h:m] **	7:21	0:28	0:40	1:16	3:04	3:42	2:58
t_b	23:40	5:00	8:40	7:20	10:30	21:50	13:10

Table 6.3. Some basic precipitation and discharge parameters for the forest stream. *) with pauses included; **) $t_{p,W}$: t_p according to definition of Wanielista (1990); $t_{p,L}$: t_p according to definition of Leopold (1991); ***) without preceding rain or pauses of rain included.

In general, it can be stated that RC is the most important variable to characterize a stream. For the forest stream, it varies between about 1 and 3 percent, which is very low. The soils exhibit moderately to high infiltration capacities[28] and will produce hardly any Hortonian overland flow. The overland flow may in most cases be saturation overland flow that originates from along the direct borders of the channel.

Another important component in the direct runoff is channel precipitation, i.e. the precipitation that directly falls on the channel area. However, the channel is approximately 1.5 km in length and 1 m in width (leading to a channel area of an estimated 1500 m^2) and the catchment size is about 440.000 m^2, so channel precipitation can only explain 0.35 percent point of the 1 to 3 % runoff due to rain. It is estimated here that for the forest stream at maximum half of the direct runoff may be due to channel precipitation. The other half may be caused by either overland flow or high-velocity shallow subsurface flow through the litter layer or uppermost soil layer from

[28] Regrettably, only one rainfall simulation was carried out in woodland. The K_{cor} calculated out of this measurement is 0.33 m / d, while the original uncorrected K was 5.26 m / d due to the high applied rainfall intensity of over 200 mm / h. The drainage was subsurface flow.

areas close to the channel. This subsurface flow was often observed to occur underneath shrubs, forest and dense grass during the rainfall simulations

The hypothesis that half of the storm runoff is caused by rapid shallow throughflow can be checked using literature values for overland flow velocities and measured values for shallow subsurface flow velocities. It is most probable that the mechanism with the highest average velocities is responsible for the runoff peak.

Data on overland flow velocities under field conditions are scarce. The most well known values are provided by Pearce (1976), who indicates velocities from 0.15 to 1.5 cm / s (130 to 1300 m / d), and Emmet (1970). Emmet (1970) converted laboratory values to field values and found velocities of about 6.1 cm / s (5270 m / d) for bare soil with only tussocks.

At seven points, the depth of the throughflow was noted during the rainfall simulations. With this quantity, the width of the rainfall simulator, the amount of drainage, the slope angle and Darcy's Law, the velocity of shallow subsurface flow can be calculated easily with the following formula:

$$v = \frac{Q}{A} = K_{lat} \cdot \sin\alpha \Leftrightarrow K_{lat} = \frac{v}{\sin\alpha} = \frac{Q}{A \cdot \sin\alpha}; \qquad \text{(Eq. 6.5a)}$$

$$A = l \cdot h \qquad \text{(Eq. 6.5b)}$$

with: v = discharge [m / d]; Q = discharge [m³ / d]; K_{lat} = lateral hydraulic conductivity [m / d]; A = seepage area [m²]; " = slope [°]; l = width of rainfall simulator = 0.24 [m]; h = depth of throughflow [m].

The noted depths indicate only shallow subsurface flow of at most 4 cm deep below ground level. Together with the discharge data from the rainfall simulations, this resulted in the values of Table 6.4. The small amount of variation in the values can almost instantly be noted; only point rs108 can be considered as an outlier. This may be due to the shrub vegetation: the shrub roots lead to a higher lateral conductivity than the small grass roots, in this case three times as high. It becomes however clear that, even if the lateral conductivity under forest is again three times higher than K_{lat} under shrubs, the overland flow velocities can reach far higher values. Therefore, it is plausible that the part in the storm runoff that is not caused by channel precipitation is caused by infiltration excess or saturation overland flow, and not by shallow subsurface flow. The throughflow will probably come to runoff during a later phase of the recession of the peak, maybe after the inflection point.

Number	rs107	rs108	rs110	rs4a	rs5a	rs7a	rs8a
Texture	silty loam	silty loam	loamy sand	humic loam	humic loam	sandy loam	loam
Vegetation	mainly grass	grass & shrubs	moss & grass	grass	grass	grass & moss	grass
h [cm]	3	1	2	4	3	3	3.5
K [m / d]	11.1	36.5	12.8	13.5	16.6	18.0	11.6

Table 6.4. Values for lateral hydraulic conductivities in cases of throughflow for seven points in the fieldwork area. See Fig. 4.1 for the locations of the three points that do not end on a.

The relatively low lateral conductivities furthermore show that the pistes — which have a higher chance of fast overland flow than non-pistes — are indeed affected, in the sense that they increase the direct runoff and peak discharges for the headwaters, which was already hypothesized in Section 4.4. This is supported by the fact that the highest discharge in the 'forest' catchment was only about 15 l / s (see Figs. 6.2 & 6.5)

and in the 'Hochsölden' catchment, which is nearly equally large but has a larger percentage of ski area and less woodland, more than 50 l/s (Fig. 6.4). The mean altitude for the forest stream is 2173 m a.s.l. with a maximum at 2507 m, while the mean altitude for the Hochsölden stream equals 2264 m and its highest point reaches 2780 m. Part of this difference can thus be explained by the fact that the stream near Hochsölden originates at a higher altitude and therefore may receive more rain or rain with higher intensities, but it is not thought that this will explain the total difference found.

6.6 Runoff coefficients for overland flow

In Section 6.5, it was mentioned that the RC is one of the most important variables in catchment hydrology. Nevertheless, the variable can also be calculated for the runoff from the rainfall simulations. Because the RC is a standardized, dimensionless variable, it can be used for comparison with literature values. Besides, the RC has a profound influence on the peak discharge of the headwaters: a high RC causes a high amount of direct runoff.

It is obvious that the RC is influenced by K and i: the higher K, the lower RC; and the higher i, the higher RC. Because K is also influenced by rainfall intensity (see also Section 4.2), rainfall intensity has to be set to one standard value, in order to be able to compare values. In literature, the most often used rainfall intensity is 100 mm/h for one hour — which is clearly very high — so this value is used here as well. Because of the interdependency RC K i, both t_p (time to runoff) and K have to be recalculated for an intensity of 100 mm/h. After this, RC can be calculated from K and i. This proceeds through the following equations (with K recalculated as K_{RC} using Eq. 4.1 with 100 [mm/h] instead of 15), the principle is illustrated in Fig. 6.12:

$$t_{p,RC} \cdot 100 = t_p \cdot i \Leftrightarrow t_{p,RC} = t_p \cdot \frac{i}{100} \qquad \text{(Eq. 6.6)}$$

$$F = \left(2.78 \cdot 10^{-5} \cdot t_{p,RC}\right) + \left(3600 - t_{p,RC}\right) \cdot \frac{K_{RC}}{86400} \qquad \text{(Eq. 6.7)}$$

$$RC = \left(\frac{0.1 - F}{0.1}\right) \cdot 100 \qquad \text{(Eq. 6.8)}$$

with: $t_{p,RC}$ = time to runoff when an intensity of 100 mm/h would be used [s]; 100 = rainfall intensity [mm/h]; t_p = time to runoff as measured with rainfall simulations [s]; F = cumulative infiltration after 1 hour of rain with an intensity of 100 mm/h [m]; $2.78 \cdot 10^{-5}$ = 100 mm/h recalculated to m/s [m/s]; K_{RC} = hydraulic conductivity for an intensity of 100 mm/h [m/d]; 86400 = conversion factor to convert from m/d to m/s [s/d]; RC = runoff coefficient [%]; 0.1 = total amount of rain in one hour when rained with 100 mm/h [m].

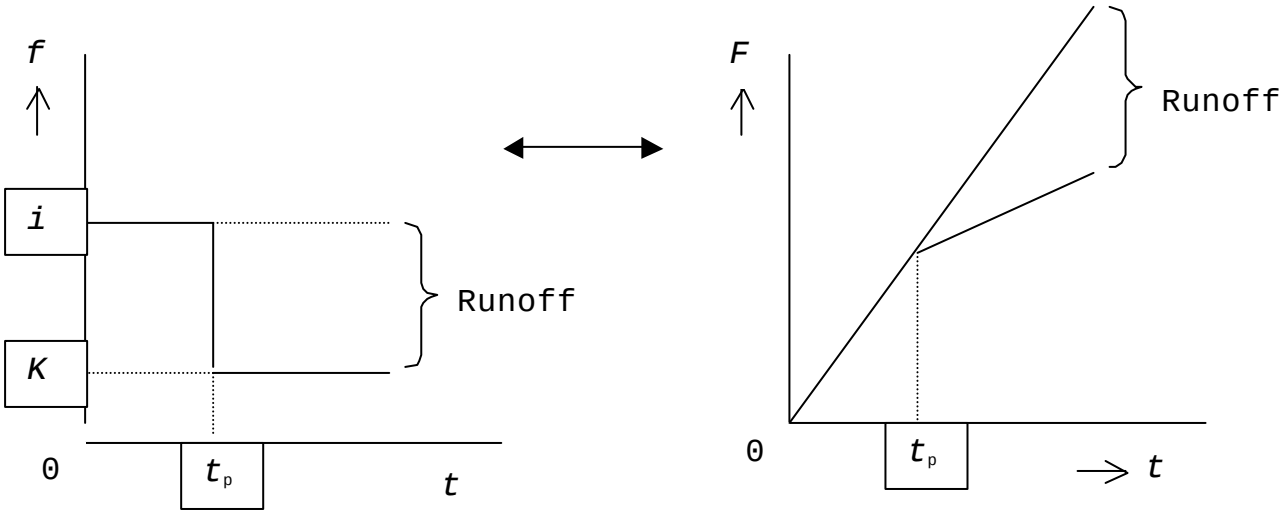

Figure 6.12. Scheme of the determination of the amount of runoff as function of t_p, time, K and rainfall intensity (i); left the momentary rainfall and infiltration, right the cumulative amounts. The rectangle in the left and the triangle in the right denote the total runoff.

The results of this exercise are summarized in Table 6.5 and Fig. 6.13. Further use will be made of the RC's when only Hortonian overland flow is considered because this is also done in literature. It can be noted that when rainfall simulation points where shallow subsurface flow was observed are also taken into account, the mean and median values drop. This shows that subsurface flow is in general related to longer times to runoff and / or higher infiltration rates.

Descriptive Statistics	RC [%], only HOF	RC [%], HOF & SSF
n	82	121
Mean	41.00	30.77
Median	33.78	28.57
Std. dev.	17.78	18.29

Table 6.5. Basic statistics for all RC's in the study area, either only Hortonian overland flow (HOF) considered, or both overland and subsurface flow (SSF).

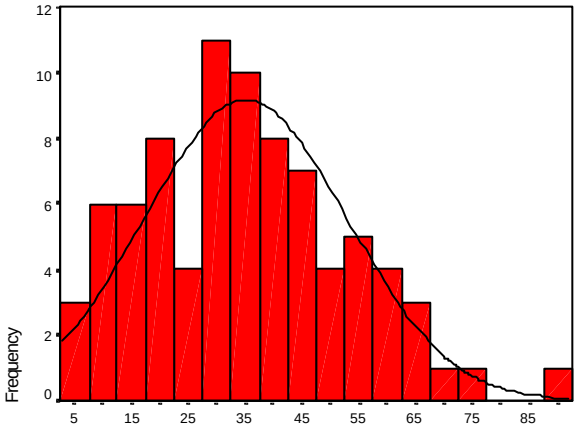

Figure 6.13a. Runoff coefficient, only HOF considered [%]

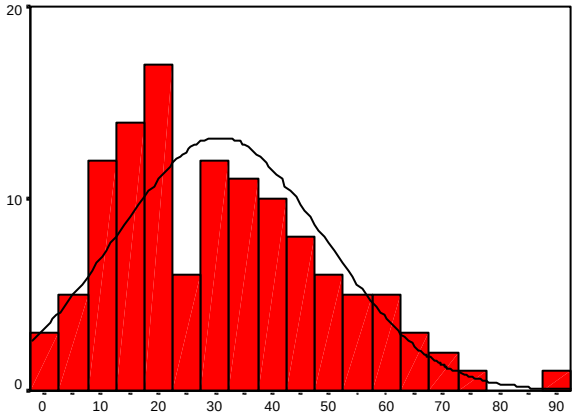

Figure 6.13b. RC, both HOF and SSF considered [%]

Figure 6.13. Histograms of runoff coefficients for two cases (with and without observations exhibiting SSF included).

Comparison with other data

In Table 6.6, the mean values for different land use covers as found in this research and in literature are shown for comparison. Only one literature value for shrubs was found in Löhmannsröben & Cernusca (1990): 10 %. Here an average RC of 30 % for shrubs was found. The data provided by Schiechtl (1975) in Section 2.4 are not used here because they are probably too high.

Nearly all values in Table 6.6 (except for this research and Ramskogler (1987)) are the result of rainfall simulations with the rainfall simulator as constructed by Karl & Toldrian (1973) and described in more detail by Bunza *et al.* (1985). This rainfall simulator can simulate rain on large areas such as 50 or 100 m^2, which is very large in comparison to the rainfall simulator area used here of only about 0.06 m^2. According to Mannaerts (1993), a standardized value as a runoff coefficient is comparable between different scales of measurement. It has however to be kept in mind that an important process such as run on-run off is hardly incorporated in the small-scale rainfall simulations as carried out in this research. It was shown in Section 4.2 and by Markart *et al.* (2000) that this process increases the apparent infiltration capacity and lowers the runoff (coefficient). This leads to values that actually are too high. This may be cancelled out by another process that is not incorporated in the calculation of the RC's. The curve as is depicted in Fig. 4.7 should flatten for higher intensities (as in Fig. 4.14). This means that the linear relationship as incorporated in Eq. 4.1 should be logarithmic and that RC increases more than linearly with intensity.

Source	*i* [mm / h]	*D* [min.]	RC forest	RC meadow	RC piste
This research	100	60	0.0 ***	32	41
Toldrian (1974, *in* Cernusca 1977)	n.a. *	n.a. *	6.4	30	80
Stauder (1974, *in* Cernusca 1977)	n.a.	n.a.	7.5		50
Karl (1977, *in* Cernusca 1977)	n.a. *	n.a. *	0.0		40
Bunza (1984a)	87	60		28	68
Ramskogler (1987)	50	50	11	27	63
Bunza (1989)	81	60		28	64
Bunza & Schauer (1989)	91	60	15		
Löhmannsröben & Cernusca (1990)	n.a. *	n.a. *	15	43	77
Bunza & Porzelt (1991)	90	60		0.0 **	6.1 **
Markart *et al.* (2000)	92	60		10	81 ***

Table 6.6. Comparison of runoff coefficients between earlier research and this research. All values are arithmetic averages. *) probably as close as possible to 100 mm / h; **) very low values due to large fissures in bedrock; ***) only one value available.

When it is assumed that these two non-incorporated aspects (missing of run on-run off process and the flattening out of the K i relationship) effectively cancel each other out, it seems that the values are quite comparable and within the range that is set by the literature values. In addition, the general trend is the same for the data as presented here: forest has the lowest runoff coefficients, pistes the highest and meadow intermediate values, but the piste runoff coefficients are rather low and the meadow runoff coefficients are rather high. Therefore, it can be stated that the pistes in the region of Sölden are less affected by skiing and piste preparation than pistes at other places (which were investigated by the other authors).

7 The effect of skiing on soil erosion

This chapter deals with the influence of skiing on the probability of rill erosion. The hydrological module of Eurosem is used together with two thresholds for incipient rilling taken from literature. When these thresholds are exceeded during a rainstorm with a recurrence interval of once in fifty years, rill erosion may start and cause damage to the ski tracks.

7.1 Model set up

The hydrological module of Eurosem is implemented in the *PCRaster Dynamic Modelling Language* by Van Dijck (2000) and Karssenberg (2000). This spatial modelling language was developed by Wesseling *et al.* (1996) and is used for dynamic modelling within the raster GIS PCRaster 2 (Karssenberg 1997). A full description of the European Soil Erosion Model — the full name for EUROSEM — can be found in Morgan *et al.* (1998a, 1998b) and a description of the hydrological module in Van Dijck (2000) and Karssenberg (2000). Here only a brief description of the hydrological part of EUROSEM will be given.

First of all, it has to be said that it is assumed that in the simulation as carried out here there is no surface storage of rain, no interception of rain by plants and no evapotranspiration. These parts of the module were all set to zero. This was done because no information is available on the amount of surface storage, interception storage was not considered because rill erosion is only possible on bare soil and evapotranspiration can be neglected during heavy rainstorms. The infiltration and routing parts of the model are thus the only two parts that were used in the simulation.

Hydrological part of Eurosem

The infiltration part of the model is rather simple. In the end, it was decided not to use the formula of Smith & Parlange (1978) — which is normally an integral part of EUROSEM — because the infiltration in the fieldwork area almost instantly reached a constant infiltration capacity at all places except one. Fig. 3.5 can be hold representative for the largest part of the area: there is hardly any matrix suction (*G* in the formula of Smith & Parlange (1978)) present. It is thought that the amount of work to fit the infiltration formula does not outweigh the improvement of the model results when a more simple solution is used. Therefore, *K* was used as potential infiltration rate. *K* was optimised for the rainfall intensity as used in the scenario. The duration of the rain was chosen to be half an hour with an intensity of 100 mm / h, resulting in a total rainfall amount of 50 mm. This rainstorm occurs once in fifty years in the Hohen Tauern (Bunza 1989), which is a mountain range about 100 km to the west of the Ötztal. This rainstorm was used because it was the only rainstorm that could be found in literature for the research area and which could serve in the modelling exercise.

For each cell, the model adds the input or rain, the amount of water on the surface and the runoff from upstream. After this, it compares the potential infiltration rate *K* with this amount of surface water. The smaller amount is the actual infiltration in that time step:

$$f_a = \text{IF } SurW > K \text{ THEN } K \text{ ELSE } SurW \qquad \text{(Eq. 7.1)}$$

with: f_a = actual infiltration [m / time step]; $SurW$ = amount of water slice on the surface [m]; K = potential infiltration rate [m / time step].

When the actual infiltration rate is determined using Eq. 7.1, this is subtracted from the amount of water slice on the surface. The infiltration surplus is routed to the downstream pixel and added to the amount of water on the surface in that pixel. This routing is done with the aid of the kinematic part of the Saint-Venant equations, which can be found in regular textbooks such as Chow *et al.* (1988, Table 9.2.1) or Anderson & Burt (1985, Eqs. 14.1 & 14.2). These two equations are both conservation equations. Eq. 7.2a is a conservation of mass equation and Eq. 7.2b is a conservation of momentum equation:

$$\frac{\partial Q}{\partial x} + \frac{\partial A}{\partial t} = q \qquad \text{(Eq. 7.2a)}$$

$$S_f = S_s \qquad \text{(Eq. 7.2b)}$$

with: Q = discharge [m / time step]; x = pixel length [m]; A = throughflow surface [m²]; t = time [time step]; q = infiltration surplus [m² / time step]; S_f = surface slope of flowing water [ ]; S_s = slope of terrain [ ].

Eq. 7.2b is part of a large equation, but this simplification is sound when it is assumed that the water does not exhibit local and convective acceleration and pressure changes. This assumption is normally valid for shallow overland flow. Eq. 7.2 can be solved using numerical methods and the Manning's equation (Chow *et al.* 1988; Karssenberg 2000). This solution also renders water height and flow velocity, of which the former is used in further calculation.

Threshold exceedance

It is commonly known that in order to start rill erosion or at least incipient rilling / micro-rilling, a certain threshold has to be exceeded (Bryan 1987, 2000). A wide range of possible thresholds is given in Thonon (1999) and Bryan (2000). A threshold is determined by both the characteristics of the water and the soil. One can imagine that in fast flowing water or on loose soil the threshold is exceeded earlier than in slowly moving water or cohesive soil. In literature, one of the most commonly used thresholds is based on the so-called shear velocity. The fact that this quantity can serve as a threshold for incipient rilling was originally found by Govers (1985). This shear velocity is defined as the square root of shear stress exerted by water on the soil (when the density of water is assumed to be one) (Pearce 1976; Kirkby 1980):

$$\hat{o}_w = \tilde{n}_w \cdot g \cdot R \cdot S_s \qquad \text{(Eq. 7.3a)}$$

$$u^* = \sqrt{g \cdot R \cdot S_s} = \sqrt{\frac{\hat{o}_w}{\tilde{n}_w}} \qquad \text{(Eq. 7.3b)}$$

with: J_w = flow shear stress [Pa]; R = hydraulic radius water height [m]; u^* = shear velocity [m / s].

When the shear velocity is calculated as a function of both slope and water height, it can be compared to the threshold for rilling, which was chosen to be 7 cm / s. This value was found by Merz & Bryan (1993) for a sandy loam texture. The u^*_{cr} for silty loams as can be found in literature are too low because they are only valid for very erodible calcareous loess soils (Bryan 2000). When the soil texture was silty loam or heavier[29], the soil was considered not to be prone to rill erosion: these soils exhibit a higher grade of cohesion that renders them less sensitive to rilling (Morgan 1995). Because u^* is a hydraulically determined threshold, no use of J_D or J_W was made. This is used in a

[29] Soil texture was interpolated by the use of Thiessen polygons, of which the theory is covered in Section 5.1.

threshold as defined by Torri *et al.* (1987) and recommended by Thonon (1999). In the end however, the u^*_{cr} threshold was chosen to prevail above the little used and less appropriate threshold from Torri *et al.* (1987).

Yet, another threshold has to be exceeded in order to get rill erosion. This is the critical slope. It was originally shown by Savat & De Ploey (1982) and later by a number of other authors (reviewed in Thonon (1999)) that the terrain slope has to be larger than 2 to 3 degrees in order to get rilling. So, when the threshold of $u^*_{cr} = 7$ cm / s is exceeded, the change of rilling is still minimal when the slope is too low. Therefore, the prerequisite was set that the local slope has to exceed 3° before rilling may occur.

A third threshold that was defined in time and taken from literature as well. Torri *et al.* (1987) examined the development of rill erosion and took 40 minutes as the time after which they checked for the occurrence of rilling. The model was run for one hour, with time steps of six seconds, resulting in 600 time steps, so at least two-third of this time u^*_{cr} had to be exceeded before a spot was considered to be potentially sensitive to rill erosion.

Two assumptions were made in the modelling. First, it was assumed that the forest and shrub areas (i.e., all the non-piste areas) and the spots on the pistes where subsurface flow was noticed[30] do not give overland flow. This was done because of the generally high infiltration capacities of forests (cf. Table 6.6) and the more frequent occurrence of subsurface flow underneath both forest and scrubland (Fig. 4.20), which does not lead to erosion or overland flow on downstream areas when there is no return flow present. Therefore, it was also assumed that return flow did not occur.

7.2 Model results and discussion

The map that resulted after the model simulation is depicted in Fig. 7.1a. After application of the time filter, the slope filter and the soil filter, the map in Fig. 7.1b resulted. This map gives the locations of potential erosion hazard: when the soil would be bare, rill erosion could be possible on these places during severe rainstorms. In Fig. 7.1c, the locations were actual erosion hazard is present are depicted. The green spots in Fig. 7.1c are places where rill erosion is potentially possible (as indicated in Fig. 7.1b) coincide with places where a bare soil was observed during the fieldwork period.

It has to be kept in mind that the surface stoniness is not incorporated in the model, the interpolation of K is rather global and that a model check was not performed. No literature with a quantitative definition of the influence of surface stoniness on thresholds for rill initiation could be found. For soil moisture content literature (Bryan *et al.* 1998; Bryan & Rockwell 1998) however indicates that this may also have an influence on the threshold for incipient rilling. Although this parameter is rather constant in time, it is not constant in space. This factor was however not incorporated in the model because up to now there is no quantitative expression for the relationship between rilling and ASM. The model outcomes can therefore only be interpreted on a high level of scale (not on a pixel scale) and with a high level of uncertainty because of the model simplicity. However, it is assumed that the model as used here is accurate enough to predict potential rill erosion, because sheet erosion was observed to occur on most spots that are potentially vulnerable to rill erosion. These spots on the potential erosion hazard map (Fig. 7.1b) mostly coincided with a damaged vegetation: either the grass cover was low or the shrubs were dead or suffering. The former was the case on three spots in the fieldwork area (1, 2 and 3 in Fig 7.1b). At the place indicated

[30] These spots were also interpolated with the use of Thiessen interpolation.

by 3, the photos in Figs. 4.4 and 4.5 were made, indicating damaged grass sods. Damage of the shrub cover was observed in the southeast of the area, indicated by 4 in Fig. 7.1b. Sheet erosion points at a low infiltration capacity, which causes overland flow to occur. When the vegetation is totally destroyed, the overland flow can rapidly concentrate in small depressions and form rivulets, which may easily evolve in rills. Fig. 7.1b thus at least indicates the areas where rill erosion might be possible when the vegetation cover is totally destroyed. The map can help the skiing company to concentrate their policy and protective measurements on the spots where rill erosion is potentially possible: only on these spots, the vegetation has to be regenerated in order to prevent rill erosion to take place. This regeneration was observed at spot 5 in Fig. 7.1c. According to Fig. 7.1b, this area is sensitive to rill erosion. Because the vegetation cover was low, the skiing company fenced off this area and gave the vegetation the time to reinstate.

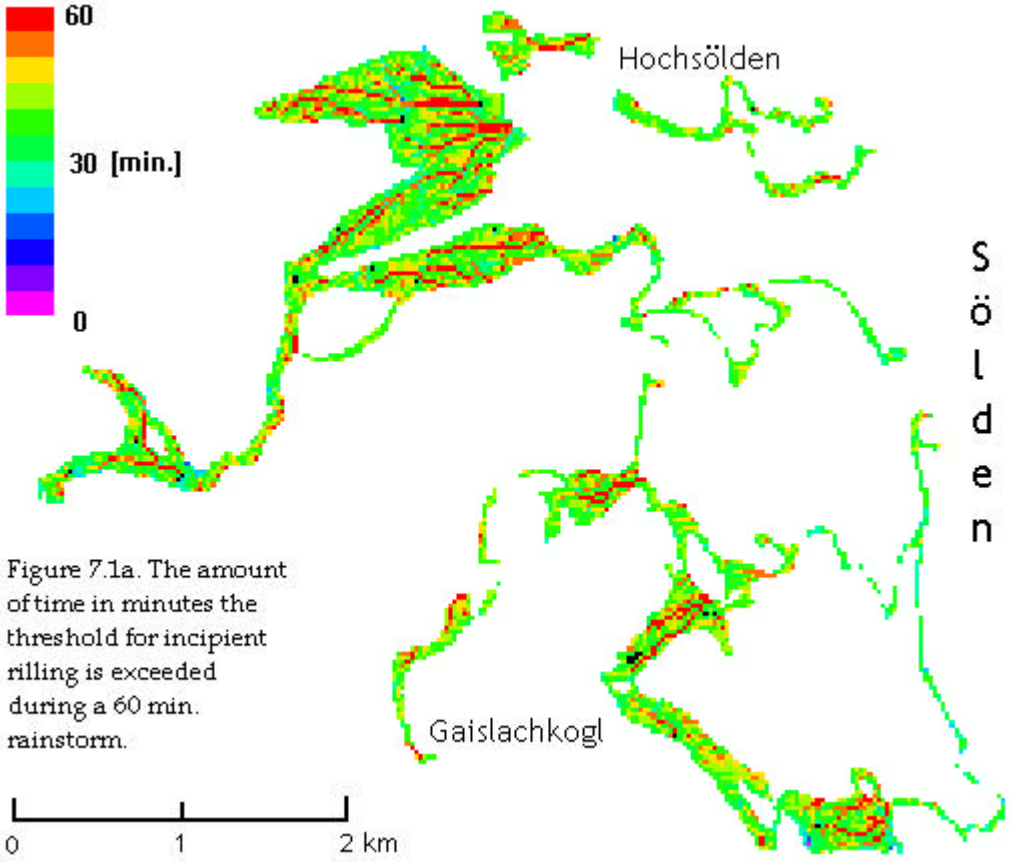

Figure 7.1a. The amount of time in minutes the threshold for incipient rilling is exceeded during a 60 min. rainstorm.

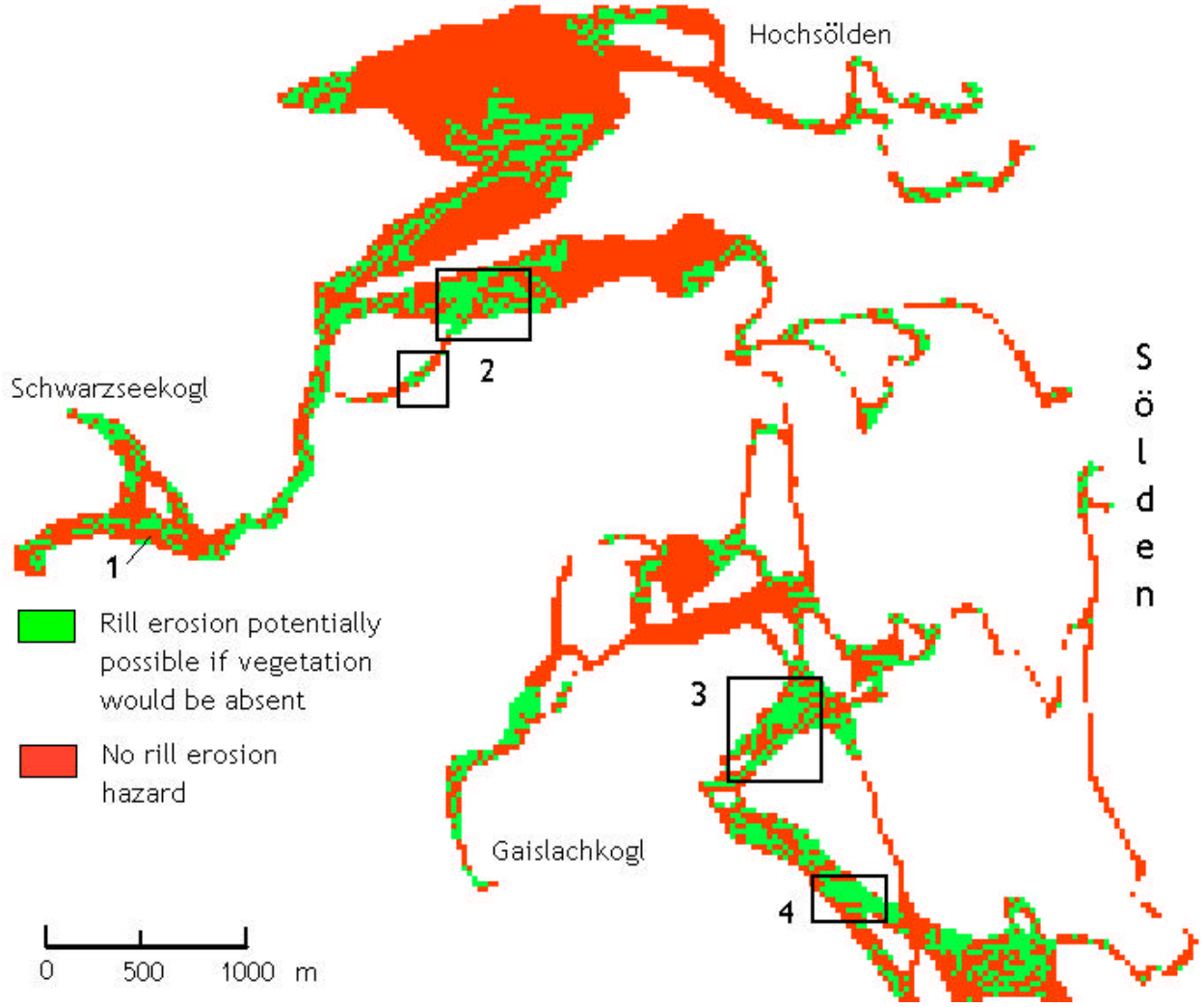

Figure 7.1b. Erosion hazard map. If the soil would be bare on the locations which are indicated by a green colour, rill erosion would be likely to occur. Often the soil is however covered with vegetation and only on the spots as indicated in Fig. 7.1c, rill erosion occurred or was likely to occur under the conditions as observed during the fieldwork period.

The results in the actual erosion map (Fig. 7.1c) are partly confirmed by field observations: at the time of fieldwork, rilling was observed to occur on the biosol[31] near the Schwarzseekogl (Pfeffer, *pers. comm.*; number 7 in Fig. 7.1c). Bunza & Porzelt (1991) also observed erosion of the same kind of artificial humic soil on ski tracks in northern Italy. This may lead to the conclusion that this humic biosol is very prone to rill erosion. A possible explanation for this high sensitivity to rilling of this artificial soil is the nearly complete lack of soil structure and its rather coarse texture (loamy sand in most of the cases).

[31] Biosol is the soil that is used on new ski tracks. It contains humic material and manure, has a sandy texture and is used to get a grass cover in a short time.

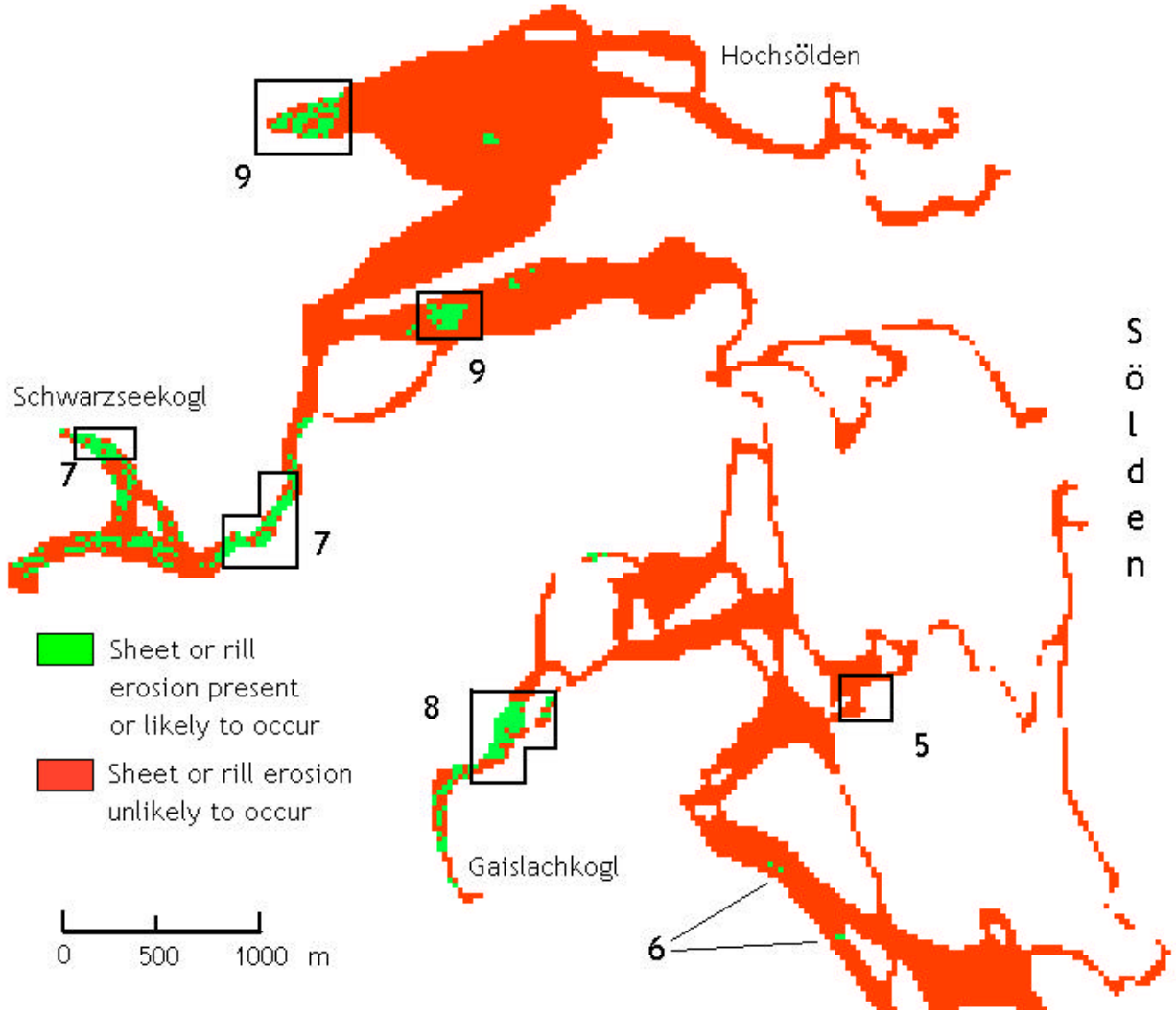

Figure 7.1c. Present rill erosion map. The green spots indicate places where erosion was observed during the fieldwork period or where erosion was due to occur according to the model outcomes combined with the vegetation conditions during the fieldwork period.

Rill erosion was also observed on rather bare normal soil in the southeast of the fieldwork area, where the small spots of Fig. 7.1c are located (number 6). On other places, however, only sheet flow was observed (numbers 9). Spot number 8 had a high degree of surface stoniness and no erosion was observed to occur here. It may be that the high degree of stones protects the soil against incision by water: a far higher shear stress has to be exerted by the water on stones and gravel in order to set these particles in motion. The threshold for setting in motion of particles is the well-known Shield's curve, but it was found that this cannot be applied to overland flow with confidence, because of several reasons given in Thonon (1999). The most important in this case is that the water level to grain size ratio has to be large to render the application of the Shields criterion to be sound (Poesen 1987), but this is hardly the case in shallow overland flow (Emmett 1970; Bryan 1974; Pearce 1976; Dunne & Dietrich 1980). The overland flow depth for the application of Shields' diagram is only sufficient in concentrated flow, but the locations of these rivulets cannot be predicted because the occurrence of these flow concentrations is mainly a stochastic process. It may therefore be concluded that the model works quite well on sandy (loamy) soils without a high degree of stones. As said before, until now no quantitative relationship between surface stoniness and rilling threshold(s) has been developed.

A disadvantage of the used data field data are their ‘smoothness’, as already indicated in Section 5.4: K changes smoothly in space (Fig. 5.16a), which is not natural, for natural changes are more abrupt. This affects the model results. Also, no use is made of the full range of K values, for kriging leads to a smaller range, with higher minimum values and lower maximum values. Van Dijck (2000) indicates that a small range of values is a reason for improper model results in overland flow modelling. This improperness cannot be checked, because model validation with hydrographs is not possible due to failure of the Sewer data loggers in the Seebach and the stream near Hochsölden. New measurements as conducted in 2000 may be used for this purpose. Furthermore, Monte Carlo simulation can be used to create a more realistic surface with the full range of data values. This method makes use of variograms and data points to simulate a more rough and realistic surface, but it has the disadvantage of its large number of simulations needed (rule of thumb: at least 100 (Burrough & McDonnell (1998)) and was therefore not used here.

8 Conclusions and recommendations

- The study area has certain inherent characteristics regarding climate (large amount of snowmelt together with rain in summer), geology (impermeable metamorphosed rocks) and geomorphology (steep rocky slopes that drain quickly and large relatively flat terraces where snow can be stored) that can lead to high amounts of runoff generation, even without skiing taking place.
- The hypothesis that hydraulic conductivity is positively correlated to rainfall intensity can be supported with the data from this research and from literature.
- Skiing and the preparation of pistes do not have a notable direct effect on porosity or vertical hydraulic conductivity. Skiing does have an indirect influence on soil bulk density via the process of vegetation damaging, which is possibly caused by a direct negative influence on the soil moisture status. Probably via the mechanism of soil compaction, ski tracks have an increased risk of overland flow as compared to undisturbed areas, which mainly drain through the harmless mechanism of subsurface flow.
- Interpolation of hydraulic conductivities is possible with the use of several methods, of which ordinary point kriging is probably the best one.
- Ordinary point kriging provides rather good results when the low number of data points is taken into consideration. It is obvious that interpolation on only ski tracks provides better results, lower estimation errors and a wider interpolated area than interpolation with incorporation of all data points. The distinct variograms supports the view that natural slopes and ski tracks are quite distinct hydrological areas, in spite of the closeness of their average hydraulic conductivity values. Improvement of interpolation is only possible by addition of data points, notably in the ‘total area’ case.
- In block kriging, it was noticed that an increase in resolution of the grid did not improve interpolation results. However, for modelling purposes interpolations on a denser grid may be needed. Both block kriging and simple kriging result in even lower estimation errors than ordinary point kriging — this is however inherent in the methods. The larger amount of smoothing makes these methods less appropriate when the results are to be used in distributed modelling. Monte Carlo simulations have an opposite result and are recommended here as a good alternative for ordinary point kriging, especially when the interpolated maps are used for modelling.
- The general view that interpolation methods are more optimal for normal distributed variables than non-Gaussian distributed variables can be supported.
- The effect of skiing on the most important catchment hydrological parameters could not be deduced from the gathered data due to apparatus failure. From manual measurements it can however be deduced that peak discharges are probably higher when a catchment exhibits a high cover percentage of ski tracks.
- The ski tracks have a higher risk of overland flow than undisturbed areas; non-pistes are mainly associated with subsurface flow. This subsurface flow cannot be held responsible for the direct runoff peak in the gauged ‘forest stream’; this is for about one third to one half caused by channel precipitation and for the remaining part by (saturation) overland flow, which probably originates directly along the channel.
- It appears that the Sölden ski area is less affected by skiing than other comparable ski areas when considering runoff coefficients.
- In this kind of research, the concept of the Dimensionless Hydrograph provides a better method for comparison of direct runoff between different catchments than the concept of the Unit Hydrograph. DH construction is less laborious and simpler than

UH construction and results in clearer figures. It is recommended that in further research, DH's are used for comparison purposes.

- Skiing enlarges the risk of (rill) erosion notably through the damage of vegetation. When the vegetation is destroyed, large areas of ski pistes may become affected by rill erosion. However, where the vegetation was already destroyed, often sheet erosion instead of rill erosion was observed. Especially the artificial soil (biosol) is very sensitive to both sheet and rill erosion. It is therefore recommended to keep the soil covered well by grass or shrub vegetation. The present policy of the skiing company, i.e. giving stressed vegetation a chance of regeneration, is sufficient when the vegetation can indeed recover. Further research on vegetation recovery and biomass production has to prove whether this is indeed the case.

References

Adams, J.E., Kirkham, D. & Nielsen, D.A. (1957): A portable rainfall-simulator infiltrometer and physical measurements of soils in place; *Soil Science Society of America Proceedings* 21 (5), 473 477.

Anderson, G., Pidgeon, J.D., Spencer, H.B. & Parks, R. (1980): A new handheld penetrometer for soil studies; *Journal of Soil Science* 31, 276–296.

Anderson, M.G. & Burt, T.P. (1985): *Hydrological forecasting*; John Wiley & Sons, New York (USA).

Ankeny, M.D., Ahmed, M., Kaspar, Th. C. & Horton, R. (1991): Simple field method for determining unsaturated hydraulic conductivity; *Soil Science Society of America Journal* 55 (2), 467–470.

Ankeny, M.D., Kaspar, Th. C. & Horton, R. (1988): Design for an automated tension infiltrometer; *Soil Science Society of America Journal* 52, 893–896.

Armstrong, M. (1998): *Basic linear geostatistics*; Springer Verlag, Berlin (Germany), 153 pp.

Aulitzky, H. (1970): Schutzfunktion des Waldes im Gebirge; *Österreichische Forstzeitung* 81 (5), 128-129 (in German).

Babalola, O. (1978): Spatial variability of soil water properties in tropical soils of Nigeria; *Soil Science* 126 (5), 269-279.

Bardossy, A., Bogardi, I., & Kelly, W.E. (1990a): Kriging with imprecise (fuzzy) variograms. I: theory; *Mathematical Geology* 22 (1), 63 79.

Bardossy, A., Bogardi, I. & Kelly, W.E. (1990b): Kriging with imprecise (fuzzy) variograms. II: application; *Mathematical Geology* 22 (1), 81 94.

Bätzing, W. (1991): *Die Alpen: Entstehung und Gefährdung einer europäischen Kulturlandschaft*; Verlag C.H. Beck, Munich (Bavaria - Germany), 287 pp. (in German).

Bätzing, W. (1997): *Kleines Alpenlexikon: Umwelt, Wissenschaft, Kultur*; *Beck'sche Reihe* 1205, Verlag C.H. Beck, Munich (Bavaria Germany), 320 pp. (in German).

Bauer, B. (1988): Ostalpen, Bau und Genese eine Skizze; *Praxis Geographie* 18 (10), 6 12 (in German).

Beven, K. (1989): Changing ideas in hydrology – the case of physically based models; *Journal of Hydrology* 105 (4), 157–172.

Beven, K. & Germann., P. (1982): Macropores and water flow in soils; *Water Resources Research* 18 (5), 1311 1325.

Blijenberg, H.M. (1998): *Rolling stones? Triggering and frequency of hillslope debris flows in the Bachelard Valley, southern French Alps*; *Nederlandse Geografische Studies/Netherlands Geographical Studies* 246, Koninklijk Nederlands Aardrijkskundig Genootschap / Faculteit Ruimtelijke Wetenschappen, Universiteit Utrecht, Utrecht (The Netherlands), 223 pp. *Also*: PhD Thesis Utrecht University.

Blijenberg, H.M., De Graaf, P.J., Hendriks, M.R., De Ruiter, J.F. & Van Tetering, A.A.A. (1996): Investigation of infiltration characteristics and debris flow initiation conditions in debris flow source areas using a rainfall simulator; *Hydrological Processes* 10, 1527 1543.

Bögel, H. & Schmidt, K. (1976): *Kleine Geologie der Ostalpen — allgemein verständliche Einführung in den Bau der Ostalpen unter Berücksichtigung der angrenzenden Südalpen*; Ott Verlag, Thun (Kanton Bern - Switzerland), 231 pp. (in German).

Bork, H.R. (1980): *Oberflächenabfluss und infiltration Qualitative und quantitatieve Analysen von 50 Starkregensimulationen in der Südheide (Ostniedersachsen)*; *Landschaftsökologie und Landschaftsgenese* 6, Lehrstuhl für Physische Geographie und Landschaftsökologie der Technischen Universität Braunschweig, Braunschweig (Lower Saxony Germany), 94 pp. (in German).

Bork, H.R. & Bork, H. (1981): *Oberflächenabfluss und infiltration Ergebnisse von 100 Starkregensimulationen im Einzugsgebiet der Ramla del Campo Santo (SE-Spanien)*; *Landschaftsökologie und Landschaftsgenese* 8, Lehrstuhl für Physische Geographie und Landschaftsökologie der Technischen Universität Braunschweig, Braunschweig (Lower Saxony Germany), 76 pp. (in German).

Bradford, J.M. & Grossman, R.B. (1982): In-situ measurement of near-surface soil strength by the fall-cone device; *Soil Science Society of America Journal* 46, 685–688.

Brakensiek, D.L. & Rawls, W.J. (1994): Soil containing rock fragments: effects on infiltration; *Catena* 23 (1), 99 110.

Bringazi, F. (1989): *Naturkatastrophen als Folge anthropogener Eingriffe in die alpine Vegetation dargestellt am Beispiel des Baues und Betriebes von Skipisten in österreich*; Hausarbeit zum Seminar für Physiogeographie, Institut für Geographie und Regionalforschung, Universität Wien, Vienna (Austria) 74 pp. (in German).

Brunori, F., Penzo, M.C. & Torri, D. (1989): Soil shear strength: its measurement and soil detachability; *Catena* 16, 59–71.

Bryan, R.B. (1974): Water erosion by splash and wash and the erodibility of Albertan soils; *Geografiska Annaler serie A* 56 (3–4), 159-181.

Bryan, R.B. (1987): Processes and significance of rill development. 1–15 *In*: Bryan, R.B. (ed.): *Rill erosion – processes and significance*; *Catena Supplement* 8, Catena Verlag, Cremlingen-Destedt (Lower Saxony Germany) 160 pp.

Bryan, R.B. (2000): Soil erodibility and processes of water erosion on hillslope; *Geomorphology* 32 (3 4), 385 415.

Bryan, R.B., Govers, G. & Poesen, J.W.A. (1989): The concept of soil erodibility and some problems of assessment and application; *Catena* 16, 393–412.

Bryan, R.B., Hawke, R.M. & Rockwell, D.L. (1998): The influence of subsurface moisture on rill system evolution; *Earth Surface Processes and Landforms* 23 (9), 773 789.

Bryan, R.B. & Rockwell, D.L. (1998): Water table control on rill initiation and implications for erosional response; *Geomorphology* 23, 151–169.

Bunza, G. (1984a): Oberflächenabfluß und Bodenabtrag in alpinen Graslandökosystemen; *Verhandlungen der Gesellschaft für Ökologie (Bern 1982)* XII, 101 109 (in German).

Bunza, G. (1984b): Oberflächenabfluß und Bodenabtrag in Meran 2000. Chapter 2 *in*: Cernusca, A. (ed.): *Ökologisches Gutachten über die Ursachen der Erosionen in Meran 2000 und Vorschläge für Sanierungsmaßnahmen*; Abteilung Ökologie, Institut für Botanik, Leopold Franzens Universität, Innsbruck (Tyrol Austria), 151 pp. (in German).

Bunza, G. (1989): Oberflächenabfluß und Bodenabtrag in der alpinen Grasheide der Hohen Tauern an der Grossglockner-Hochalpenstraße. *In*: Cernusca, A. (ed.): *Struktur und Funktion von Graslandökosystemen im Nationalpark Hohe Tauern*; *Veröffentlichungen des österreichischen MaB-Programms* 13, Universitätsverlag Wagner, Innsbruck (Tyrol Austria), 155 199 (in German).

Bunza, G., Deisenhofer, H.-E., Karl, J., Porzelt, M. & Riedl, J. (1985): Beiträge zu Oberflächenabfluß und Stoffabtrag bei künstlichen Starkniederschlägen; *DVWK Schriften* 71, 3 35.

Bunza, G. & Porzelt, M. (1991): *Abfluß- und Erosionsversuche auf Pistenflächen und naturnahen Standorten des Skigebietes am Monte Bondone, Autonome Provinz Trient*; Bayerisches Landesamt für Wasserwirtschaft, Munich (Bavaria Germany), 10 pp. (unpublished, in Germann).

Bunza, G. & Schauer, Th. (1991): Der Einfluß von Vegetation, Geologie und Nutzung auf den Oberflächenabfluß bei künstlichen Starkregen in Waldbachgebieten der Bayerischen Alpen; *Informationsbericht des Bayerischen Landesamt für Wasserwirtschaft* 89 (2), 127 150 (internal publication, in Germann).

Burden, D.S. & Selim, H.M. (1989): Correlation of spatially variable soil water retention for a surface soil; *Soil Science* 148 (6), 436 447.

Burrough, P.A. & McDonnell, R.A. (1998): *Principles of geographical information systems*; *Spatial information systems and geostatistics*, Oxford University Press, Oxford (Oxfordshire UK), 333 pp.

Cameron, D.R. (1978): Variability of soil water retention curves and predicted hydraulic conductivity on a small plot; *Soil Science* 126(6), 364-371.

Casagrande, A. (1932): Research on the Atterberg limits of soils; *Public Roads* 10.

Casagrande, A. (1948): Classification and identification of soils; *Transactions ASCE* 113, 901.

Cernica, J. N. (1995): *Geotechnical engineering soil mechanics*; John Wiley & Sons, New York (USA), 453 pp.

Cernusca, A. (1977): Ökologische Veränderungen im Bereich von Schipisten. 81 150 *In*: Sprung. R. & König, B. (eds.): *Das österreichische Skirecht*; Innsbruck (in German).

Cernusca, A. (1984a): Zusammenfassung der Ergebnisse der Studie; Chapter 1 *in*: Cernusca, A. (ed.): *Ökologisches Gutachten über die Ursachen der Erosionen in Meran 2000 und Vorschläge für Sanierungsmaßnahmen*; Abteilung Ökologie, Institut für Botanik, Leopold Franzens Universität, Innsbruck (Tyrol Austria), 151 pp. (in German).

Cernusca, A. (1984b): Erläuterungen zum Fragenkreis „Schaden an der Vegetation und Ertragseinbußen durch den Betreib von Schipisten“. Chapter 5 *in*: Cernusca, A. (ed.): *Ökologisches Gutachten über die Ursachen der Erosionen in Meran 2000 und Vorschläge für Sanierungsmaßnahmen*; Abteilung Ökologie, Institut für Botanik, Leopold Franzens Universität, Innsbruck (Tyrol Austria), 151 pp. (in German).

Chapman, T.G. (1996a): Common Unitgraphs for sets of runoff events. Part 1: unitgraph identification from streamflow data; *Hydrological Processes* 10, 773 782.

Chapman, T.G. (1996b): Common Unitgraphs for sets of runoff events. Part 2: comparisons and inferences for rainfall loss models; *Hydrological Processes* 10, 783 792.

Chow, V.T., Maidment, D.R., Mays, L.W. (1988): *Applied hydrology*; *MacGraw-Hill series in water resources and environmental engineering*, McGraw-Hill, New York (USA), 572 pp.

Coelho, M.A. (1974): *Spatial variability of water related soil physical properties*; PhD Thesis, University of Arizona, Tucson (Arizona USA), 88 pp.

Coles, N. & Trudgill, S. (1985): The movement of nitrate fertilizer from the soil surface to drainage waters by preferential flow in weakly structured soils, Slapton; *South Devon Agriculture and Ecosystem Environment* 13, 241 259.

Corradini, C., Melone, F. , Ubertini, L., Singh, V.P. (1986): Geomorphologic approach to synthesis of direct runoff hydrograph from the upper Tiber river basin, Italy. Chapter 4 *in*: Gupta, V.K., Rodríguez-Iturbe, I. & Wood, E.F. (eds.): *Scale problems in hydrology*; D. Reidel, Dordrecht (The Netherlands), 246 pp.

Cressie, N. (1990): The origins of kriging; *Mathematical Geology* 22 (3), 239 252.

Crouch, R.J. & Novruzi, T. (1989): Threshold conditions for rill initiation on a Vertisol, Gunnedah, New South Wales, Australia; *Catena* 16, 101–110.

Cruse, R.M. & Larson, W.E. (1977): Effect of soil shear strength on soil detachment due to raindrop impact; *Soil Science Society of America Journal* 41, 777–781.

Csikos, O. (1975): Landeskunde Tirols. Chapter 1.1 *in*: Aulitzky, H., Feist, H. & Grubinger, H. (ed.): *Hochwasser- und Lawinenschutz in Tirol*; Land Tirol, Innsbruck, (Tyrol - Austria), 412 pp. (in German).

Davis, J.C. (1986): *Statistics and data analysis in geology*; John Wiley & Sons, New York (USA), 646 pp.

Dikau, R. (1986): *Experimentelle Untersuchungen zu Oberflächenabfluss und Bodenabtrag von Meßparzellen und landwirtschaftlichen Nutzflächen*; *Heidelberger Geographische Arbeiten 81,* Selbstverlag des Geografischen Instituts der Universität Heidelberg, Heidelberg (Baden-Württemberg Germany) 195 pp. (in German).

De Roo, A.P.J., Offermans, R.J.E. & Cremers, N.H.D.T. (1996a): LISEM: a single event physically based hydrological and soil erosion model for drainage basins. II: Sensitivity analysis, validation and application; *Hydrological processes* 10 (8), 1119 1126.

De Roo, A.P.J. & Riezebos, H.Th. (1992): Infiltration experiments on loess soils and their implications for modelling surface runoff and soil erosion; *Catena* 19 (2), 221–239.

De Roo, A.P.J., Wesseling, C.G. & Ritsema, C.J. (1996b): LISEM: a single event physically based hydrological and erosion model for drainage basins; I: Theory, input and output; *Hydrological processes* 10 (8), 1107 1117.

Domenico, P.A. & Schwartz, F.W. (1990): *Physical and chemical hydrogeology*; John Wiley & Sons, New York (USA), 824 pp.

Dongus, H. (1984): Grundformen des Reliefs der Alpen; *Geographische Rundschau* 36 (8), 388-394 (in German).

Drungil, C.E.C., Abt, K. & Gish, T.J. (1989): Soil moisture determination in gravelly soils with Time Domain Reflectrometry; *Transactions ASAE* 32 (1), 177 180.

Dunne, Th. & Dietrich, W.E. (1980): Experimental studies of Hortonian overland flow: II. Hydraulic characteristics and hillslope hydrographs; *Zeitschrift für Geomorphologie NF Supplement Band* 35, 60 80.

Dunne, Th., Zhang, W. & Aubry, B.F. (1991): Effects of rainfall, vegetation and microtopography on infiltration and runoff; *Water Resources Research* 27 (9), 2271 2285.

Edwards, W.M., Shipitalo, M.J., Dick, W.A. & Owens, L.B. (1992): Rainfall intensity affects transport of water and chemicals through macropores in no-till soil; *Soil Science Society of America Journal* 56 (1), 52 58.

ELE (2000): *Online catalog*; http://www.soiltest.com/index3.html.

Emmett, W.W. (1970): Hydraulics of overland flow on hillslopes; *USGS Professional Paper* 662-A, 68 pp.

Ernst, M. (1984): Ökologische Gefahren in den Hochgebirgsräumen Mitteleuropas; *Geographie und Schule* 7 (37), 1-7 (in German).

Fliri, F. (1974): *Niederschlag und Lufttemperatur im Alpenraum*; *Wissenschaftliche Alpenvereinshefte* 24, Hauptausschüssen des Deutschen und Österreichischen Alpenvereins, Innsbruck (Tyrol Austria), 110 pp. (in German).

Fliri, F. (1975): Die klimatologische Stellung von Tirol im Alpenraum. Chapter 1.4 *in*: Aulitzky, H., Feist, H. & Grubinger, H. (ed.): *Hochwasser- und Lawinenschutz in Tirol*; Land Tirol, Innsbruck (Tyrol Austria), 412 pp. (in German).

Fullen, M.A. & Reed, A.H. (1987): Rill erosion on arable loamy sands in the West Midlands of England. 85 96 *In*: Bryan, R.B. (ed.): *Rill Erosion Processes and Significance*; *Catena Supplement* 8, Catena Verlag, Cremlingen-Destedt (Lower Saxony Germany), 160 pp.

Foster, E.A. (1948): *Rainfall and runoff*; The Macmillan Company, New York (USA), 487 pp.

Geiger, R. (1961): *Das Klima der bodennahen Luftschicht*; Verlag F. Vieweg, Braunschweig (Lower Saxony - Germany), 645 pp. (in German).

Giessübel, J. (1988): Nutzungsschäden, Bodendichte und rezente Geomorphodynamik auf Skipisten der Alpen und Skandinaviens; *Zeitschrift für Geomorphologie NF Supplementband* 70, 205 219. (in German).

Goovaerts, P. (1992): Factorial kriging analysis: a useful tool for exploring the structure of multivariate spatial soil information; *Journal of Soil Science* 43 (4), 597–619.

Goovaerts, P. & Journel, A.G. (1995): Integrating soil map information in modelling the spatial variation of continuous soil properties; *European Journal of Soil Science* 46 (3), 397-414.

Govers, G. (1985): Selectivity and transporting capacity of thin flows in relation to rill erosion; *Catena* 12, 35–49.

Govers, G., Everaert, W., Poesen, J.W.A., Rauws, G., De Ploey, J. (1987): Susceptibilité d'un sol limoneux à l'érosion par rigoles: essais dans le grand canal de Caen; *Bulletin de Centre Géomorphologie du C.N.R.S. Caen* 33, 85–106 (in French).

Govers, G., Everaert, W., Poesen, J.W.A., Rauws, G., De Ploey, J., Lautridou, J.P. (1990): A long flume study of the dynamic factors affecting the resistance of a loamy soil to concentrated flow erosion; *Earth Surface Processes and Landforms* 15 (4), 313–328.

Glauert, G. (1975): *Die Alpen eine Einführung in die Landeskunde*; Verlag Ferdinand Hirt, Kiel (Schleswig-Holstein - Germany), 104 pp. (in German).

Gupta, V.K, Waymire, R. & Wang, C.Y. (1980): A representation of an instantaneous unit hydrograph from geomorphology; *Water Resources Research* 16, 855 862.

Haimayer, P. (1984): Tourismus im Alpenraum; *Geographische Rundschau* 36 (8), 417 423 (in German).

Hall, M.J. (1970): A critique of methods of simulating rainfall; *Water Resources Research* 6 (4), 1104 1114.

Hawkins, D.M. & Cressie, N. (1984): Robust kriging – a proposal; *Journal of the International Association for Mathematical Geology* 16, 3–18.

Heißel, W. (1975): Der geologische Bau von Tirol. Chapter 1.2 *in*: Aulitzky, H., Feist, H. & Grubinger, H. (ed.): *Hochwasser- und Lawinenschutz in Tirol*; Land Tirol, Innsbruck (Tyrol Austria), 412 pp. (in German).

Hupke, K.D. (1990): *Das Gletscherskigebiet Rettenbach-Tiefenbachferner (Sölden im Ötztal / Tirol) - ein Beitrag zur Wirksamkeit kapitalintensiver touristischer Einrichtungen im peripheren Raum*; *Stuttgarter Geographische Studien* 114, Geograpisches Institut der Universität Stuttgart, Stuttgart (Baden-Württemberg - Germany), 196 pp. (in German, with English summary).

Imeson, A.C. (1977): A simple field-portable rainfall simulator for difficult terrain; *Earth Surface Processes* 2 (4), 431 436.

Isaaks, E.H. & Srivastava, R.M. (1989): *An introduction to applied geostatistics*; Oxford University Press, New York (USA), 561 pp.

Jean, J.-S., Ai, K.-F., Shih, K. & Hung, K.-C. (2000): Stone cover and slope factors influencing hillside surface runoff and infiltration: laboratory investigation; *Hydrological Processes* 14 (10), 1829 1849.

Jetten, V.G., Riezebos, H.Th., Hoefsloot, F. & Van Rossum, J. (1993): Spatial variability of infiltration and related properties of tropical soils; *Earth Surface Processes and Landforms* 18 (6), 477–488.

Karl, J. (1977): Erosionsversuche auf zwei Schiabfahrten und im angrenzenden Wald bei Achenkirch, Tirol. *In*: Cernusca, A. (ed.): *Ökologische Veränderungen durch das Anlegen von Schiabfahrten an Waldhängen*; Fonds für Umweltstudien, Bonn (Nordrhein-Westfalen Germany) (in German).

Karl, J. & Toldrian, H. (1973): Eine transportable Beregnungsanlage für die Messung von Oberflächenabfluß und Bodenabtrag; *Wasser und Boden* 25 (3), 63 65 (in German).

Karssenberg, D. (1997): *PCRaster version 2 manual*; Vakgroep Fysische Geografie, Faculteit Ruimtelijke Wetenschappen, Universiteit Utrecht, Utrecht (The Netherlands), 368 pp.

Karssenberg, D. (2000): *Rainfall-runoff modelling in PCRaster EUROSEM in PCRaster*; http://www.geog.uu.nl/pcraster/runoff.

Kessler, J. & Oosterbaan, R. (1974): Determining hydraulic conductivity of soils; *Drainage Principles and Applications* 16 (3), ILRI (International Institute for Land Reclamation and Improvement), Wageningen (The Netherlands), 253–296.

Kirkby, M.J. (1980): Modelling water erosion processes. Chapter 6 *in*: Kirkby, M.J. & Morgan, R.P.C. (eds.): *Soil Erosion*; John Wiley & Sons, Chichester (East Sussex UK), 312 pp.

Kolmogorov, A.N. (1941): Interpolated and extrapolated stationary random sequences; *Seriya Matematicheskaya* 5 (1), Isvestia Akademii Nauk SSSR (former Soviet Union) (in Russian).

Kraak, M.J. & Ormeling, F.J. (1996): *Cartography: visualisation of spatial data*; Longman Group, Harlow (Essex UK), 222 pp.

Krige, D.G. (1966): Two-dimensional weighted moving average trend surface for ore-evaluation; *Journal of the South African Institute of Mining Metallurgy* 66, 13–38.

Kureha, M. (1995): *Wintersportgebiete in Österreich und Japan*; *Innsbrucker Geograpische Studien* 24, Selbstverlag des Instituts für Geographie der Universität Innsbruck, Innsbruck (Tyrol - Austria), 188 pp. (in German, with English summary).

Kutiel, P., Lavee, H., Segev, M. Benyamini, Y. (1995): The effect of fire-induced surface heterogeneity on rainfall-runoff-erosion relationships in an eastern Mediterranean ecosystem, Israel; *Catena* 24 (1 4), 77 87.

Kutílek, M. & Nielsen, D.R. (1994): *Soil hydrology: textbook for students of soil science, agriculture, forestry, geoecology, hydrology, geomorphology or other related disciplines*; *GeoEcology*, Catena Verlag, Cremlingen-Destedt (Lower Saxony Germany), 370 pp.

Langbein, W.R. (1940): Channel storage and unit hydrograph studies; *Transactions AGU* 21, 620 627.

Leopold, L.B. (1991): Lag times for small drainage basins; *Catena* 18, 157 171.

Löhmannsröben, R. (1984): Erosionzprozesse in Meran 2000: Kausalanalytische Geländeuntersuchung unter besondererer Berücksichtigung der Bodenverhältnisse. Chapter 3 *in*: Cernusca, A. (ed.): *Ökologisches Gutachten über die Ursachen der Erosionen in Meran 2000 und Vorschläge für Sanierungsmaßnahmen*; Abteilung Ökologie, Institut für Botanik, Leopold Franzens Universität, Innsbruck (Tyrol Austria), 151 pp. (in German).

Löhmannsröben, R. & Cernusca, A. (1990): Bodenverhältnisse, Oberflächenabfluß und Erosionsgefährdung im Skigebiet am Stubnerkogel; *Verhandlungen der Gesellschaft für Ökologie* 19, 15 pp. (submitted version, in German).

Luk, S.-H. (1985): Effect of antecedent soil moisture content on rainwash erosion; *Catena* 12, 129 139.

Luk, S.-H., Abrahams, A.D. & Parsons, A.J. (1986): A simple rainfall simulator and trickle system for hydro-geomorphological experiments; *Physical Geography* 7 (4), 34 356.

Luk, S.-H. & Morgan, C. (1981): Spatial variation of rainwash and runoff within apparently homogeneous areas; *Catena* 8, 383 402.

Lusby, G.C. & Toy, T.J. (1976): An evaluation of surface mine spoils area restoration in Wyoming using rainfall simulation; *Earth Surface Processes* 1 (4), 375 386.

Mannaerts, Ch. (1993): *Assessment of the transferability of laboratory rainfall runoff and rainfall soil loss relationships to field and catchment scales a study in the Cape Verde Islands*; *ITC Publication* 19, ITC (International Institute for Aerospace Survey and Earth Sciences), Enschede (The Netherlands), 217 pp.

Markart, G., Kohl, B., Poscher, G., Wanker, W., Schnetzer, I. (1999): Assessment of runoff characteristics in a torrent catchment area; *Proceedings of the XXVII IAHR Congress*, 9 pp. (CD-ROM publication).

Markart, G., Kohl, B., Pramstraller, A., Gallmetzer, W. (2000): *Wirkung von Begrünungen auf das Abflußverhalten in Wildbacheinzugsgebieten bei Starkregen*; Interpraevent, Villach (Karinthia Austria), 12 pp. (unpublished, in German).

Mason, D.D., Lutz, J.F. & Petersen, R.G. (1957): Hydraulic conductivity as related to certain soil properties in a number of great soil groups sampling errors involved; *Soil Science Society of America Proceedings* 21 (5), 554 560.

McGrew, J.C. & Monroe, C.B. (1993): *An introduction to statistical problem solving in geography*; William C. Brown Publishers, Dubuque (Iowa USA), 305 pp.

Merz, W. & Bryan, R.B. (1993): Critical conditions for rill initiation on sandy loam brunisols: laboratory and field experiments in southern Ontario, Canada; *Geoderma* 57, 357–385.

Meurer, M. (1984): Höhenstufung von Klima und Vegetation; *Geographische Rundschau* 36 (8), 395-403 (in German).

Meyer, L.D. & McCue, D.L. (1958): Rainfall simulator for runoff plots; *Agricultural Engineering* 39 (10), 644 648.

Moore, I.D., Hirschi, M.C., Barfield, B.J., Barnhisel, R.I. & Leopold, M. (1981): A new portable rainfall simulator for erosion and runoff yield. 233 239 *In*: Text for poster session Erosion and sediment

transport measurement, *Proceedings of the Florence Symposium 22 26 June 1981*, Instituto di Ingegneria Civile, Università di Firenze, Florence (Toscane Italy), 313 pp.

Morgan, R.P.C. (1995): *Soil erosion and conservation*; Longman Technical and Scientific, Harlow (Essex UK), 198 pp.

Morgan, R.P.C., Quinton, J.N., Smith, R.E., Govers, G.J., Poesen, J.W.A., Auerswald, K., Chisci, G., Torri, D., Stycen, M.E., Folly, A.J.V. (1998a): *The European Soil Erosion Model (EUROSEM): documentation and user guide, version 3.6*; Silsoe College, Cranfield University, Silsoe (Bedford UK), 22 pp.

Morgan, R.P.C., Quinton, J.N., Smith, R.E., Govers, G.J., Poesen, J.W.A., Auerswald, K., Chisci, G., Torri, D., Stycen, M.E. (1998b): The European Soil Erosion Model (EUROSEM): a dynamic approach for predicting sediment transport from fields and small catchments; *Earth Surface Processes and Landforms* 23, 527 544.

Mosimann, Th. (1981): Geoökologische Standortsindikatoren für die Erosionsanfälligkeit alpiner Hänge nach Geländeeingriffen für Pistenanlagen; *Geomethodica* 6, 143 174 (in Germann).

Mosimann, Th. (1983): Landschaftsökologischer Einfluss von Anlagen für den Massenskisport. II. Bodenzustand und Bodenstörungen auf planierten Skipisten in verschiedenen Lagen (Beispiel Crap Sogn Gion, Laax). *Materialien zur Physiogeographie* 3, *Basler Beträge zur Physiogeographie*, Ordinariat für Physiogeographie, Geographisches Institut der Universität Basel, Basel (Switserland), 72 pp.

Mosimann, Th. (1985): Landschaftsökologischer Einfluss von Anlagen für den Massenskisport. III. Ökologische Entwicklung von Pistenflächen Entwicklungstendenzen im Erosionsgeschehen und beim Wiederbewuchs planierter Pisten im Skigebiet Crap Sogn Gion / Laax GR; *Materialien zur Physiogeographie* 9, *Basler Beträge zur Physiogeographie*, Ordinariat für Physiogeographie, Geographisches Institut der Universität Basel, Basel (Switserland), 40 pp.

Mosimann, Th. (1986): Skitourismus und Umweltbelastung im Hochgebirge; *Geographische Rundschau* 38, 303–311 (in German).

Neibling, W.H., Foster, G.R., Nattermann, R.A., Nowlin, J.D., & Holbert, P.V. (1981): Laboratory and field testing of a programmable plot-sized rainfall simulator; Erosion and sediment transport measurement, *Proceedings of the Florence Symposium 22 26 June 1981*, *IAHS Publication* 133, 405 414.

Netto, A.M., Pieritz, R.A. & Gadet, J.P. (1999): Field study on the local variability of soil water content and solute concentration; *Journal of Hydrology* 215, 23 37.

Neweseley, Ch., Cernusca, A., Bodner, M. (1994): Entstehung und Auswirkung von Sauerstoffmangel im Bereich unterschiedlich präparierter Schipisten; *Verhandlungen der Gesellschaft für Ökologie* 23, 277 282 (in German, with English synopsis).

Neweseley, Ch. (1997): *Auswirkungen der künstlichen Beschneiung von Schipisten auf Aufbau, Struktur und Gasdurchlässigkeit der Schneedecke, sowie auf den Verlauf der Bodentemperatur und das Auftreten von Bodenfrost*; PhD Thesis, Abteilung Ökologie, Institut für Botanik, Leopold Franzens Universität, Innsbruck (Tyrol Austria) (in German, with English abstract).

Nicolau, J.M., Solé-Benet, A., Puigdefábregas, J. & Guttiérez, L. (1996): Effects of soil and vegetation on runoff along a catena in semi-arid Spain; *Geomorphology* 14 (1), 297 309.

Nielsen, D.R., Biggar, J.W. & Erh, K.T. (1973): Spatial variability of field measured soil water properties; *Hilgardia* 42, 215 259.

Noomen, M.F. & Kooijman, C.M.H. (2000): *Untitled*; MSc Thesis, Vakgroep Fysische Geografie, Faculteit Ruimtelijke Wetenschappen, Universiteit Utrecht, Utrecht (The Netherlands), 53 pp. (draft version, in Dutch).

Oliver, M.A. & Webster, R. (1986): Semi-variograms for modelling the spatial patterns of landform and soil properties; *Earth Surface Processes and Landforms* 11 (5), 491–504.

Overbeek, J. & Wiersma, J. (1996): Puinstroomsystemen in de Franse Alpen infiltratiekarakteristieken en dateringen; MSc Thesis, Vakgroep Fysische Geografie, Faculteit Ruimtelijke Wetenschappen, Universiteit Utrecht, Utrecht (The Netherlands), 110 pp. (in Dutch).

Parsons, A.J. & Lascelles, B. (eds.) (2000): Special Issue: Rainfall simulations in geomorphology; *Earth Surface Processes and Landforms* 25 (7), 679 741.

Pearce, A.J. (1976): Magnitude and frequency of erosion by Hortonian overland flow; *Journal of Geology* 84, 65–80.

Pebesma, E.J. & Wesseling, C.G. (1998): Gstat: a program for geostatistical modelling, prediction and simulation; *Computers & Geosciences* 24 (1), 17-31.

Perroux, K.M. & White, I. (1988): Design for disc permeameter; *Soil Science Society of America Journal* 52, 1205–1215.

Poesen, J.W.A. (1986): Surface sealing as influenced by slope angle and position of simulated stones in the top layer of loose sediments; *Earth Surface Processes and Landforms* 11 (1), 1 10.
Poesen, J.W.A. (1987): Transport of rock fragments by rill flow – a field study. 35–54 *In*: Bryan, R.B. (ed.): *Rill Erosion – Processes and Significance*; *Catena Supplement* 8, Catena Verlag, Cremlingen-Destedt (Lower Saxony Germany), 160 pp.
Poesen, J.W.A. & Lavee, H. (1994): Rock fragments in top soils: significance and processes; *Catena* 23 (1), 1 28.
Purtscheller, F. (1978): *Ötztaler und Stubaier Alpen*; *Sammlung Geologische Führer* 53, Gebrüder Borntraeger (Berlin - Germany), 127 pp. (in German).
Prakash, A. (2000): *GETS/Objectives – Research objectives and content*; http://www.itc.nl/~gets/objectives.html.
Ramskogler, K. (1987): Schierschließungen Auswirkungen auf Boden und Bestand am Beispiel des Schigroßraumes Gasteinertal; *Österreichische Forstzeitung* 98 (6), 5 8.
Rauws, G. & Govers, G. (1988): Hydraulic and soil mechanical aspects of rill generation on agricultural soils; *Journal of Soil Science* 39, 111–124.
Rawls, W.J. (1983): Estimating soil bulk density from particle size analysis and organic matter content; *Soil Science* 135 (2), 123 125.
Reichardt, K., Bachi, O.O.S., De las Mercedes Villagra, M., Turatti, A.I. & Pedrosa, Z.O. (1993): Hydraulic variability in space and time in a dark red latosol of the tropics; *Geoderma* 60, 159–168.
Riezebos, H. Th. & Seyhan, E. (1977): Essential conditions of rainfall simulation for laboratory water erosion experiments; *Earth Surface Processes* 2 (2), 185 190.
Rodríguez-Iturbe, I. & Valdes, J.B. (1979): The geomorphological structure of hydrologic response; *Water Resources Research* 15, 1409 1420.
Roels, J.M. (1984): Surface runoff and sediment yield in the Ardèche Rangeland; *Earth Surface Processes and Landforms* 9 (4), 371–381.
Roth, C.H., Meyer, B., & Frede, H.-G. (1985): A portable rainfall simulator for studying factors affecting runoff infiltration and soil loss; *Catena* 12, 79 85.
Rowell, D.L. (1994): *Soil science methods and applications*; Longman Scientific & Technical, Harlow (Essex UK), 350 pp.
Russo, D. & Bresler, E. (1981): Soil hydraulic properties as stochastic processes: I. An analysis of field spatial variability; *Soil Science Society of America Journal* 45 (4), 682–687.
Russo, D. & Bresler, E. (1982): Soil hydraulic properties as stochastic processes: II. Errors of estimates in a heterogeneous field; *Soil Science Society of America Journal* 46 (1), 20–26.
Sander, B. (1912): Über einige Gesteinsgruppen des Tauernwestendes; *Jahresbuch der Geologische Reichsanstalt* 62 (in German).
Savat, J. & De Ploey, J. (1982): Sheetwash and rill development by surface flow. Chapter 6 *in*: Bryan, R.B. & Yair (eds.): *Badland Geomorphology and Piping*; GeoBooks, Norwich (Norfolk UK), 408 pp.
Schauer, T. (1981): Vegetationsveränderungen und Florenverlust auf Skipisten in den bayerische Alpen; *Jahresbuch des Vereines zur Schutze der Bergwelt* 46, 149 179.
Schiechtl, H.M. (1975): Die Vegetation Tirols. Chapter 1.5 *in*: Aulitzky, H., Feist, H. & Grubinger, H. (ed.): *Hochwasser- und Lawinenschutz in Tirol*; Land Tirol, Innsbruck (Tyrol Austria), 412 pp. (in German).
Schmidegg, O. (1933): Neue Ergebnisse aus den südlichen Ötztaler Alpen; *Verhandlungen der Geologischen Bundesanstalt* (in German).
Schmidt, W. (1922): Zur Phasenfolge in Ostalpenbau; *Verhandlungen der Geologischen Reichsanstalt* (in German).
Sevruk, B. (1996): Adjustment of tipping-bucket precipitation gauge measurements; *Atmospheric Research* 42, 237 246.
Sharma, M.L., Gander, G.A., & Hunt, C.G. (1980): Spatial variability of infiltration in a watershed; *Journal of Hydrology* 45 (3), 101–122.
Sherman, L.K. (1932): Stream flow from rainfall by the unit-graph method; *Engineering News Record* 108, 501 505.
Shipitalo, M.J., Edwards, W.M., Dick, W.A. & Owens, L.B. (1990): Initial storm effects on macropore transport of surface-applied chemicals in no-till soil; *Soil Science Society of America Journal* 54 (6), 1530 1536.
Sisson, J. & Wieringa, P.J. (1981): Spatial variability of steady-state infiltration rates as a stochastic process; *Soil Science Society of America Journal* 45 (4), 699–704.

Smith, R.E. & Parlange, J.Y. (1978): A parameter-efficient hydrologic infiltration model; *Water Resources Research* 14 (3), 533 538.

Sorriso-Valvo, M., Bryan, R.B., Yaï r, A., Iovino, F. & Antronico, L. (1995): Impact of afforestation on hydrological response and sediment production in a small Calabrian catchment; *Catena* 25 (1 4), 89 104.

Stanley, S.M. (1989): *Earth and life through time*; W. H. Freeman, New York (USA), 689 pp.

Stauder, S. (1974): Die Beeinflussung des Wasserhaushaltes im Wald durch Schiabfahrten; *Allgemeine Forstzeitung* 85, 171 172 (in German).

Strik, L.-A. (2000): *Degradatie van skipistes door oppervlakkige landslides in het skigebied rondom Sölden, Tirol verslag van een doktoraalveldwerk te Oostenrijk, 1999*; MSc Thesis, Vakgroep Fysische Geografie, Faculteit Ruimtelijke Wetenschappen, Universiteit Utrecht, Utrecht (The Netherlands) 22 pp. (draft version, in Dutch).

Sudicky, E.A. (1986): A natural gradient experiment on solute transport in a sand aquifer: spatial variability of hydraulic conductivity and its role in the dispersion process; *Water Resources Research* 22 (13), 2069–2082.

Tenschert, E. (1974): *Petrographische und Geochemische Untersuchungen am Granit bis Granodioritgneis Acherkogl/Sellrain und Engelswand*; PhD Thesis, Universität Innsbruck, Innsbruck (Tyrol - Austria) (in German).

Terwindt, J.H.J. (1990): Geologie. Chapter A.1 *in*: Beukenkamp, P.C. & Terwindt, J.H.J. (ed.): *Alpen-excursie 1990 - deel A*; Vakgroep Fysische Geografie, Faculteit Ruimtelijke Wetenschappen, Universiteit Utrecht, Utrecht (The Netherlands), 224 pp. (in Dutch).

Thiessen, A.H. (1911): Precipitation for large areas; *Monthly Weather Review* 39, 1082–1089.

Thonon, I. (1999): *Thresholds for incipient rilling and particle entrainment*; Vakgroep Fysische Geografie, Faculteit Ruimtelijke Wetenschappen, Universiteit Utrecht, Utrecht (The Netherlands) (unpublished).

Thonon, I. (2000): *Interpolation of hydraulic conductivities with the aid of different methods applied at measurements from Sölden, Tyrol, Austria*; Vakgroep Fysische Geografie, Faculteit Ruimtelijke Wetenschappen, Universiteit Utrecht, Utrecht (The Netherlands), 40 pp. (unpublished).

Tietje, O. (1993): *Räumliche Variabilität bei der Modellierung der Bodenwasserbewegung in der ungesättigten Zone*; *Landschaftökologie und Umweltforschung* 21, Selbstverlag Institut für Geographie und Geoökologie der Technischen Universität Braunschweig, Braunschweig (Lower Saxony Germany), 118 pp. (in German).

Tivy, J. (1993): *Biogeography - a study of plants in the ecosphere*; Longman Group, Harlow (Essex - UK), 452 pp.

Tobler, W. (1979): Smooth pycnophylactic interpolation for geographic regions; *Journal of the American Statistical Association* 74 (367), 519–536.

Toldrian, H. (1974): Wasserabfluß und Bodenabtrag in verschiedenen Waldbeständen; *Allgemeine Forstzeitung* 49, 1107 1109 (in German).

Torri, D., Sfalanga, M. & Chisci, G. (1987): Threshold conditions for incipient rilling. 97–105 *In*: Bryan, R.B. (ed.): *Rill erosion – Processes and Significance*; *Catena Supplement* 8, Catena Verlag, Cremlingen-Destedt (Lower Saxony Germany), 160 pp.

Torri, D., Poesen, J.W.A., Monaci, F., Busoni, E. (1994): Rock fragment content and fine soil bulk density; *Catena* 23 (1), 65 71.

Van Asch, Th.W.J. (1980): Water erosion on slopes and landsliding in a Mediterranean landscape; Utrechtse Geografische Studies 20, Faculteit Ruimtelijke Wetenschappen, Universiteit Utrecht (Utrecht The Netherlands), 238 pp. *Also*: PhD Thesis Utrecht University.

Van den Berg, J.A. (1989): *Variability of soil parameters for modelling soil moisture content studies on loamy to silty soils on marly bedrock in the Ardèche drainage basin, France*; *Nederlandse Geografische Studies/Netherlands Geographical Studies* 93, Koninklijk Nederlands Aardrijkskundig Genootschap / Faculteit Ruimtelijke Wetenschappen, Universiteit Utrecht, Utrecht (The Netherlands), 214 pp. *Also*: PhD Thesis Utrecht University.

Van Dijck, S.J.E. (2000): *Effects of agricultural land use on surface runoff and erosion in a Mediterranean area*; *Nederlandse Geografische Studies/Netherlands Geographical Studies* 265, Koninklijk Nederlands Aardrijkskundig Genootschap / Faculteit Ruimtelijke Wetenschappen, Universiteit Utrecht, Utrecht (The Netherlands), 234 pp. *Also*: PhD Thesis Utrecht University.

Verhees, L. (1998): De indringingsweerstand als basis voor kwantificatie van overland flow en compactie van zandige leem in een Zuid-Frans wijbouw gebied; MSc Thesis, Vakgroep Fysische Geografie, Faculteit Ruimtelijke Wetenschappen, Universiteit Utrecht, Utrecht (The Netherlands), 47 pp. (in Dutch).

Vieira, S.R., Nielsen, D.R. & Biggar, J.W. (1981): Spatial variability of field-measured infiltration rate; *Soil Science Society of America Journal* 45 (6), 1040–1048.

Von Klebelsberg, R. (1935): *Geologie von Tirol*; (Verlag von) Gebrüder Borntraeger, Berlin (Germany), 872 pp. (in German).

Waniliesta, M. (1990): *Hydrology and water quantity control*; John Wiley & Sons, New York (USA), 565 pp.

Ward, R.C. & Robinson, M. (1990): *Principles of hydrology*; McGraw-Hill, Maidenhead (Berkshire UK), 365 pp.

Webster, R. (1994): The development of pedometrics; *Geoderma* 62 (1), 1–15.

Wesseling, C.G., Karssenberg, D., Burrough, P.A. & van Deursen, W.P.A. (1996): Integrating dynamic environmental models in GIS: the development of a Dynamic Modelling Language; *Transactions in GIS* 1 (1), 40 – 48.

Whalley, W.R. (1993): Considerations on the use of time-domain reflectrometry (TDR) for measuring soil water content; *Journal of Soil Science* 43, 1 9.

Wilding, L.P. & Drees, L.R. (1978): Spatial variability: a pedologist's viewpoint. Chapter 1 *in*: Drosdorff, M., Daniels, R.B. & Nicholaides, J.J. (eds.): *Diversity of soils in the tropics*; *Soil Science Society of America Special Publication* 34, Soil Science Society of America & American Society of Agronomy, Madison (Wisconsin USA), 119 pp.

Wilding, L.P. & Drees, L.R. (1983): Spatial variability and pedology. Chapter 4 *in*: Wilding, L.P., Smeck, N.E. & Hall, G.F. (eds.): *Pedogenesis and soil taxonomy I. Concepts and interactions*; *Developments in Soil Science* 11A, Elsevier Science Publishers, Amsterdam (The Netherlands), 303 pp.

Reference abbreviations

ASAE	American Society of Agricultural Engineers
ASCE	American Society of Civil Engineers
AGU	American Geophysical Union
DVWK	Deutsche Verein für Wasserkunde (German for 'German Association for Water Science')
IAHR	International Association of Hydrological Research
IAHS	International Association of Hydrological Sciences
ITC	formerly known as International Training Centre, now International Institute for Aerospace Survey and Earth Sciences
NF	Neue Folge (German for 'new series')
UK	United Kingdom
USA	United States of America
USGS	United States Geological Survey